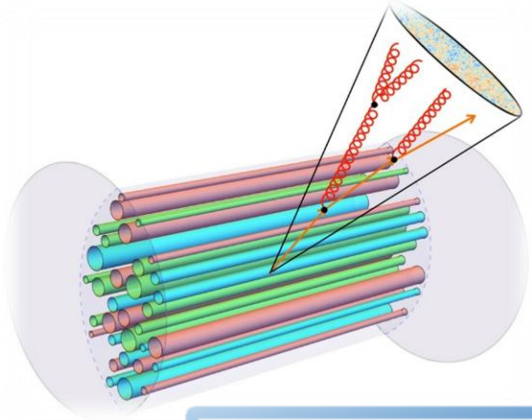

Bulk medium and hard probe transport coefficients in the strongly interacting QGP

Olga Soloveva (GSI & HFHF & ITP Goethe University Frankfurt)

I. Grishmanovskii, G. Ingrosso, T. Song,

E. Bratkovskaya, C. Greiner

2608.xxxx

17 July 2026

Emmi Workshop

“Probing the early stages with jets“

GSI

HFHF

EMMI

CRC-TR 211

Strong-interaction matter under extreme conditions

GOETHE UNIVERSITÄT FRANKFURT AM MAIN

How do microscopic QGP degrees of freedom control heavy-quark and jet observables?

Relevant for observables

- heavy-flavour $\mathbf{R_{AA}}$ and $\mathbf{v_2}$
- charm / bottom diffusion
- jet and HQ energy loss
- elastic vs radiative mechanisms

Microscopic input

- EoS and finite-**(T, μ_B)** properties
- quasiparticle masses and widths
- off-shell spectral functions
- non-perturbative scattering rates

Transport link

- transport coefficients, relaxation times and diffusion matrix
- bridge to hydro / lQCD constraints
- comparison to phenomenology

η/s, ζ/s, D_BQS, σ_e/T, D_s, κ, $\hat{q}$, $A(p)$, $B_0(p)$, $B_1(p)$

PHSD/DQPM advantage: **the same microscopic quasiparticle picture can be tested from transport coefficients to final-state heavy-flavour and jet observables.**

Heavy quarks and jets are inverse probes of the microscopic structure of the strongly interacting QGP.

Properties of QGP: transport coefficients

"Numerical simulations are now essential to make contact between theory and experiment" - J. Kapusta

! One has to specify transport and microscopic properties as well as EoS for theoretical simulations of HICs (hydro / transport approaches)

EoS(ε,n)

$\boldsymbol{\sigma(\sqrt{s}, m_q, m_q, T, \mu_B)}$

$\mathbf{m}(\boldsymbol{T, \mu_B})$

On practice: effective models for QGP

Transport simulations with QGP phase:

Catania transport – QuasiParticle Model

F. Scardina, S. K. Das, V. Minissale, S. Plumari, and V. Greco, PRC 96, 044905 (2017).

PHSD – Dynamical QPM for partonic phase

W. Cassing, E. Bratkovskaya, PRC 78 (2008) 034919
P. Moreau, O. S , L. Oliva, T. Song, W. Cassing, E. Bratkovskaya, PRC 100 (2019) , 014911;
O. S, P. Moreau, L. Oliva, V. Voronyuk, V. Kireyeu, T. Song, E. Bratkovskaya, Particles 3 (2020), 178-192

AMPT – PNJL EoS (Mean field potentials)

K.J. Sun, C. M. Ko, and Z.-W. Lin, PRC 103(2021)

Hybrid simulations with QGP:

vHLLE/Music+UrQMD/SMASH

Iu.A. Karpenko, P. Huovinen, H. Petersen and M. Bleicher PRC 91 (2015), 064901.
S. Ryu, J.F.Paquet, C. Shen, G.S. Denicol, B. Schenke PRL 115 (2015), 132301

Degrees of freedom of QGP

lQCD: QGP EoS at finite μ_B

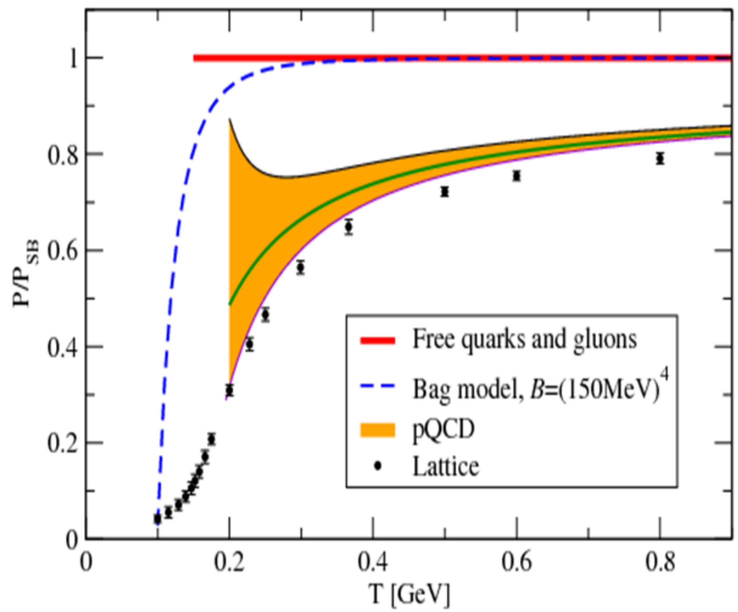

Non-perturbative QCD ← pQCD

pQCD: (Yang-Mills) shear viscosity η

J. Ghiglieri, G.D. Moore, D. Teaney, JHEP 1803 (2018) 179

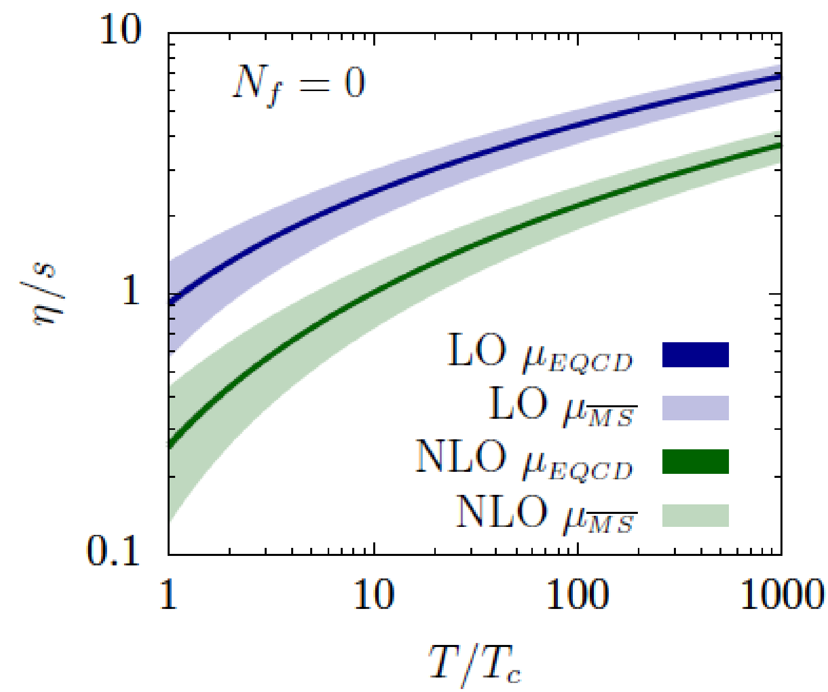

pQCD:

- **weakly interacting system**
- **massless quarks and gluons**

Thermal (non-perturbative) QCD:

- **strongly interacting system**
- **massive quarks and gluons**

➔ Quasiparticles = effective degrees-of-freedom

Dynamical Quasi-Particle Model (DQPM)

DQPM – effective model for the description of non-perturbative (strongly interacting) QCD based on lQCD EoS

Degrees-of-freedom: strongly interacting dynamical quasiparticles - quarks and gluons

$$\rho_j(\omega,\mathbf{p}) = \frac{\gamma_j}{\tilde{E}_j}\left(\frac{1}{(\omega-\tilde{E}_j)^2+\gamma_j^2} - \frac{1}{(\omega+\tilde{E}_j)^2+\gamma_j^2}\right)$$

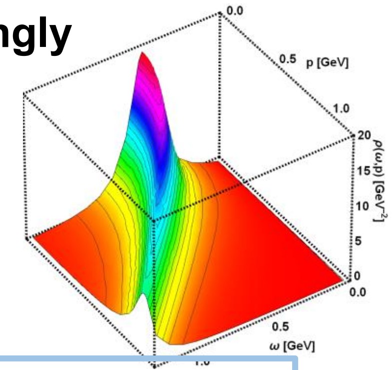

resummed propagators: $\Delta_i(\omega,\mathbf{p}) = \dfrac{1}{\omega^2-\mathbf{p}^2-\Pi_i}$ & self-energies: $\Pi_i = m_i^2 - 2i\gamma_i\omega$

Re $\boldsymbol{\Pi_i}$: thermal mass $(\boldsymbol{M_g}, \boldsymbol{M_q})$

$$m^2_{q(\bar{q})}(T,\mu_\mathrm{B}) = C_q \frac{g^2(T,\mu_\mathrm{B})}{4} T^2 \left[1+\left(\frac{\mu_B}{3\pi T}\right)^2\right]$$

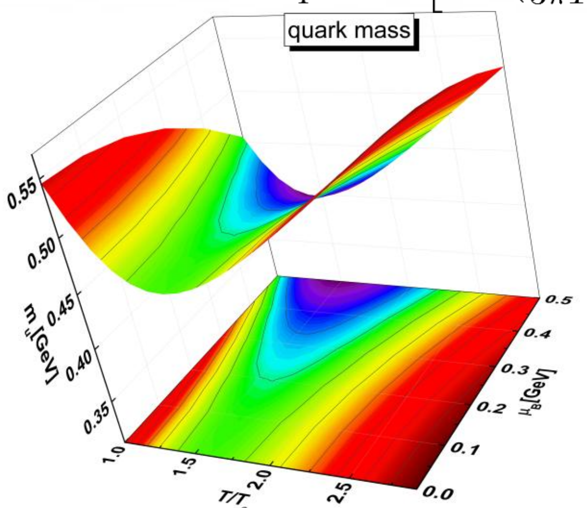

Im $\boldsymbol{\Pi_i}$: interaction width $(\boldsymbol{\gamma_g}, \boldsymbol{\gamma_q})$

$$\gamma_j(T,\mu_\mathrm{B}) = \frac{1}{3} C_j \frac{g^2(T,\mu_\mathrm{B})T}{8\pi} \ln\left(\frac{2c_m}{g^2(T,\mu_\mathrm{B})}+1\right)$$

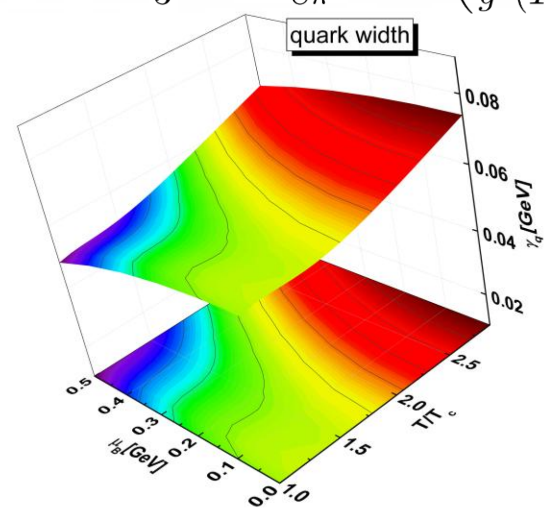

Peshier, Cassing, PRL 94 (2005) 172301; Cassing, NPA 791 (2007) 365; H. Berrehrah, E. Bratkovskaya, T. Steinert, W. Cassing, Int. J. Mod. Phys. E 25 (2016), 164200; P. Moreau, O. Soloveva , L. Oliva, T. Song, W. Cassing, E. Bratkovskaya, PRC 100 (2019) , 014911;

DQPM: Parton properties

Realization concept:

- introduce an ansatz (HTL; with few parameters) for the (T, μ_B) dependence of masses/widths
- evaluate the QGP thermodynamics in equilibrium using the Kadanoff-Baym theory
- fix DQPM parameters by comparison of the DQPM entropy density to lQCD at $\mu_B=0$

- **Masses** and **widths** of quasiparticles depend on T and μ_B

$$m_g^2(T,\mu_B) = C_g \frac{g^2(T,\mu_B)}{6} T^2 \left(1 + \frac{N_f}{2N_c} + \frac{1}{2}\frac{\sum_q \mu_q^2}{T^2\pi^2}\right)$$

$$m_{q(\bar{q})}^2(T,\mu_B) = C_q \frac{g^2(T,\mu_B)}{4} T^2 \left(1 + \frac{\mu_q^2}{T^2\pi^2}\right)$$

$$\gamma_j(T,\mu_B) = \frac{1}{3} C_j \frac{g^2(T,\mu_B) T}{8\pi} \ln\left(\frac{2c_m}{g^2(T,\mu_B)} + 1\right)$$

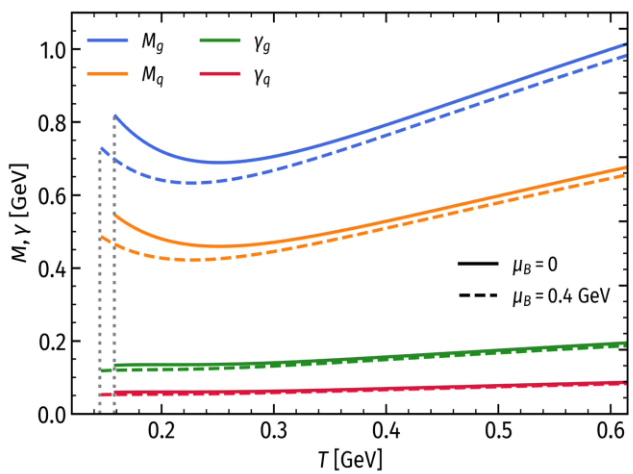

- **Strong coupling** (g) is defined from **lQCD entropy density** at $\mu_B=0$, using

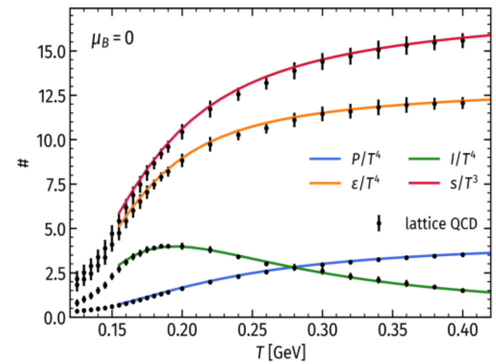

$$g^2(s/s_{SB}) = d((s/s_{SB})^e - 1)^f$$

$$s_{SB}^{QCD} = 19/9\,\pi^2 T^3$$

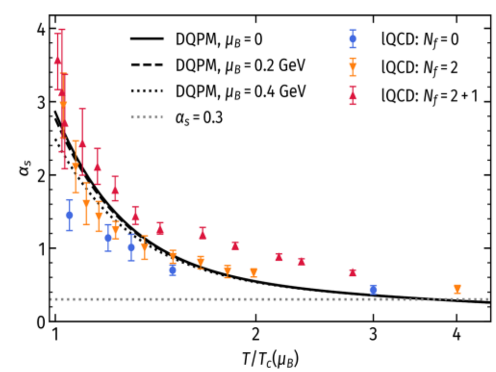

$$\alpha_s = g^2(T,\mu_B)/(4\pi)$$

→ DQPM allows to explore QCD in the **non-perturbative regime** of the (T, μ_B) phase diagram

Partonic interactions: matrix elements

DQPM partonic cross sections → leading order diagrams

- **Propagators for massive bosons and fermions:**

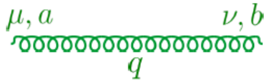

$$= -i\delta_{ab}\frac{g^{\mu\nu} - q^\mu q^\nu / M_g^2}{q^2 - M_g^2 + 2i\gamma_g q_0}$$

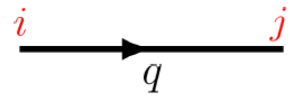

$$= i\delta_{ij}\frac{\not{q} + M_q}{q^2 - M_q^2 + 2i\gamma_q q_0}$$

- **(Quasi-) elastic channels:**

qq' → qq' scattering

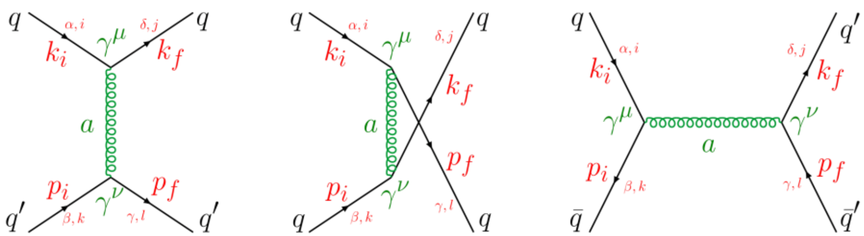

$t-$ channel $\quad u-$ channel $\quad s-$ channel

gq → gq scattering

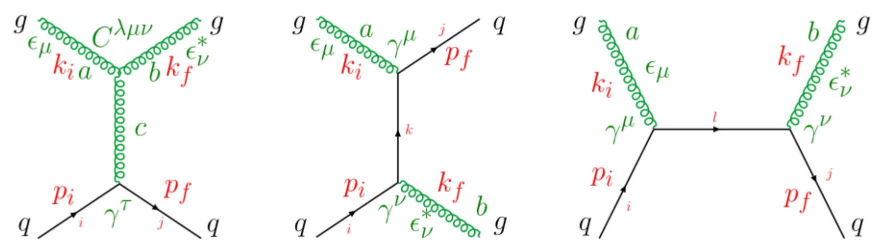

$t-$ channel $\quad u-$ channel $\quad s-$ channel

gg→ gg scattering

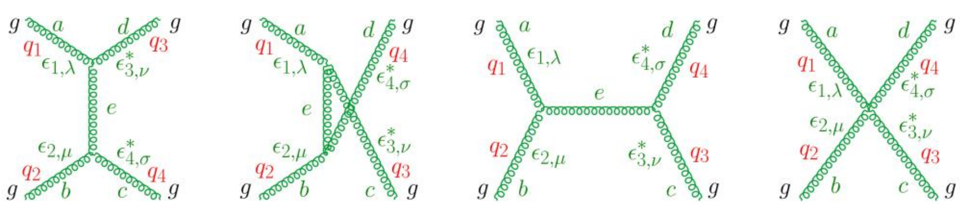

$t-$ channel $\quad u-$ channel $\quad s-$ channel $\quad 4-$ point

- **Inelastic channels:**

$$\mathrm{q} + \bar{\mathrm{q}} \to \mathrm{g}$$
$$\mathrm{g} \to \mathrm{q} + \bar{\mathrm{q}}$$

H. Berrehrah et al, PRC 93 (2016) 044914, Int.J.Mod.Phys. E25 (2016) 1642003, → P. Moreau, O.S., et al., PRC100 (2019) 014911

Differential cross section

On-shell:

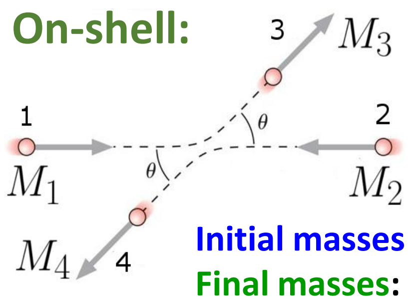

Initial masses: pole masses
Final masses: pole masses

Off-shell:

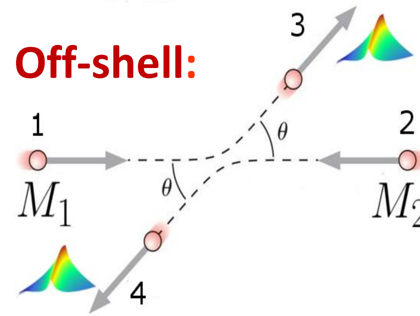

Initial masses: pole masses
Final masses: integration over spectral functions

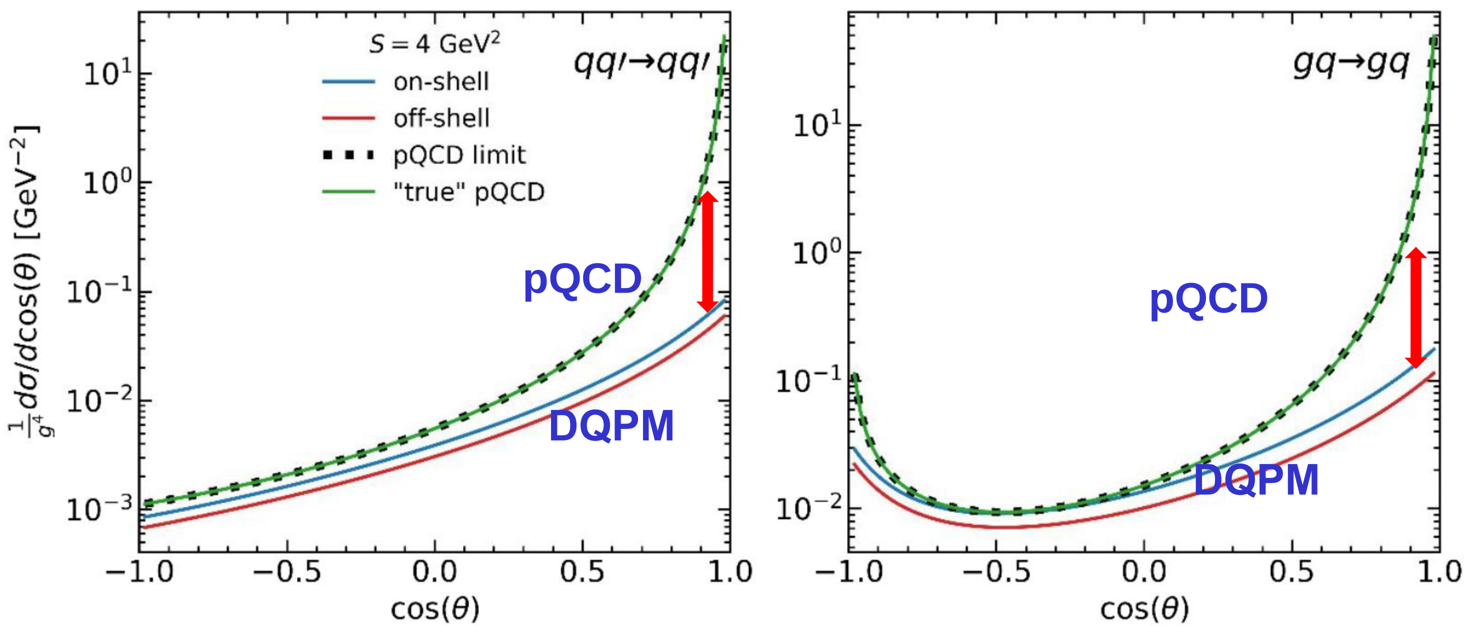

Plot by Ilia Grishmanovskii

- DQPM: M→0, γ→0 ➔ reproduces pQCD limits
- Differences between DQPM and pQCD : less forward peaked angular distribution leads to more efficient momentum transfer

P. Moreau, O.S. et al., PRC100 (2019) 014911

Probing the properties of the sQGP with jet partons

Extension of DQPM (T, μ_q)

elastic (2→2) + inelastic (2→3) scattering

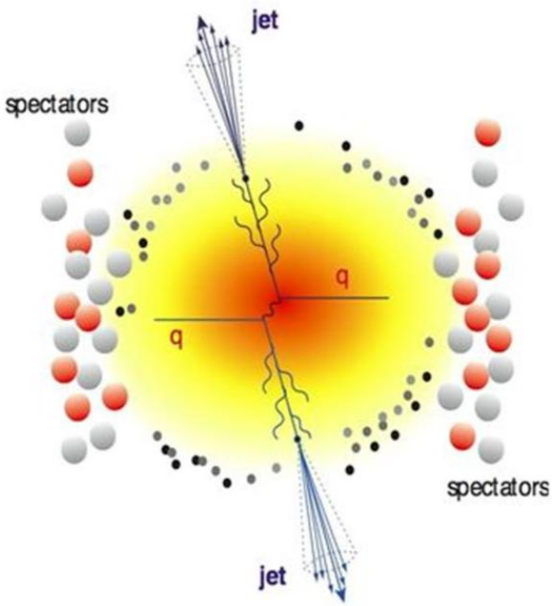

Partonic inelastic 2→3 interactions

quark + quark

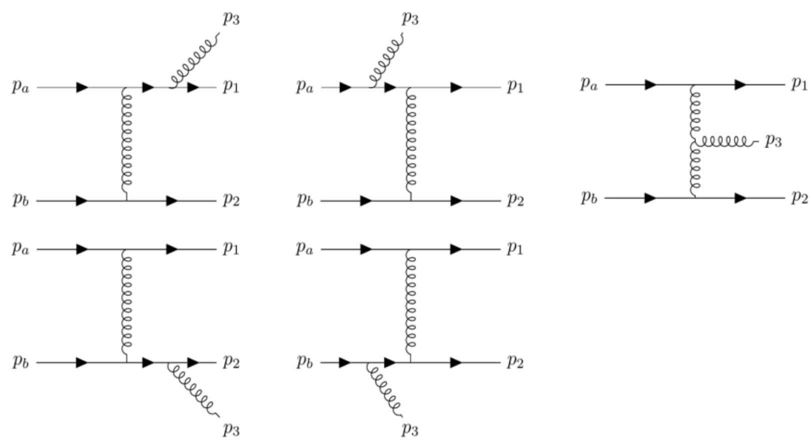

quark + gluon (t-channel)

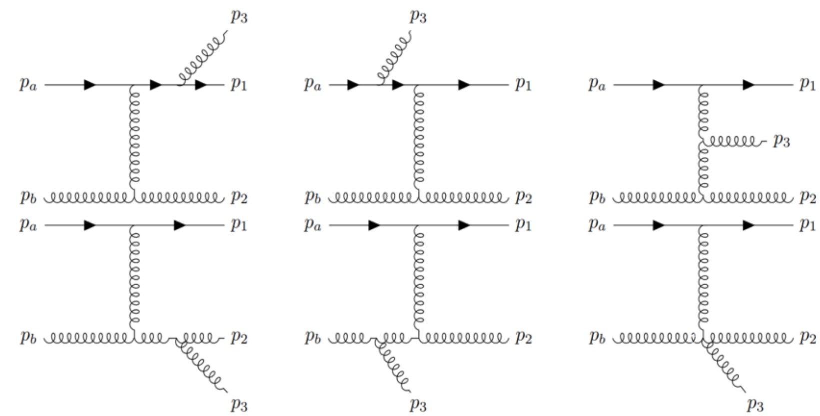

quark + gluon (u-channel)

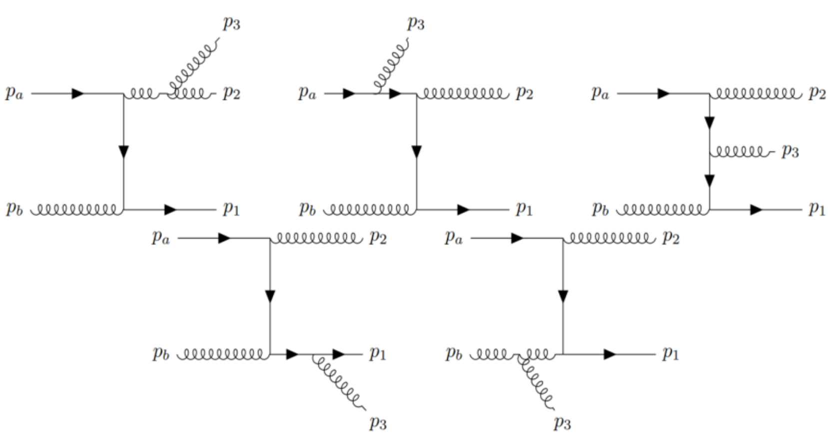

quark + gluon (s-channel)

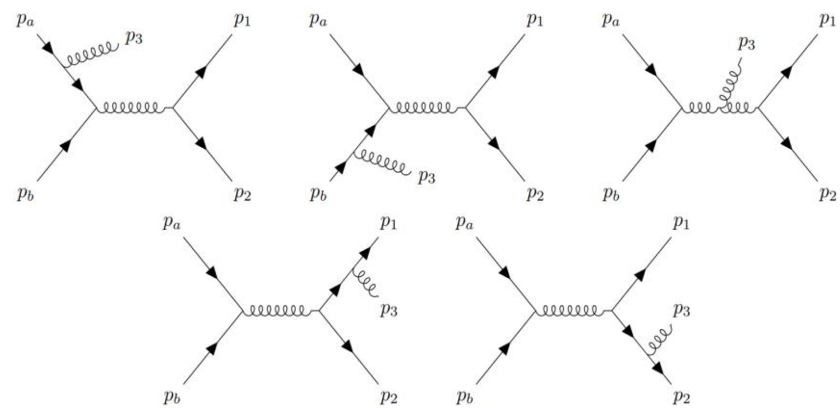

- **No approximations applied**
- **All interference terms included**
- **Emitted gluon is massive in DQPM**

I. Grishmanovskii, O.S. et al., PRC 109, 024911 (2024)

Properties of QGP: transport coefficients

Hydrodynamics

$$\begin{cases} \partial_\mu T^{\mu\nu} = 0 & T^{\mu\nu} = -Pg^{\mu\nu} + wu^\mu u^\nu + \Delta T^{\mu\nu} \\ \partial_\mu J_B^\mu = 0 & J_B^\mu = n_B u^\mu + \Delta J_B^\mu \end{cases}$$

$$\boxed{\eta}\left(D^\mu u^\nu + D^\nu u^\mu + \tfrac{2}{3}\Delta^{\mu\nu}\partial_\rho u^\rho\right) - \boxed{\zeta}\Delta^{\mu\nu}\partial_\rho u^\rho$$

$$\Delta J_B^\mu = \boxed{\kappa_B} D^\mu\left(\frac{\mu_B}{T}\right)$$

input for hydro

Transport coefficients:

Shear viscosity

$\eta \nabla^{<\mu} u^{\nu>}$

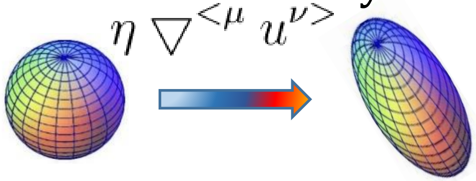

Bulk viscosity

$-\zeta \nabla u$

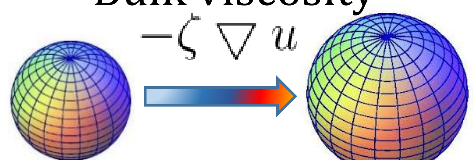

(B, Q, S) diffusion coefficients

$\kappa_q \nabla \frac{\mu_q}{T}$

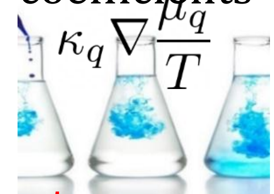

Model predictions for QGP: ! same EoS but different transport coefficients

Transport coefficients can serve a bridge for comparison transport and hydro

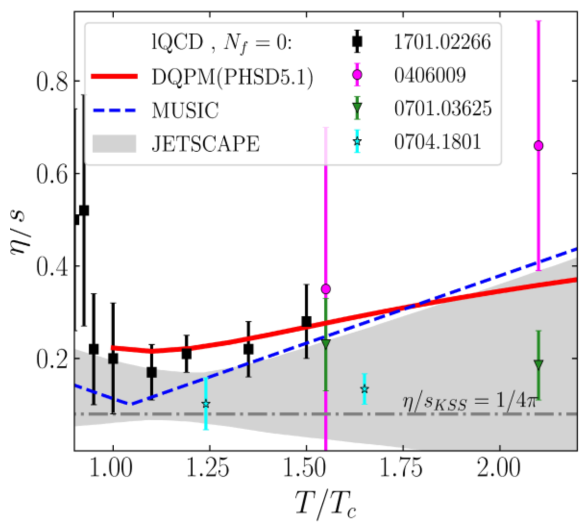

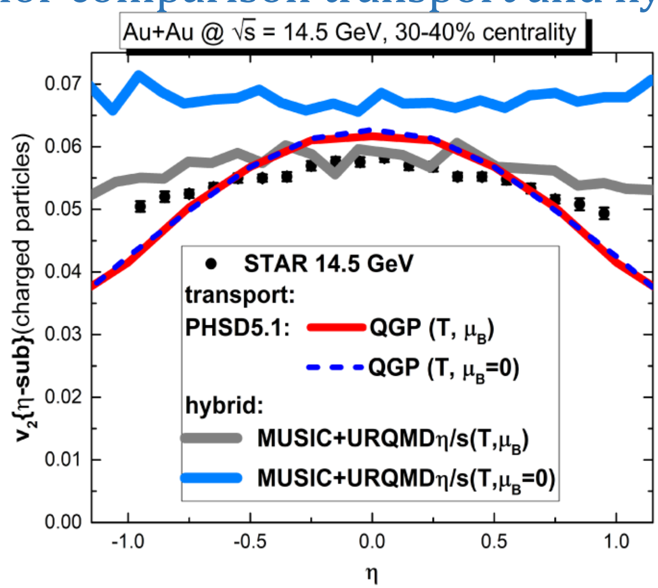

MUSIC:
C. Shen,
S.Alzhrani, PRC
102 (2020) 1,
014909

Transport coefficients at finite μ_B

$$\eta^{\mathrm{RTA}}(T,\mu_B) = \frac{1}{15T}\sum_{i=q,\bar{q},g}\int \frac{d^3p}{(2\pi)^3}\frac{\mathbf{p}^4}{E_i^2}\tau_i(\mathbf{p},T,\mu_B)\, d_i(1\pm f_i)f_i$$

$$\boxed{\tau_i(\mathbf{p},T,\mu_B) = \frac{1}{\Gamma_i(\mathbf{p},T,\mu_B)}}$$

2⟷2 scatterings

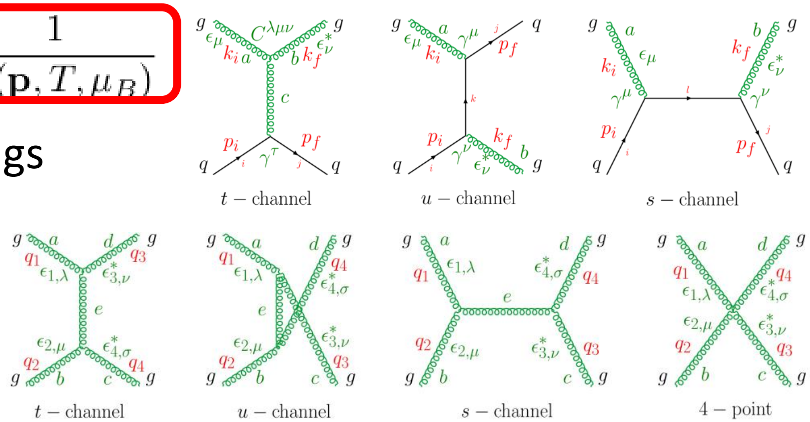

Relaxation times

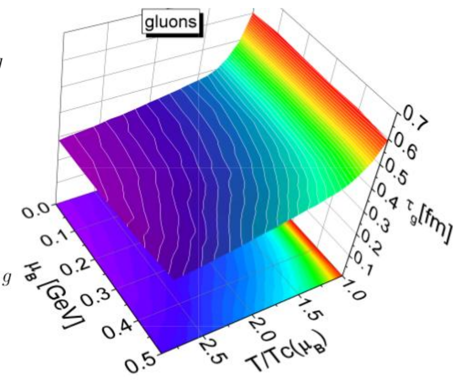

Specific shear viscosity

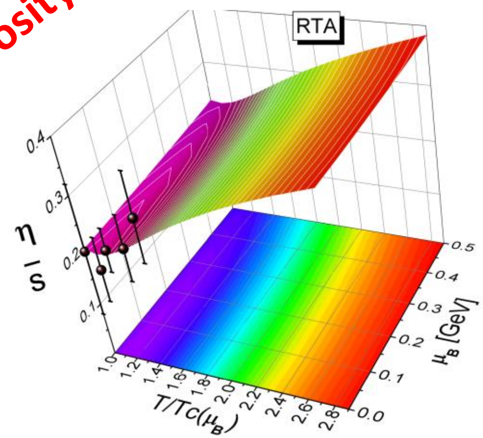

μ_B

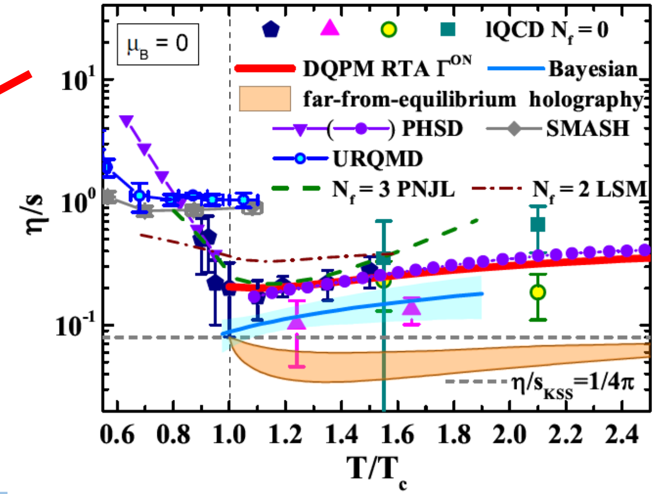

O. S., P. Moreau and E. Bratkovskaya, PRC 101 (2020), 045203

- Good agreement with lQCD predictions and Bayesian estimates
- Light increase with μ_B in the crossover region for viscosities and electric conductivity

Transport coefficients at finite μ_B

η/s versus (T,μ_B)

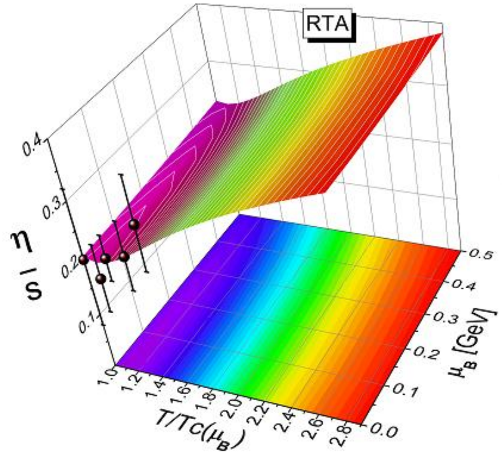

Bulk viscosity ζ/s

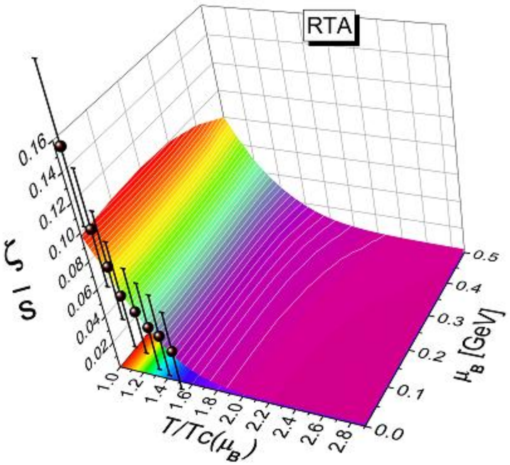

Speed of sound c_s^2

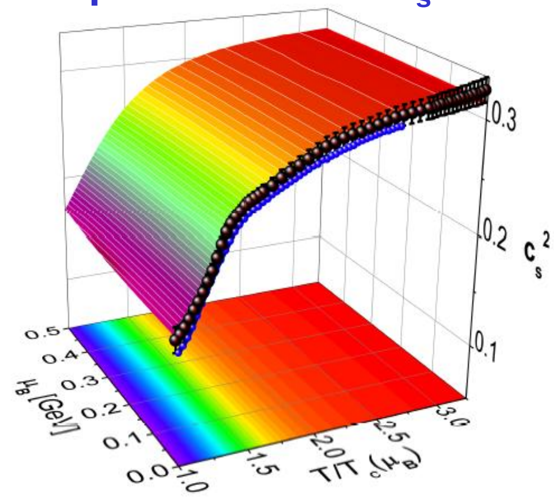

P. Moreau et al., PRC100 (2019) 014911;
O. Soloveva et al., PRC110 (2020) 045203

Electric conductivity σ_e/T

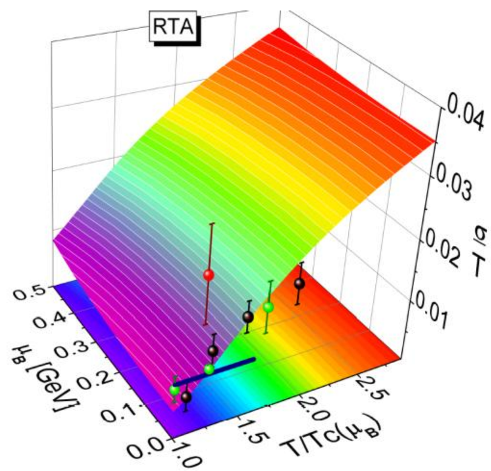

Baryon diffusion coefficient κ_B/T^2

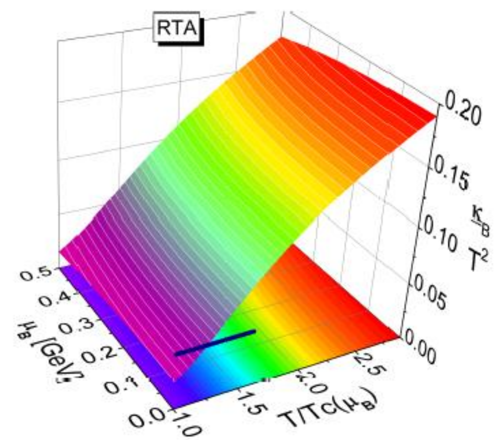

Full diffusion coefficient matrix:

$$\begin{pmatrix} j_B^\mu \\ j_Q^\mu \\ j_S^\mu \end{pmatrix} = \begin{pmatrix} \kappa_{BB} & \kappa_{BQ} & \kappa_{BS} \\ \kappa_{QB} & \kappa_{QQ} & \kappa_{QS} \\ \kappa_{SB} & \kappa_{SQ} & \kappa_{SS} \end{pmatrix} \cdot \begin{pmatrix} \nabla^\mu \alpha_B \\ \nabla^\mu \alpha_Q \\ \nabla^\mu \alpha_S \end{pmatrix}$$

J. A. Fotakis,O.S. et al., PRD 104 (2021) , 034014

- Weak dependence on μ_B in the crossover region

Transport coefficients at finite μ_B

$$\eta^{\mathrm{RTA}}(T,\mu_B) = \frac{1}{15T}\sum_{i=q,\bar{q},g}\int \frac{d^3p}{(2\pi)^3}\frac{\mathbf{p}^4}{E_i^2}\tau_i(\mathbf{p},T,\mu_B) \quad d_i(1\pm f_i)f_i$$

Relaxation times

$$\tau_i(\mathbf{p},T,\mu_B) = \frac{1}{\Gamma_i(\mathbf{p},T,\mu_B)}$$

2⟷2 + 2⟷3 scatterings

Specific shear viscosity

μ_B

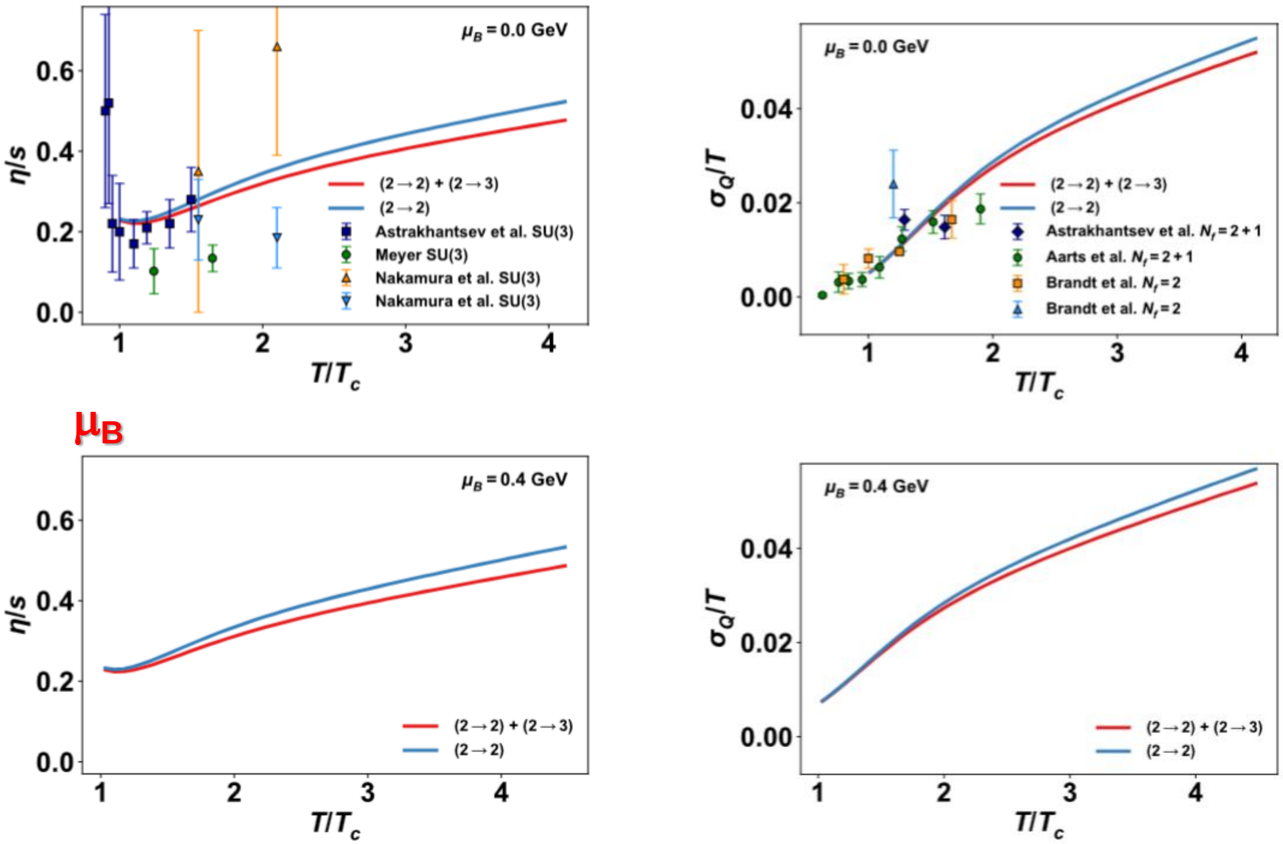

G. Ingrosso, O. S., I. Grishmanovskii and E. Bratkovskaya, arxiv:2606.13363

- Good agreement with lQCD predictions and Bayesian estimates
- Light increase with μ_B in the crossover region for viscosities and electric conductivity

Transport coefficients at finite μ_B

$$\eta^{\mathrm{RTA}}(T,\mu_B) = \frac{1}{15T}\sum_{i=q,\bar{q},g}\int \frac{d^3p}{(2\pi)^3}\frac{\mathbf{p}^4}{E_i^2}\tau_i(\mathbf{p},T,\mu_B)\, d_i(1\pm f_i)f_i$$

Relaxation times

$$\boxed{\tau_i(\mathbf{p},T,\mu_B) = \frac{1}{\Gamma_i(\mathbf{p},T,\mu_B)}}$$

$2 \leftrightarrow 2\ + 2 \leftrightarrow 3$
scatterings

Specific bulk viscosity

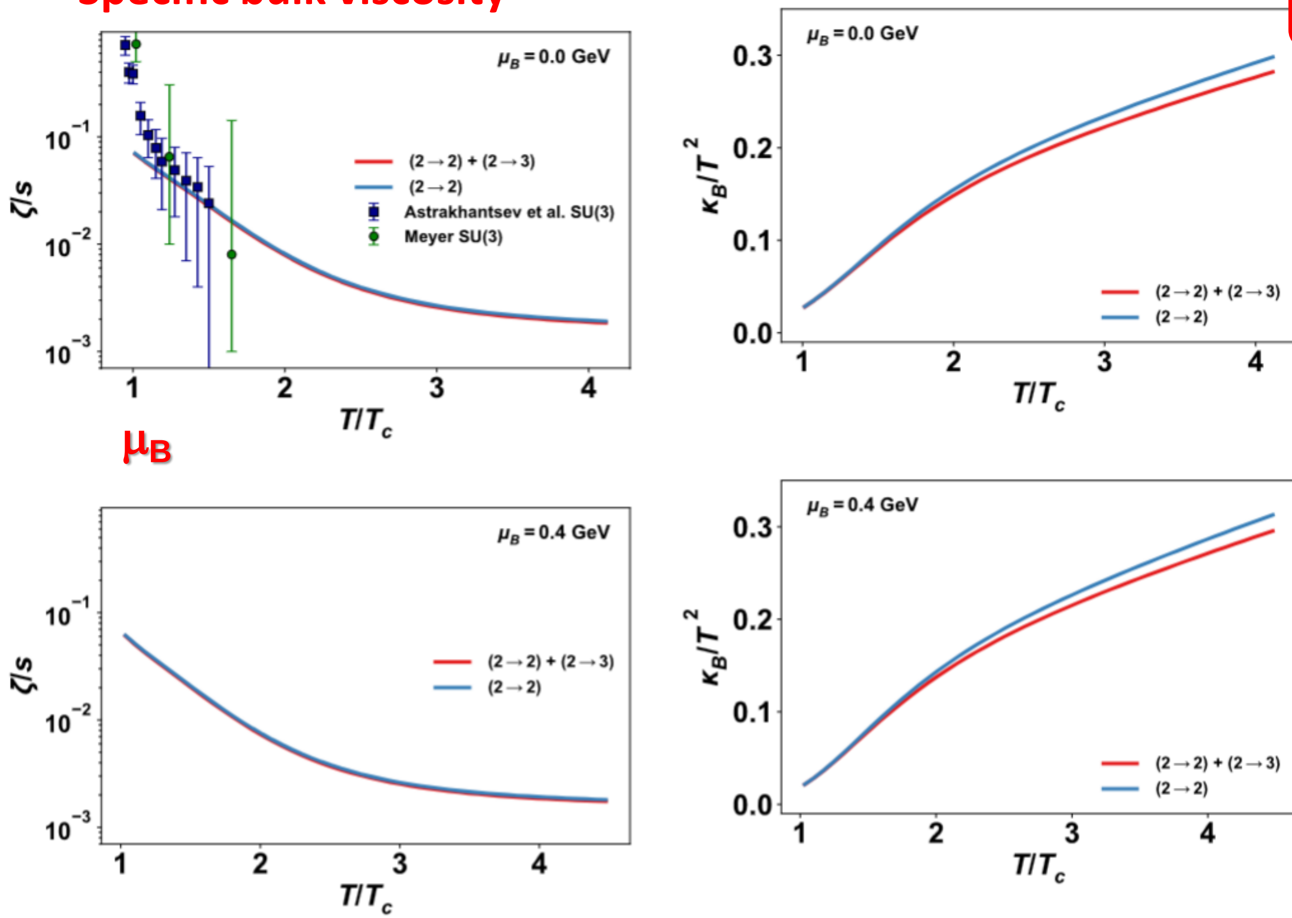

G. Ingrosso, O. S., I. Grishmanovskii and E. Bratkovskaya, arxiv:2606.13363

- Good agreement with lQCD predictions and Bayesian estimates
- Light increase with μ_B in the crossover region

Jet transport coefficients

On-shell:

- **integration over momenta**
- **masses = pole masses**

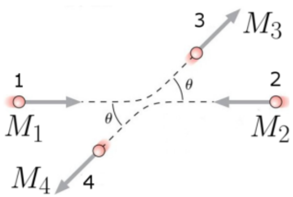

$$E^2 = m^2 + p^2$$

$$\langle \mathcal{O} \rangle^{\mathrm{on}} = \frac{1}{2E_i} \sum_{j=q,\bar{q},g} d_j f_j \int \frac{d^3 p_j}{(2\pi)^3 2E_j} \times \int \frac{d^3 p_1}{(2\pi)^3 2E_1} \int \frac{d^3 p_2}{(2\pi)^3 2E_2} \times (1 \pm f_1)(1 \pm f_2)\mathcal{O}|\overline{\mathcal{M}}|^2 (2\pi)^4 \delta^{(4)}(p_i + p_j - p_1 - p_2)$$

Off-shell:

- **integration over momenta**
- **+ two additional integrations over medium parton energies**

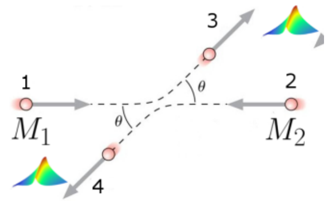

$$\frac{1}{2E} \rightarrow \int \frac{d\omega}{(2\pi)} \rho(\omega, \mathbf{p}) \theta(\omega)$$

$$\langle \mathcal{O} \rangle^{\mathrm{off}} = \frac{1}{2E_i} \sum_{j=q,\bar{q},g} d_j f_j \int \frac{d^4 p_j}{(2\pi)^4} \rho(\omega_j, \mathbf{p}_j)\theta(\omega_j) \times \int \frac{d^3 p_1}{(2\pi)^3 2E_1} \int \frac{d^4 p_2}{(2\pi)^4} \rho(\omega_2, \mathbf{p}_2)\theta(\omega_2) \times (1 \pm f_1)(1 \pm f_2)\mathcal{O}|\overline{\mathcal{M}}|^2 (2\pi)^4 \delta^{(4)}(p_i + p_j - p_1 - p_2)$$

$$\langle \mathcal{O} \rangle_u = \sum_q \langle \mathcal{O} \rangle_{uq} + \sum_{\bar{q}} \langle \mathcal{O} \rangle_{u\bar{q}} + \langle \mathcal{O} \rangle_{ug} = \langle \mathcal{O} \rangle_{uu\to uu} + \langle \mathcal{O} \rangle_{ud\to ud} + \langle \mathcal{O} \rangle_{us\to us} + \langle \mathcal{O} \rangle_{u\bar{u}\to u\bar{u}} + \langle \mathcal{O} \rangle_{u\bar{d}\to u\bar{d}} + \langle \mathcal{O} \rangle_{u\bar{s}\to u\bar{s}} + \langle \mathcal{O} \rangle_{ug\to ug}$$

- **Scattering rate Γ :** $\mathcal{O} = 1$
- **Transverse momentum transfer squared per unit length $\hat{q}$:** $\mathcal{O} = |\vec{p_T} - \vec{p_T}'|^2 \rightarrow \langle O \rangle = \hat{q}$
- **Energy loss per unit length dE/dx:** $\mathcal{O} = (E - E') \rightarrow \langle O \rangle = dE/dx$
- **Drag coefficient A:** $\mathcal{O} = p_L - p_L'$

Partonic interaction rates in equilibrated sQGP

Interaction rate

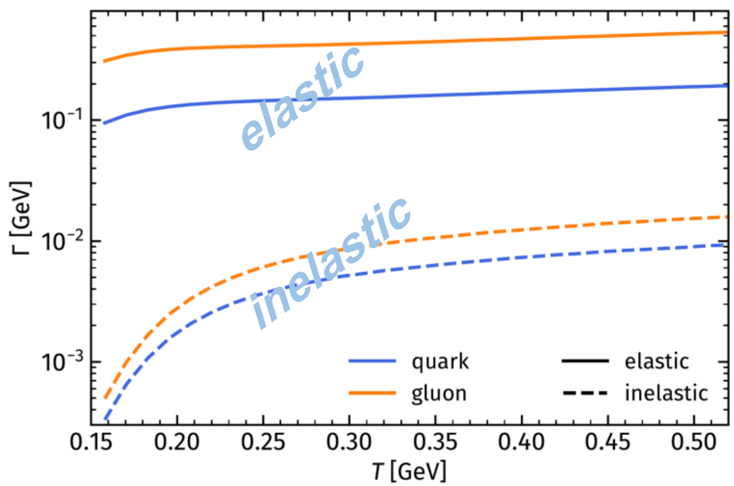

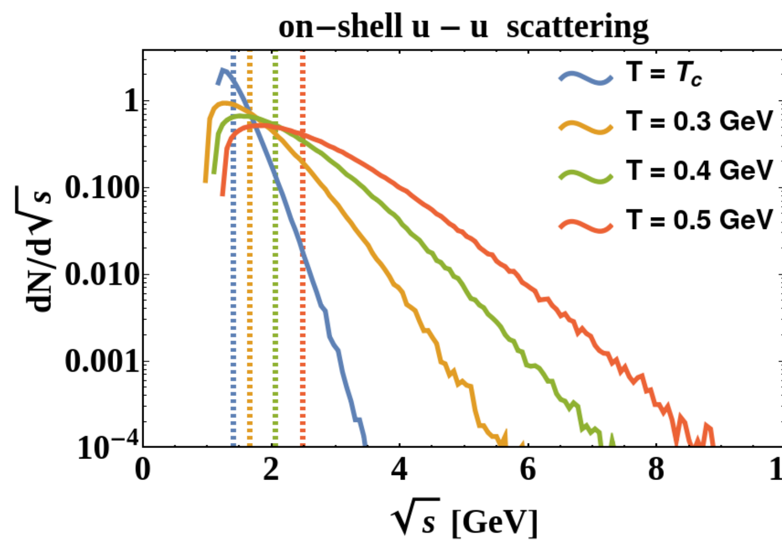

Relaxation time **(τ ~ 1/Γ)**

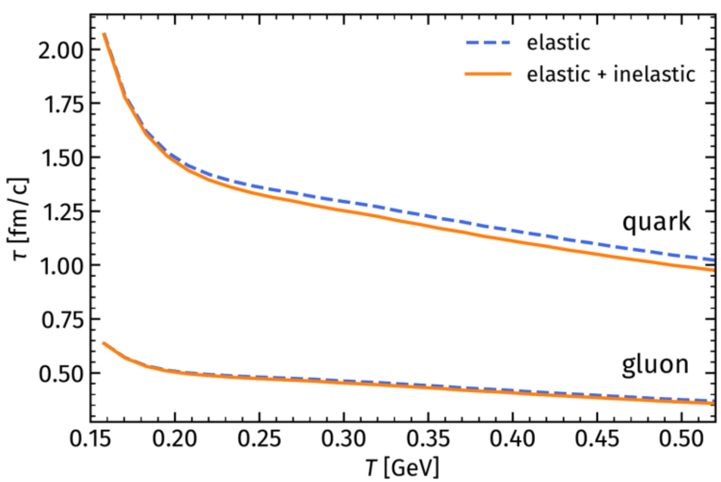

In thermalized QGP low energies are favored where the elastic scatterings dominate

- ➔ **The partonic interaction rate and relaxation time are primarily governed by elastic scattering**
- ➔ **Inelastic processes – with massive gluon emission – are suppressed in the thermalized QCD medium**

I. Grishmanovskii,OS et al., PRC 109, 024911 (2024)

Jet transport coefficients in sQGP

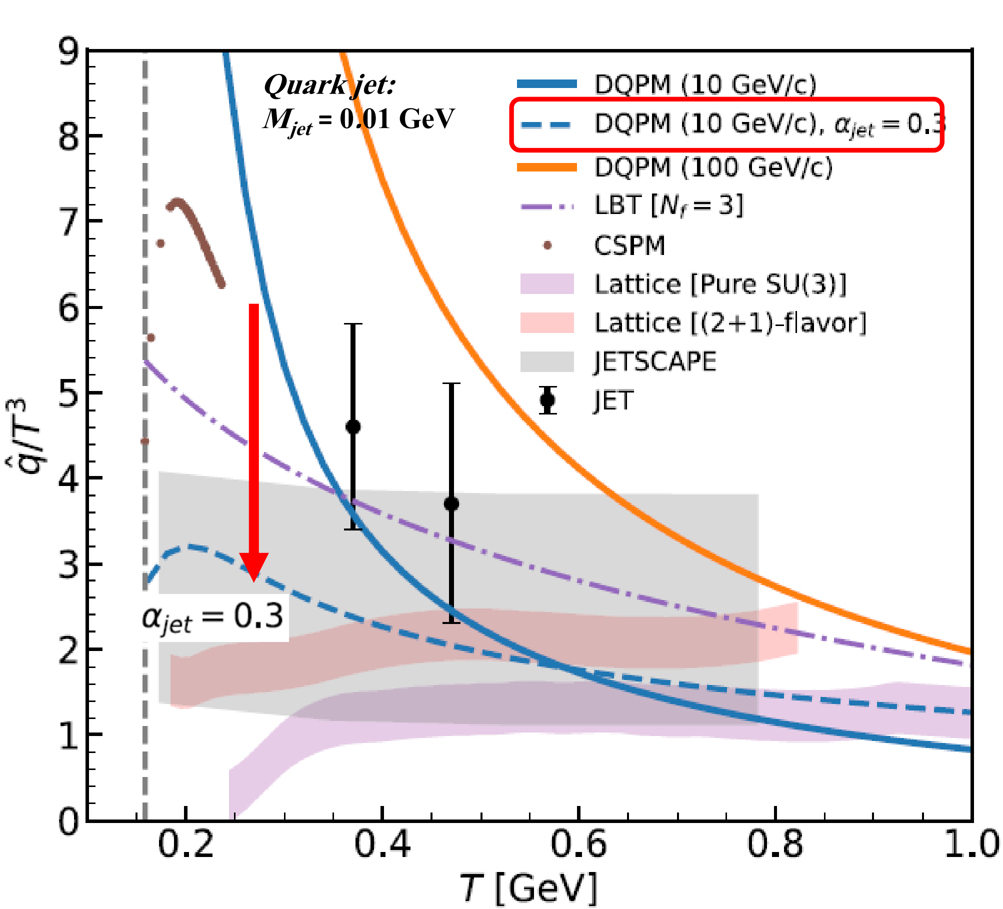

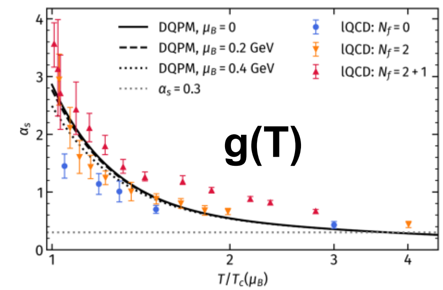

LA, Lee, Winn, Prog.Part.Nucl.Phys. 127 (2022) 103990]

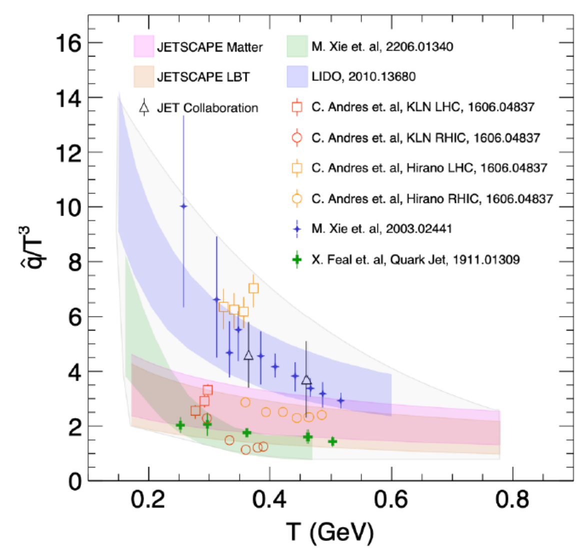

→ **Agreement with the other models at low jet energy**

→ **Rapid rise with decreasing medium temperature due to strong increase of g(T)**

LPM effect: coherent vs independent emission in QGP

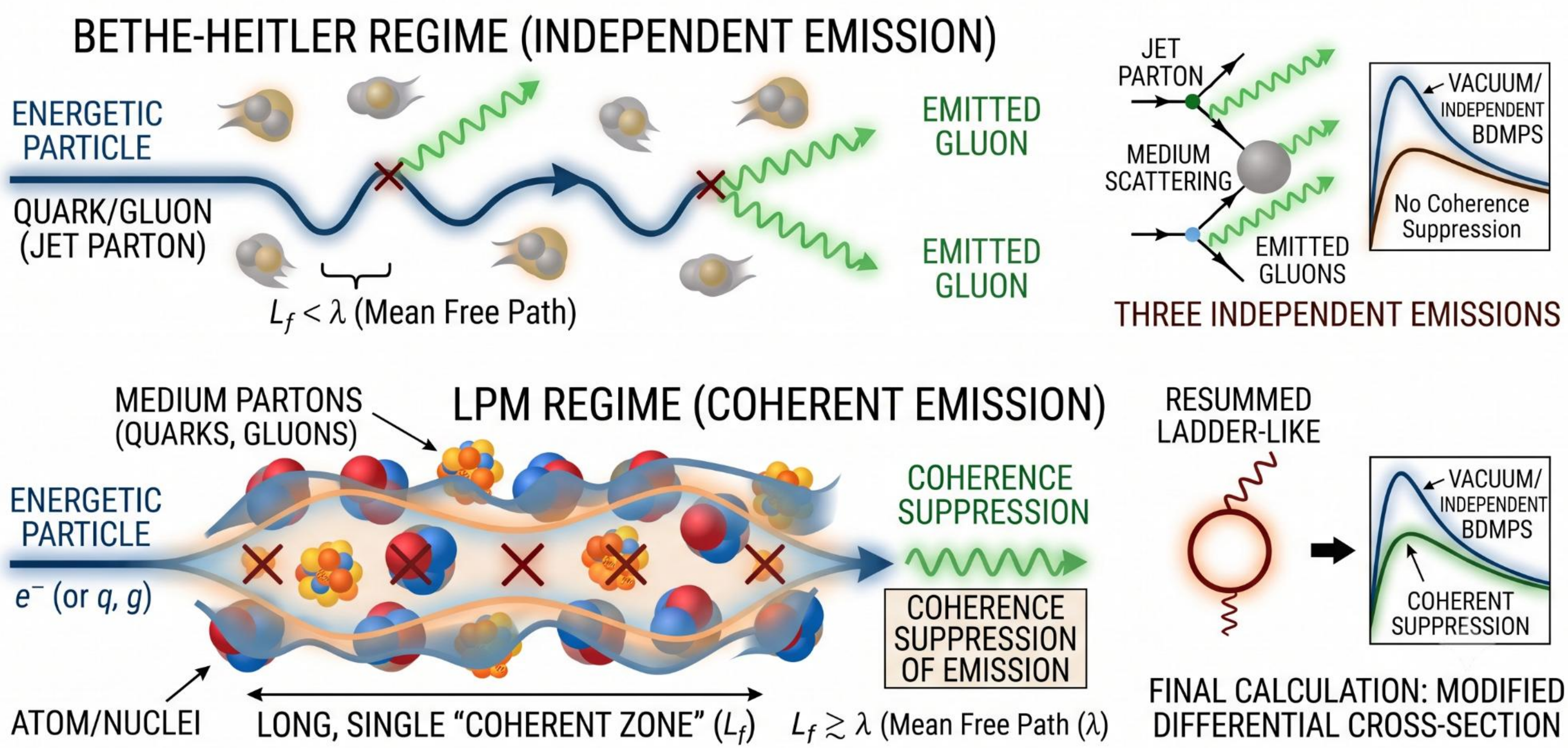

LPM: Local formation-time

$$\tau_f = \frac{2x(1-x)E_j}{k_\perp^2 + x^2 M_j^2 + (1-x)m_3^2},$$

$$\hat{q}_{\rm rad}^{\rm LPM} = \sum_i \int d\Gamma_{ji\to jig}^{\rm DQPM}\, S_{\rm LPM}\, q_\perp^2.$$

$$\begin{aligned} \text{mode 0:} \quad & S_{\rm LPM} = 1, \\ \text{mode 1 (smooth):} \quad & S_{\rm LPM}^{\rm smooth} = \min\left(1, \frac{\lambda_{\rm el}}{\tau_f}\right), \\ \text{mode 2 (sharp):} \quad & S_{\rm LPM}^{\Theta} = \Theta(\lambda_{\rm el} - \tau_f). \end{aligned}$$

Smooth: long-formation-time configurations remain, but with reduced weight.
Sharp: all configurations with $\tau_f > \lambda_{\rm el}$ are rejected.

$\tau_f \ll \lambda_{\rm el}$: the gluon forms before the next scattering, Bethe–Heitler-like emission is approximately valid.
$\tau_f \gtrsim \lambda_{\rm el}$: several interactions occur during formation; emission amplitudes interfere.
Adding independent $2 \to 3$ probabilities overestimates long-formation-time radiation.

- The LPM effect **is not merely a reduction of a cross section**
- It reflects **the loss of independence between scatterings** occurring within one formation time
- We use the ratio $\tau_f/\lambda_{\rm el}$ as a **local diagnostic** of whether the sampled emission is likely to overlap with subsequent scatterings

Formation time: Physical meaning

$$N_{\mathrm{coh}} \sim \frac{\tau_f}{\lambda_{\mathrm{el}}} = r. \qquad S_{\mathrm{LPM}} \sim \frac{1}{N_{\mathrm{coh}}} \sim \frac{\lambda_{\mathrm{el}}}{\tau_f} \qquad (r > 1)$$

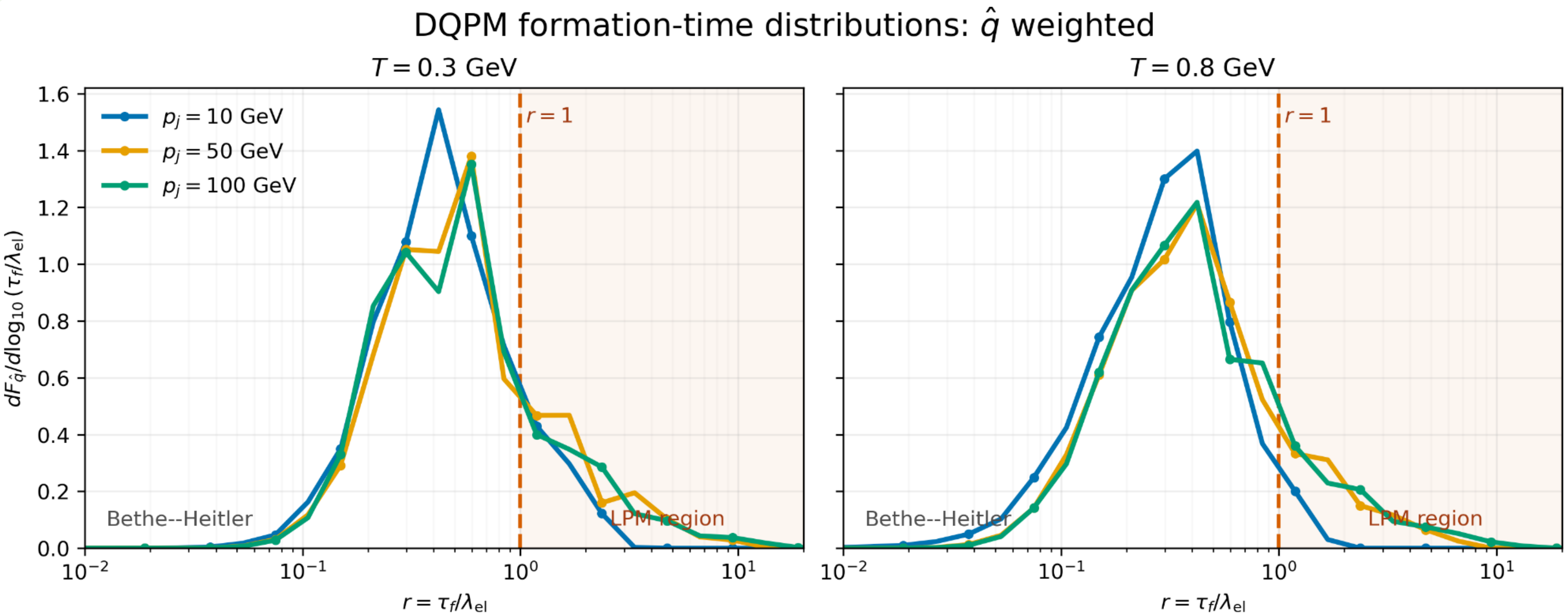

! integrated transport coefficients may be only moderately modified even when a visible long-τ_f tail exists

Since the dominant observable weight can still originate from $\tau_f < \lambda_{\mathrm{el}}$

Why 2 - 3 reactions are insufficient?

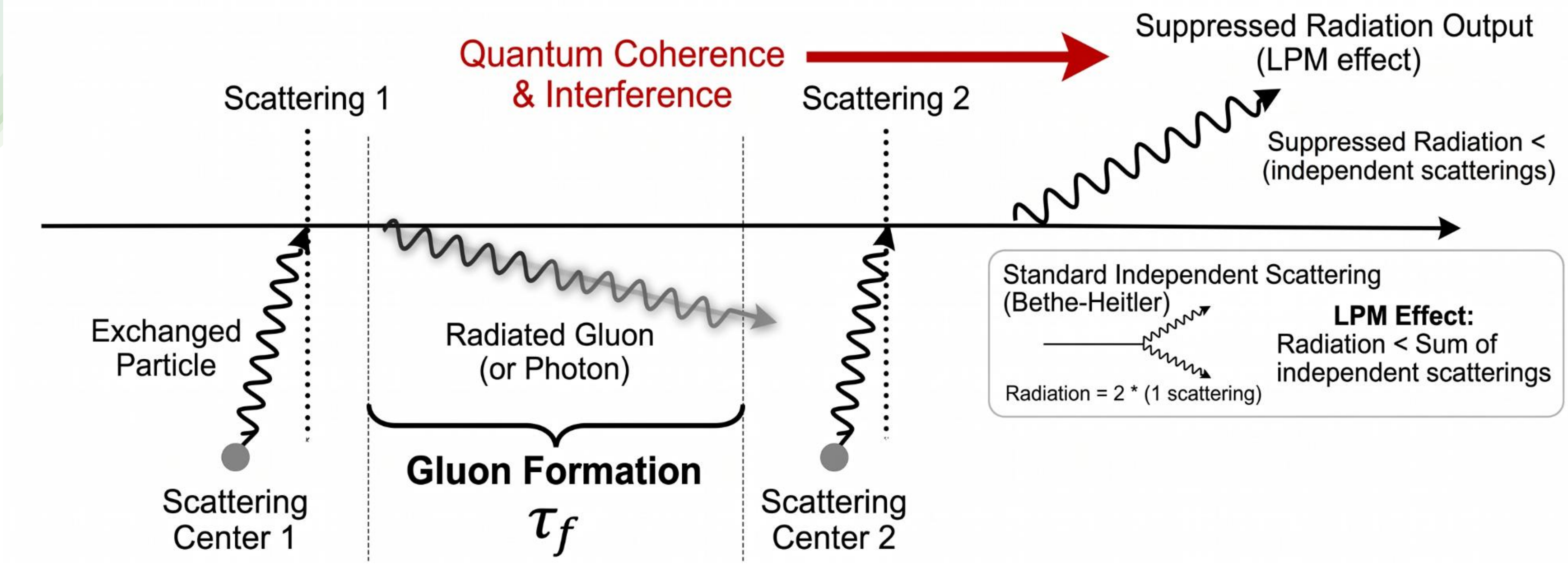

$\tau_f \ll \lambda_{\mathrm{el}}$: the gluon forms before the next scattering; Bethe–Heitler-like emission is approximately valid.

$\tau_f \gtrsim \lambda_{\mathrm{el}}$: several interactions occur during formation; emission amplitudes interfere. Therefore, simply adding independent $2 \rightarrow 3$ probabilities overestimates long-formation-time radiation.

Connection to BDPMS - Z

$$k_\perp^2 \sim \hat{q}\,\tau_f, \qquad \tau_f \sim \frac{2\omega}{k_\perp^2},$$

$$\tau_f^{\rm BDMPS} \sim \sqrt{\frac{2\omega}{\hat{q}}}.$$

emitted gluon accumulates transverse momentum during its formation; many soft interactions are coherently resummed;

τ_f and $k_\perp$ are dynamically linked; the result is a medium-induced radiation spectrum rather than a local veto on individual $2 \to 3$ events.

BDMPS-Z and Zakharov formulate the LPM problem through a full quantum multiple-scattering treatment

DQPM local implementation	BDMPS-Z
Samples one complete $2 \to 3$ event	Resums multiple interactions during formation
Uses sampled $k_\perp$ in τ_f	Builds $k_\perp$ dynamically through broadening
Local $S(\tau_f/\lambda_{\rm el})$	Quantum interference at amplitude level
Produces corrected $\hat{q}_{\rm rad}$, dE/dx	Produces medium-induced gluon spectrum
Massive off-shell quasiparticles	Usually formulated in high-energy/eikonal limits

Connection to SUBA-Jet

SUBA-Jet :

elastic/inelastic collision → preformed virtual gluon → additional medium kicks → phase accumulation → real emitted gluon.

arxiv:2404.14579

Present DQPM work	SUBA-Jet
Gluon is generated as part of a complete $2 \to 3$ event	Starts from a preformed virtual gluon
Formation time evaluated locally	Formation evolves after successive kicks
No propagation during formation	Explicit evolution during formation
Coherence encoded by $S_{\mathrm{LPM}}(r)$	Coherence encoded through accumulated phase
Exact off-shell DQPM matrix element	Gunion–Bertsch radiation seed
Main results: $\hat{q}_{\mathrm{rad}}$, dE/dx	Main benchmark: $dN_g/d\omega$, $dN_g/dk_\perp$
Natural PHSD embedding	Full jet Monte Carlo architecture

Standard massive DQPM result

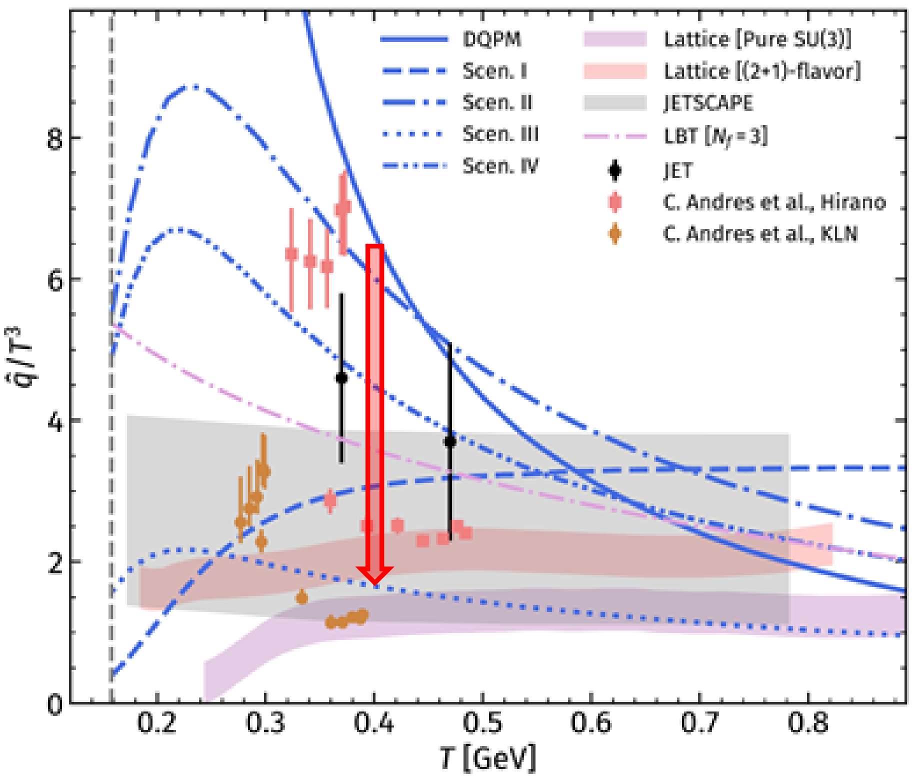

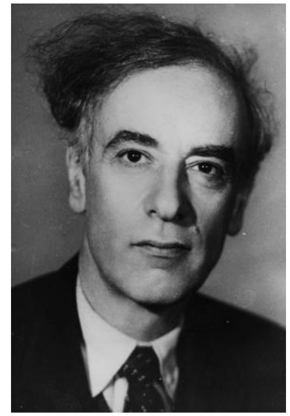

LPM quiz

High energy diagnostics

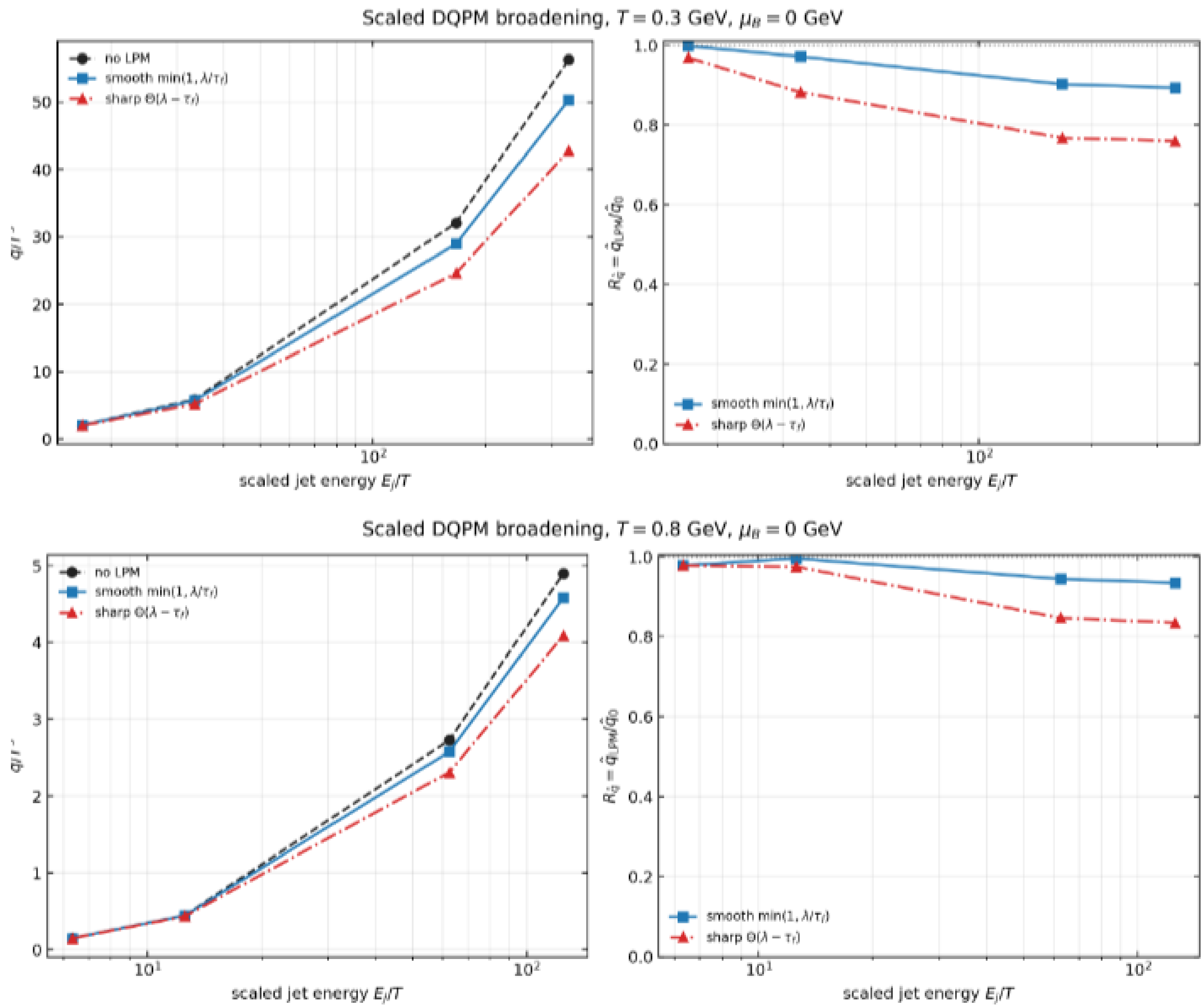

Massless-emission diagnostics

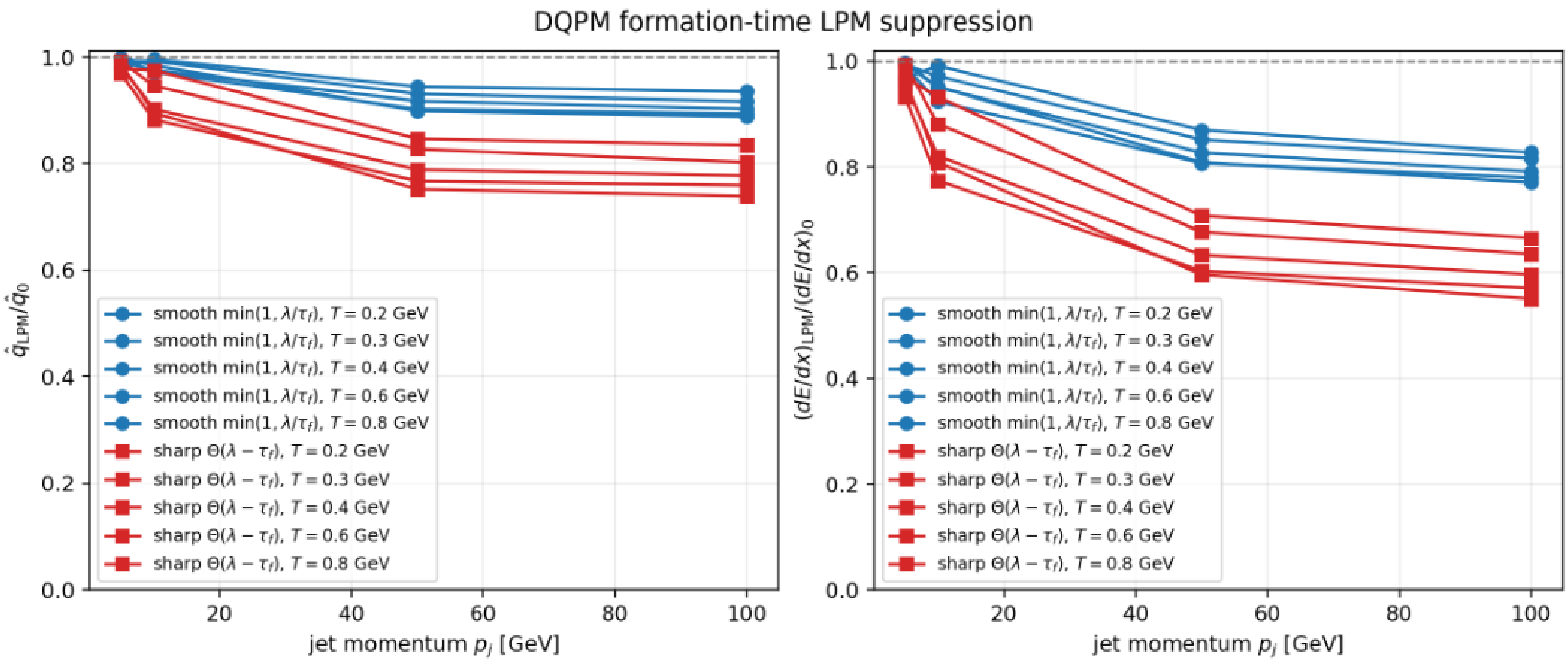

- suppression increases with E/T
- higher-energy emissions can have longer formation times
- more radiative weight enters the region $\tau_f \gtrsim \lambda_{\rm el}$

High energy and massless-emission diagnostics

Quark jet E= GeV

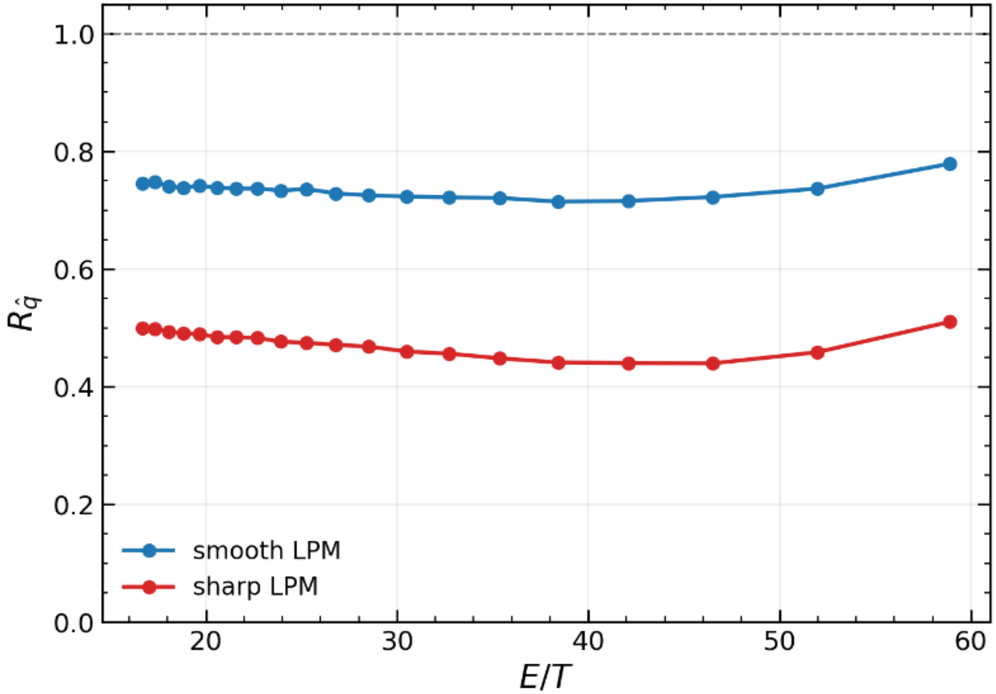

- removing the emitted-gluon mass increases τ_f;
- the result becomes more sensitive to the coherence prescription;
- gluon jets show a stronger modification than quark jets.

Coherence increases with jet energy

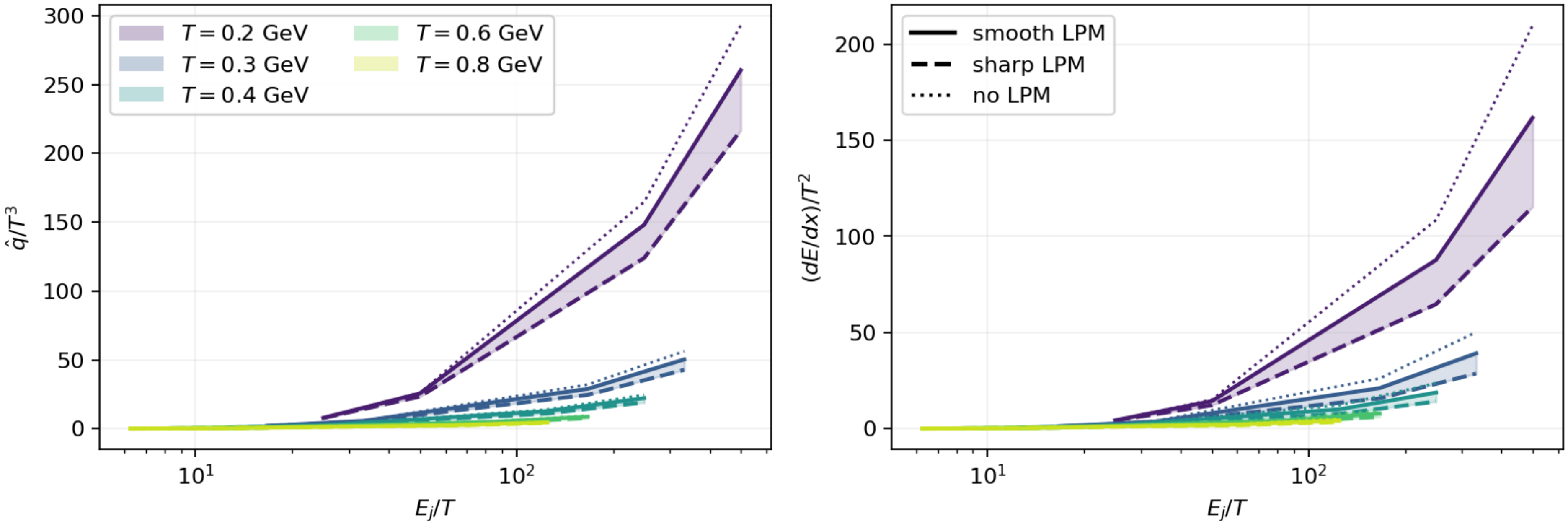

Antenna

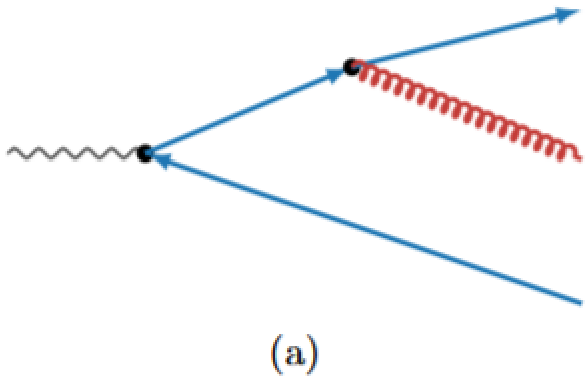

Antenna interference within the exact DQPM matrix element

$$\mathcal{M} = \sum_i \mathcal{M}_i,$$

$$|\mathcal{M}|^2 = \underbrace{\sum_i |\mathcal{M}_i|^2}_{Q_{\text{diag}}} + \underbrace{\sum_{i<j} 2\,\mathrm{Re}\left(\mathcal{M}_i \mathcal{M}_j^*\right)}_{Q_{\text{int}}}.$$

$$R_{\text{ant}} = \frac{Q_{\text{full}}}{Q_{\text{diag}}} = \frac{Q_{\text{diag}} + Q_{\text{int}}}{Q_{\text{diag}}}.$$

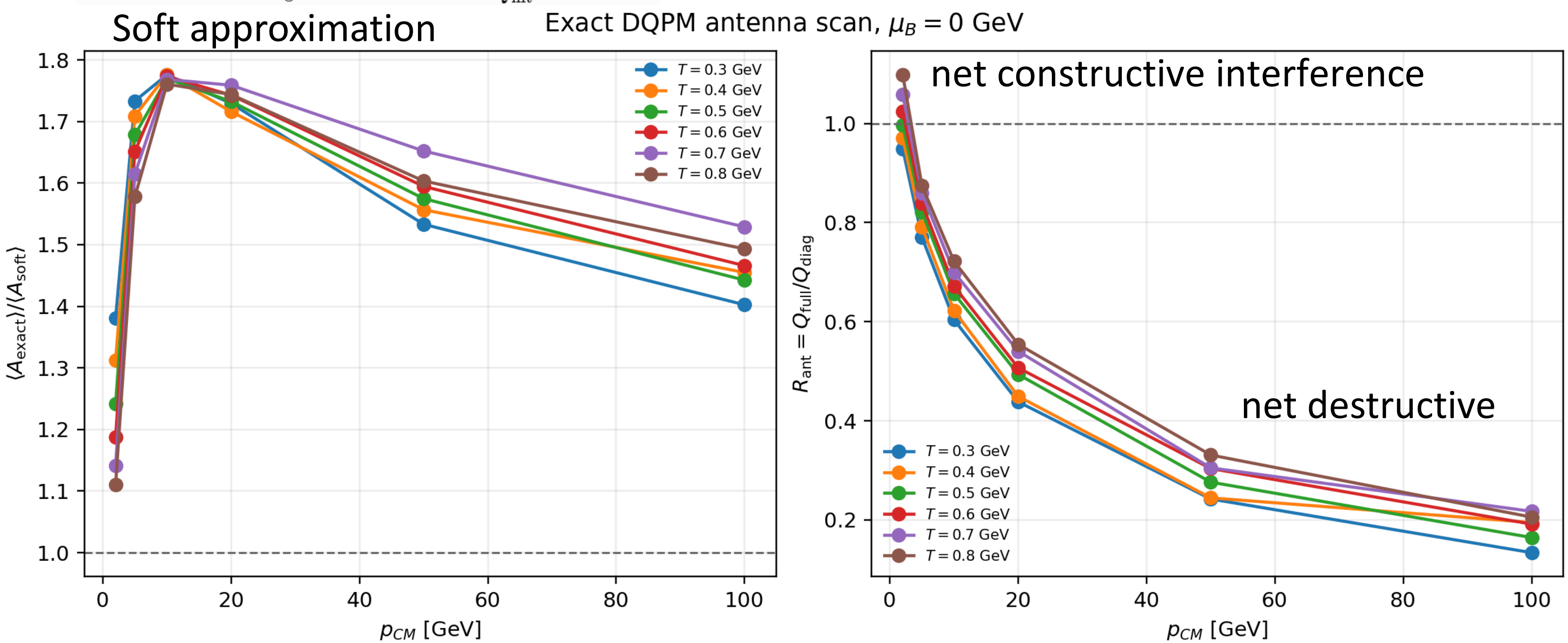

At high momentum, **<u>destructive interference</u>** cancels roughly 80% or more of the incoherent diagonal contribution.

Summary

- Local LPM suppression has been embedded consistently into the off-shell DQPM $2 \to 3$kernel
- Coherence effects increase with jet energy and affect dE/dx more strongly than $\hat{q}$.
- The standard massive setup gives moderate suppression; the massless-emission and gluon-jet cases are much more sensitive.
- The method is BDMPS-Z-inspired but remains less dynamical than the SUBA-Jet phase-accumulation approach
- $D_S(T)$ for heavy quarks is not sensitive to inelastic reactions
- Antenna interference is substantial and motivates a future unified treatment in thermal transport and PHSD

Summary

Local LPM suppression has been embedded consistently into the off-shell DQPM $2 \to 3$kernel

Coherence effects increase with jet energy and affect dE/dx more strongly than $\hat{q}$.

The standard massive setup gives moderate suppression; the massless-emission and gluon-jet cases are much more sensitive.

The method is BDMPS-Z-inspired but remains less dynamical than the SUBA-Jet phase-accumulation approach

$D_S(T)$ for heavy quarks is not sensitive to inelastic reactions

Antenna interference is substantial and motivates a future unified treatment in thermal transport and PHSD

Thank you for your attention!

Outlook

- Implement the LPM-modified $2 \to 3$rates in PHSD
- Benchmark study against BDMPS-Z and SUBA-Jet
- Move beyond the local suppression factor
- Jet transport in an anisotropic and flowing medium

From heavy-quark diffusion to thermal charm production in PHSD

Charm quark pair production

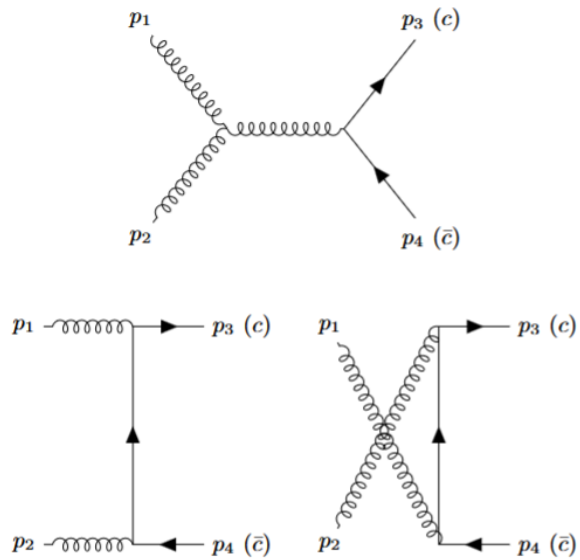

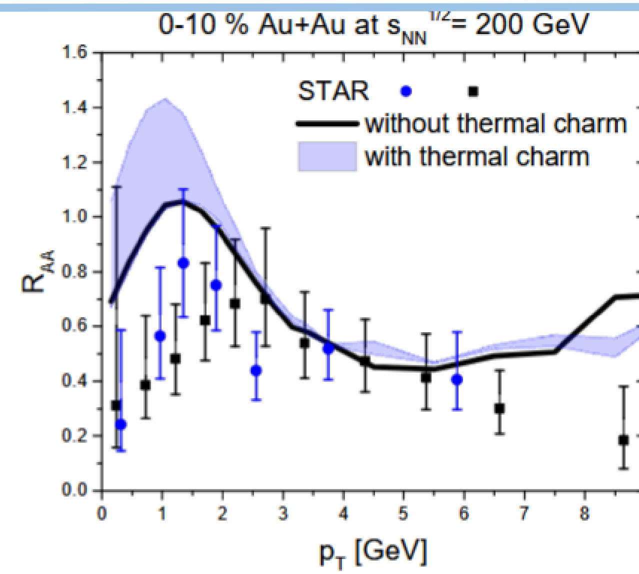

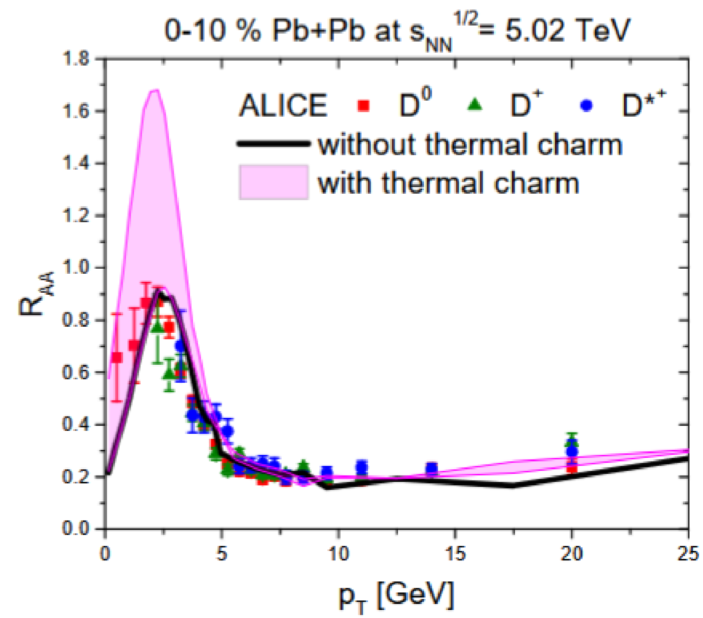

- Thermal production is concentrated in the earliest, hottest partonic stage
- Comparison to D-meson R_{AA} favors charm quarks gaining additional thermal mass in the QGP
- This connects open heavy flavour directly to microscopic QGP quasiparticle properties

T.Song, I. Grishmanovskii, O.S., E. Bratkovskaya, PRC110 (2024) 3, 034906

Properties of QGP: transport coefficients

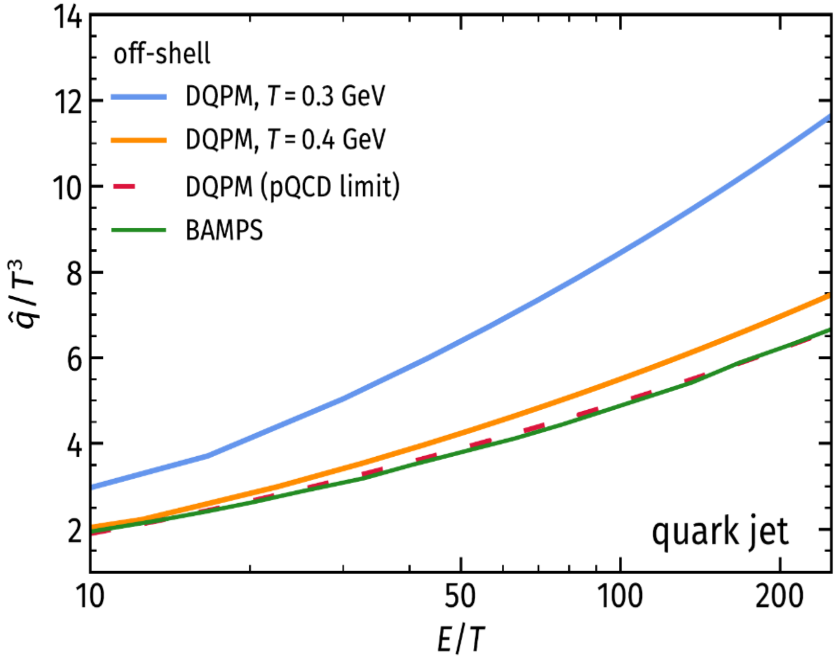

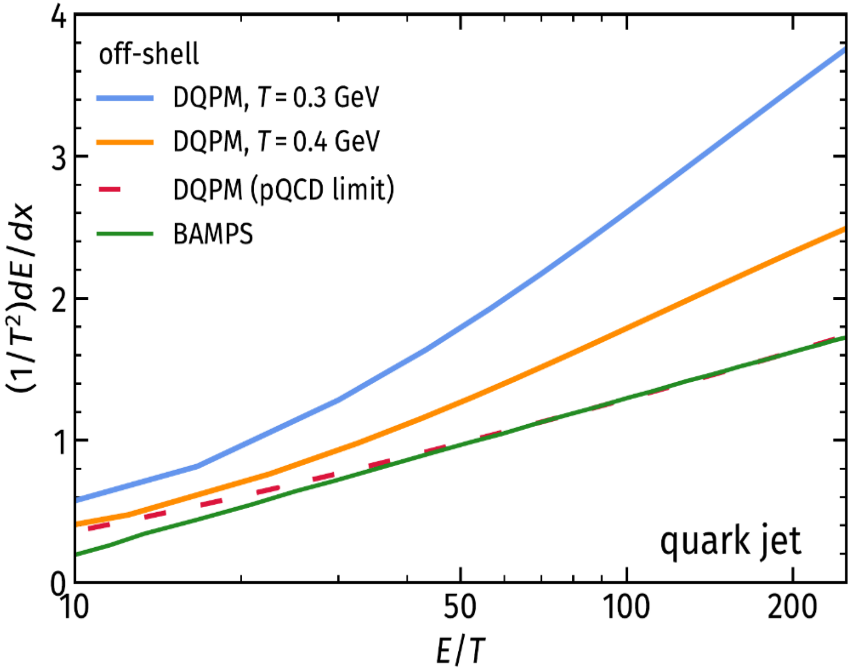

- ➔ **Logarithmic growth of q-hat and energy loss dE/dx with jet energy E**
- ➔ **DQPM predicts stronger suppression than pQCD**
- ➔ **Aligning with pQCD-based calculations in the pQCD-limit**

I. Grishmanovskii, O.S. et al., PRC 106, 014903 (2022)

$\hat{q}$ from elastic (2→2) vs. inelastic (2→3) scattering

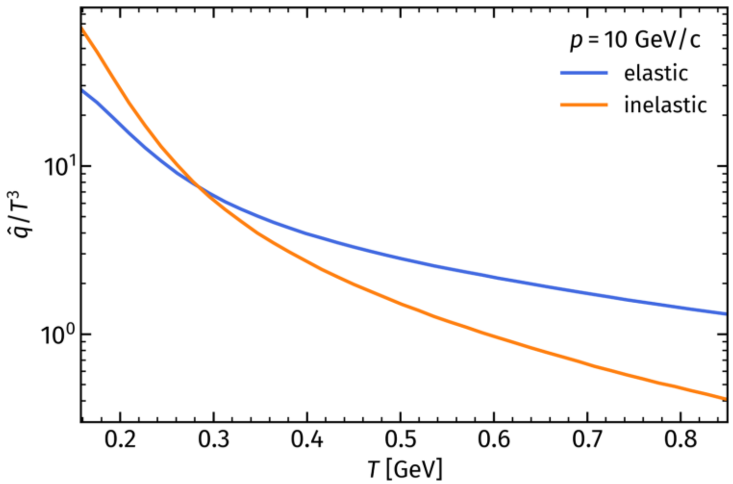

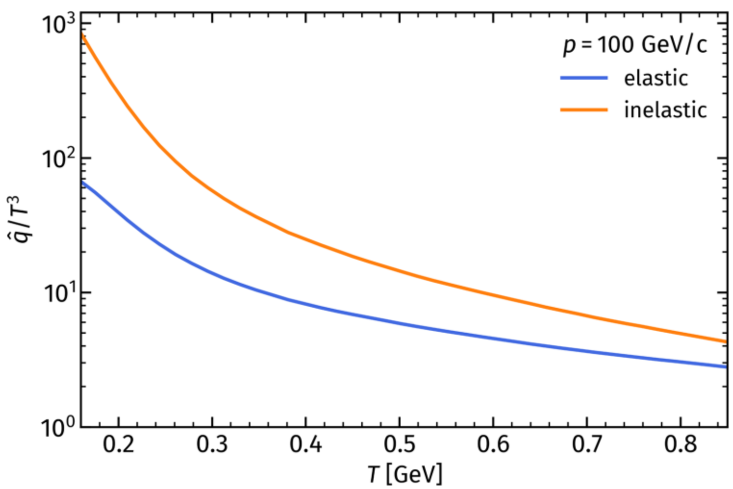

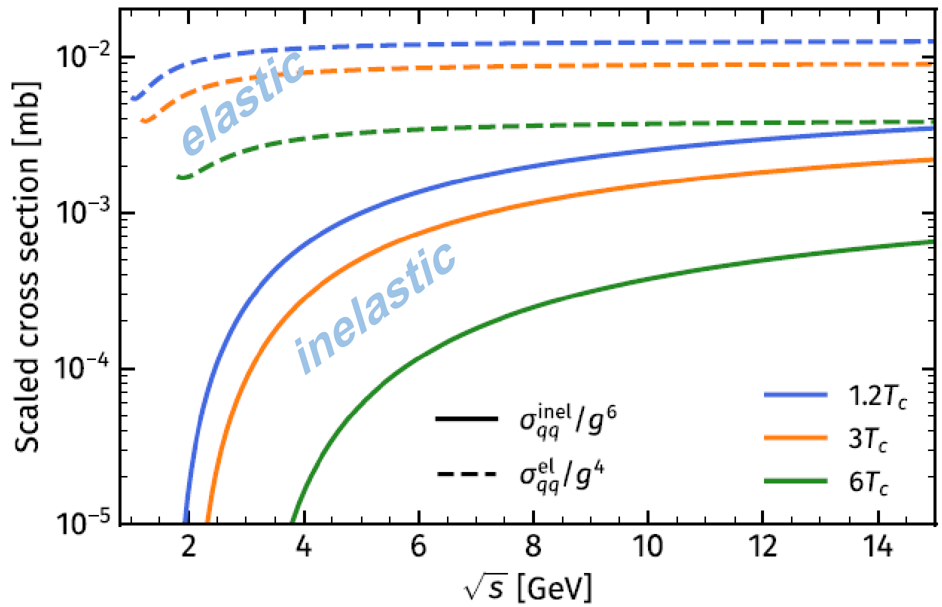

➔ Strong dependence of elastic (~g^4) and inelastic (~g^6) cross sections on strong coupling g

➔ Temperature and momentum dependence is stronger for inelastic reactions

➔ Stronger energy loss at large jet energies and small temperatures

→ ? 'questionable' suppression of jets in heavy-ion collisions

Different scenarios for strong couplings

- **Jet is not a part of the QGP medium → strong coupling is not thermal**

  → consider different strong couplings

  in *thermal* (●), *jet* (●), and *radiative* (●) vertices

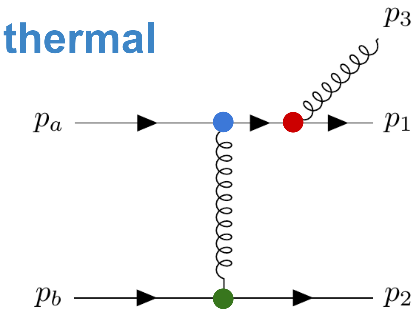

		Vertex		
	Model	● medium parton	● jet parton	● emitted gluon
	Scenario 0	$g^{\mathrm{DQPM}}(T)$		
	Scenario I	$g = \sqrt{4\pi \times 0.3}$		
Zakharov model	Scenario II	$g^{\mathrm{DQPM}}(T)$	$g(Q^2)$	$g(k_t^2)$
QLBT model	Scenario III	$g^{\mathrm{DQPM}}(T)$	$g(E)$	$g(E)$
DREENA framework	Scenario IV	$g^{\mathrm{DQPM}}(T)$	$g(ET)$	$g(Q^2)$

Scenario 0 → **"default" DQPM (thermal coupling)**

Scenario I → **constant strong coupling**

Scenarios II–IV:

$$g^2(t) = \frac{48\pi^2}{(11N_c - 2N_f)} \frac{1}{\ln\left(\frac{t}{\Lambda^2}\right)}$$

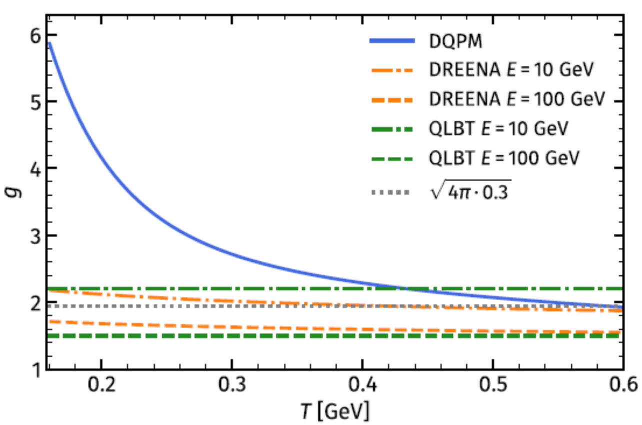

[II] B. G. Zakharov, JETP Lett. 112, 681 (2020).
[III] F.-L. Liu et al., Eur. Phys. J. C 82, 350 (2022).
[IV] D. Zigic et al, Front. Phys. 10, 957019 (2022).

$\hat{q}$ from elastic + inelastic scattering

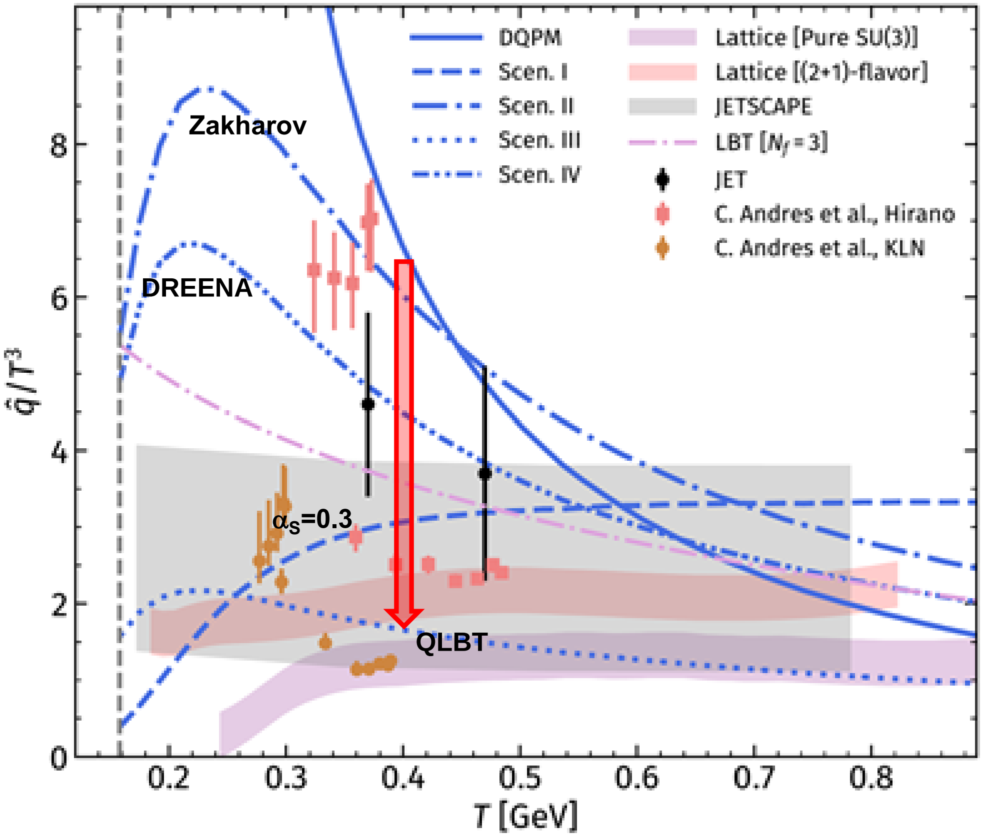

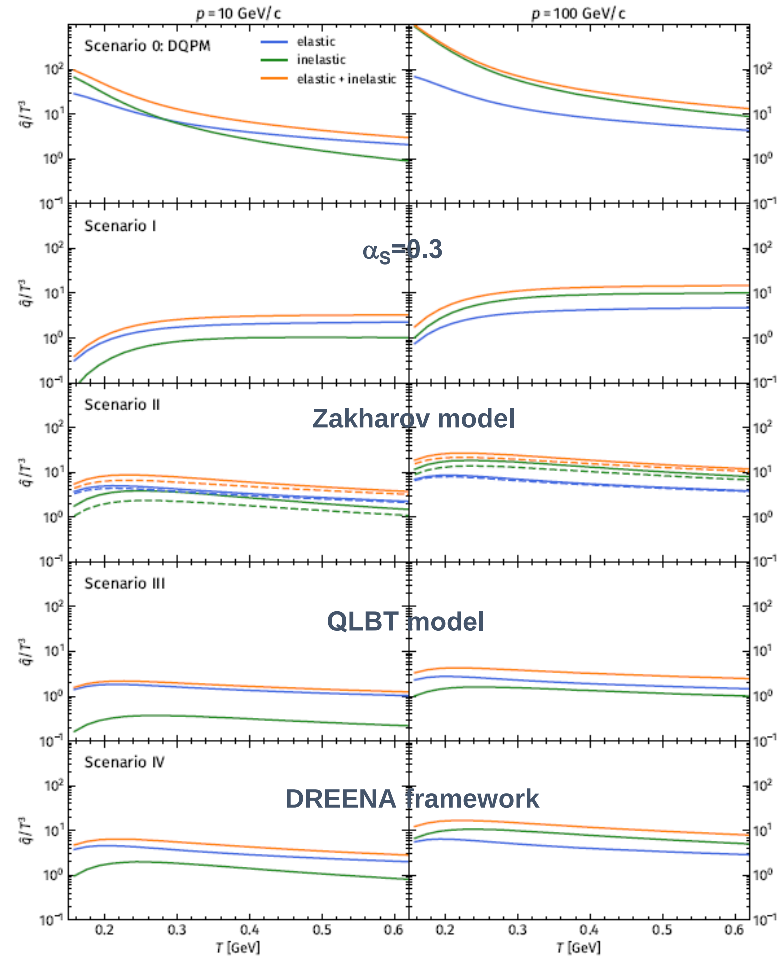

➔ **High sensitivity to the choice of the strong coupling ("scenario")**

➔ **The "default" DQPM with the thermal couplings produces the highest values of the transport coefficients**

I. Grishmanovskii et al., PRC 110, 014908 (2024)

Total elastic cross sections

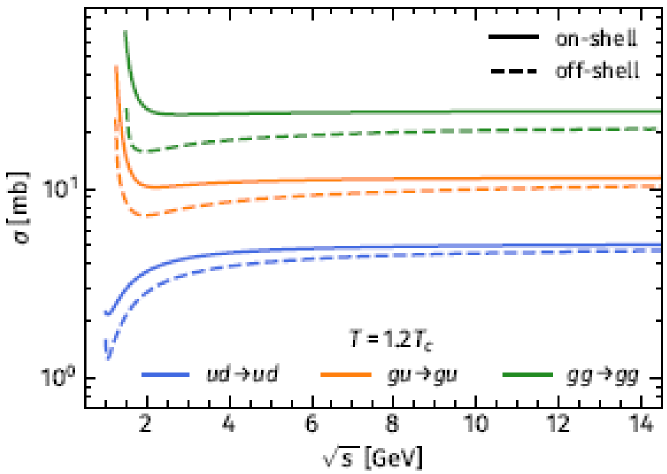

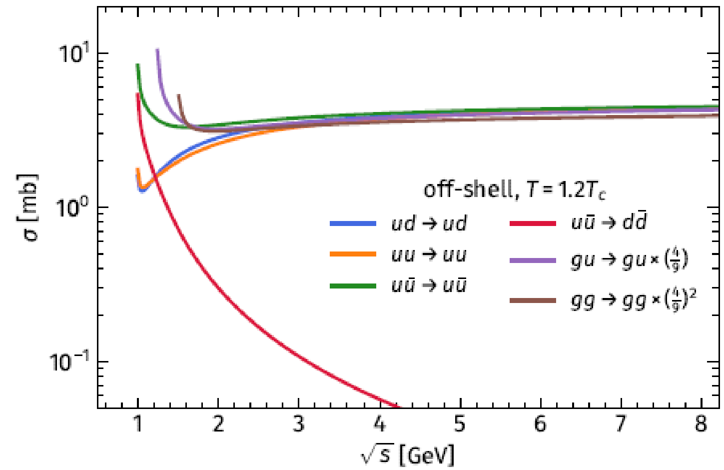

- ❑ off-shell effects are stronger at low $s^{1/2}$
- ❑ strong channel dependence at low $s^{1/2}$

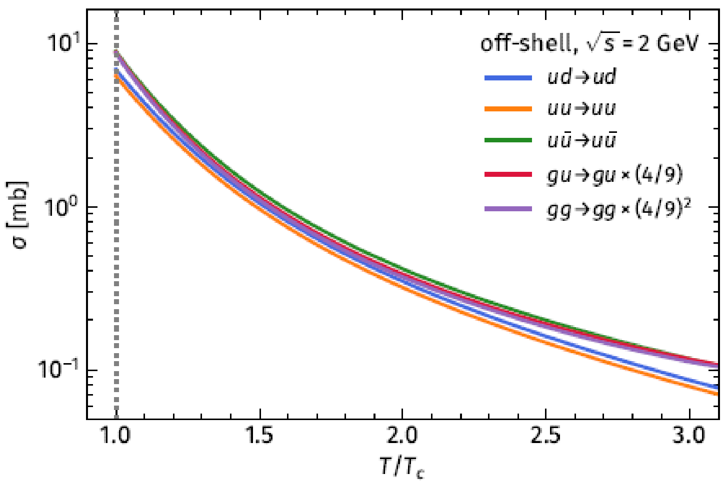

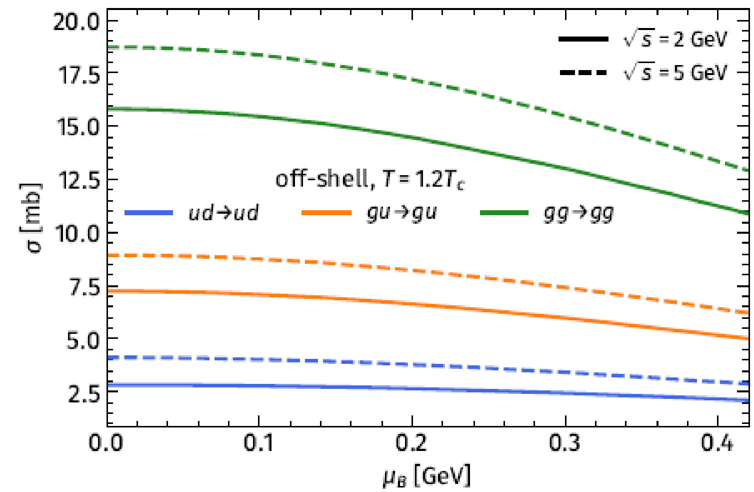

- ❑ strong T dependence
- ❑ ~ scaling with color ratio

$$|\overline{\mathcal{M}}_{gg}|^2 \approx \frac{C_g}{C_q} |\overline{\mathcal{M}}_{gq}|^2 \approx \left(\frac{C_g}{C_q}\right)^2 |\overline{\mathcal{M}}_{qq}|^2$$

- ❑ weak μ_B dependence

I. Grishmanovskii, O.S. et al., PRC 110, 014908 (2024)
plots from PhD Thesis

Spatial diffusion coefficient $D_S(T)$ for heavy quarks

Charm quark | **Bottom quark**

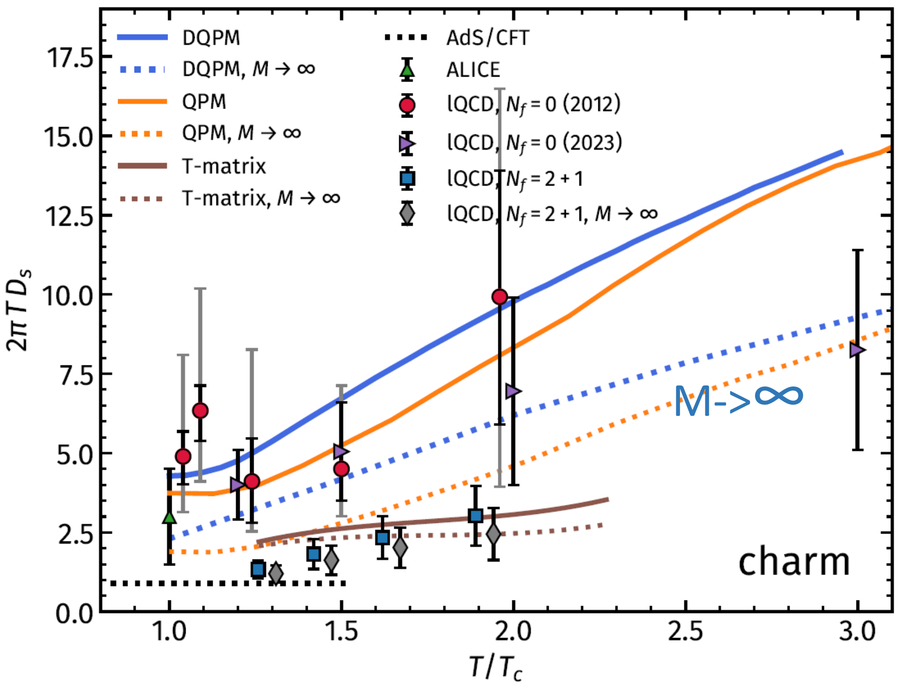

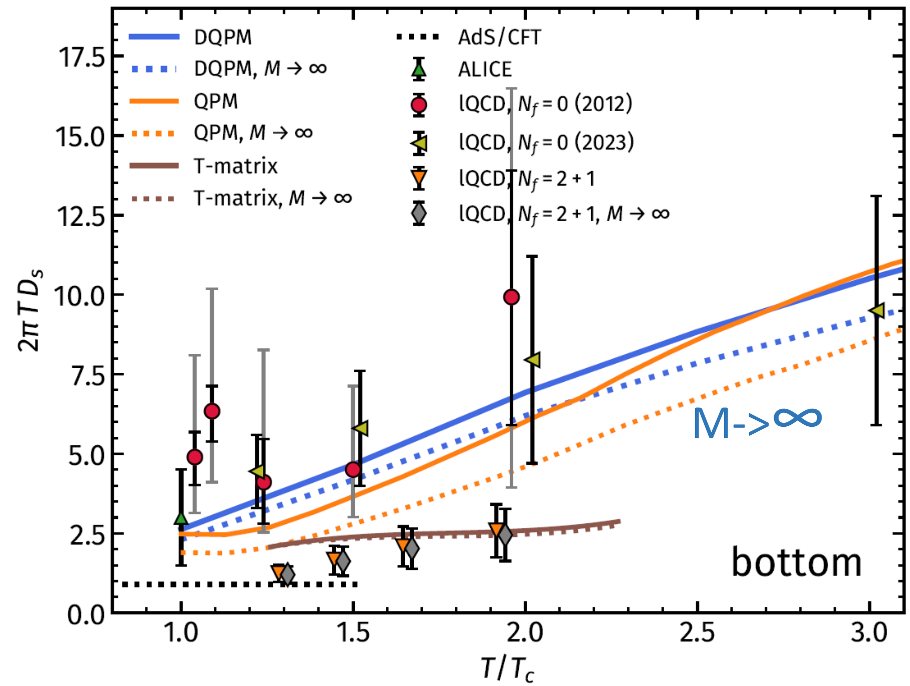

➔ **Inelastic reactions play a minor role (vs. elastic reactions) in the determination of D_S which is obtained for p→0 limit**

$$D_s = \lim_{p \to 0} \frac{T}{(\mathcal{A}/p)M}$$

➔ **D_S decreases with increasing mass of the heavy quark**

I. Grishmanovskii et al., PRC 110, 014908 (2024)

Summary

- DQPM provides a self-consistent approach to study partonic interactions and transport properties of the sQGP
- Inelastic interactions are suppressed in a thermalized QGP medium, but are crucial in the context of jet attenuation
- Jet energy loss of hard jet partons is larger within the DQPM compared to the pQCD-based calculations
- transport coefficients are highly sensitive to the choice of the strong coupling
- $D_S(T)$ for heavy quarks is not sensitive to inelastic reactions

Thank you for your attention!

Back up slides

dE/dx from elastic + inelastic scattering

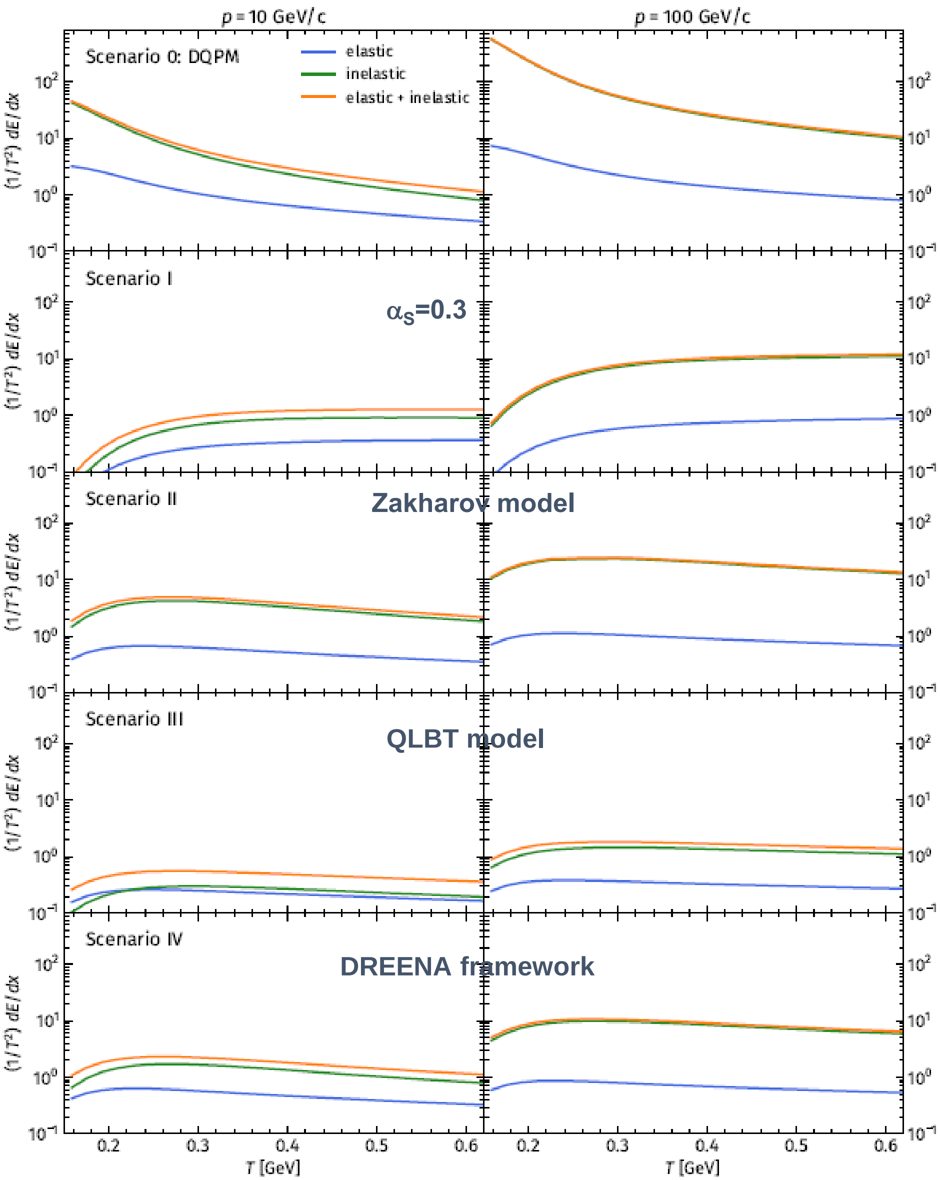

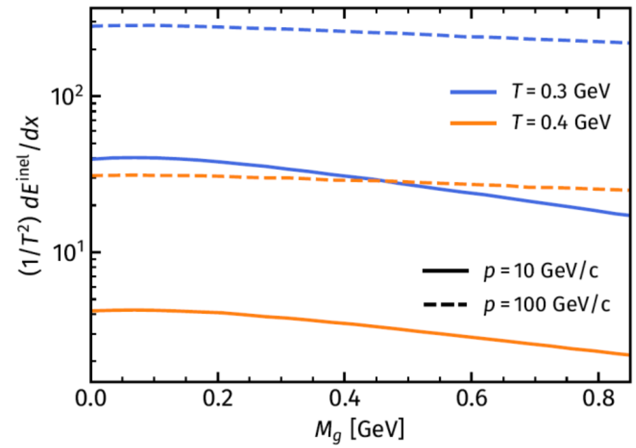

➔ **High sensitivity to the choice of the strong coupling ("scenario")**

➔ **The "default" DQPM with the thermal couplings produces the highest energy loss**

➔ **Energy loss is decreasing with increasing m_g**

Jet suppression

C. Adler et al. [STAR], Phys. Rev. Lett. 90 (2003) 082302

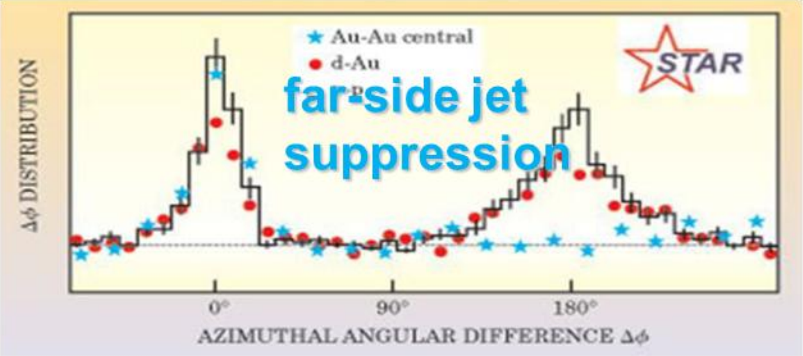

STAR (2003):
Discovery of "Jet Quenching": strong suppression of far-side jet in A+A vs p+p and d+A

HSD (Hadron-String Dynamics) microscopic transport approach (2004):

W. Cassing, K. Gallmeister, C. Greiner, J.Phys.G30 (2004) S801; NPA 748 (2005) 41

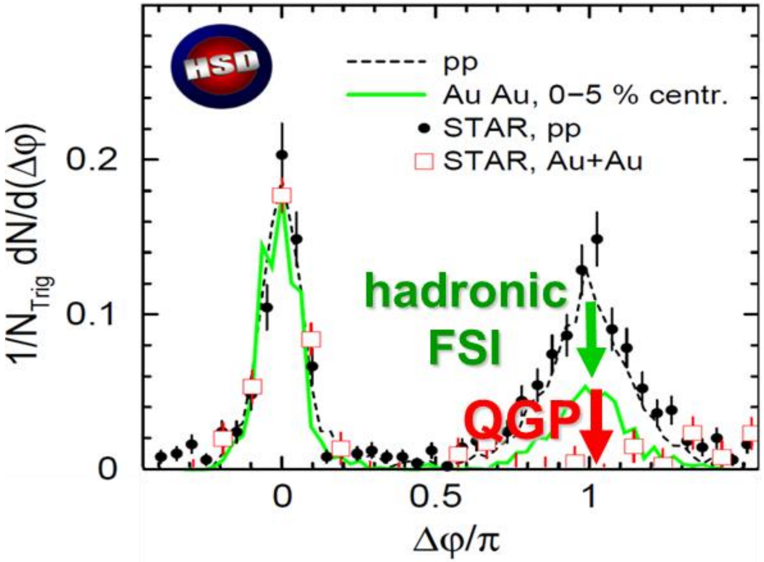

- **good description of jet quenching in p+p, d+A and near-side jet angular correlation for central Au+Au**
- **strong underestimation of suppression of the far-side jet due to hadronic interaction**

➔ **indication for strong jet suppression in QGP**

⇨ **Modeling of interaction of jet partons with sQGP**

DQPM: EoS

Entropy and baryon density in the quasiparticle limit
(G. Baym 1998, Blaizot et al. 2001):

$$s^{dqp} = - \int \frac{d\omega}{2\pi} \frac{d^3p}{(2\pi)^3} \left[d_g \frac{\partial n_B}{\partial T} \left(\mathrm{Im}(\ln -\underline{\Delta^{-1}}) + \mathrm{Im}\,\underline{\Pi}\,\mathrm{Re}\,\underline{\Delta} \right) + \sum_{q=u,d,s} d_q \frac{\partial n_F(\omega-\mu_q)}{\partial T} \left(\mathrm{Im}(\ln -\underline{S_q^{-1}}) + \mathrm{Im}\,\underline{\Sigma_q}\,\mathrm{Re}\,\underline{S_q} \right) + \sum_{\bar{q}=\bar{u},\bar{d},\bar{s}} d_{\bar{q}} \frac{\partial n_F(\omega+\mu_q)}{\partial T} \left(\mathrm{Im}(\ln -\underline{S_{\bar{q}}^{-1}}) + \mathrm{Im}\,\underline{\Sigma_{\bar{q}}}\,\mathrm{Re}\,\underline{S_{\bar{q}}} \right) \right]$$

$$n^{dqp} = - \int \frac{d\omega}{2\pi} \frac{d^3p}{(2\pi)^3} \left[\sum_{q=u,d,s} d_q \frac{\partial n_F(\omega-\mu_q)}{\partial \mu_q} \left(\mathrm{Im}(\ln -\underline{S_q^{-1}}) + \mathrm{Im}\,\underline{\Sigma_q}\,\mathrm{Re}\,\underline{S_q} \right) + \sum_{\bar{q}=\bar{u},\bar{d},\bar{s}} d_{\bar{q}} \frac{\partial n_F(\omega+\mu_q)}{\partial \mu_q} \left(\mathrm{Im}(\ln -\underline{S_{\bar{q}}^{-1}}) + \mathrm{Im}\,\underline{\Sigma_{\bar{q}}}\,\mathrm{Re}\,\underline{S_{\bar{q}}} \right) \right]$$

- Input: entropy density as a f(T , $\boldsymbol{\mu_B = 0}$)

$$g^2(s/s_{SB}) = d\left((s/s_{SB})^e - 1\right)^f$$

$$s^{DQPM}(\Pi, \Delta, S_q, \Sigma) = s^{lattice}$$

fix the parameters

- Scaling hypothesis for the crossover region at finite $\boldsymbol{\mu_B}$

$$g^2(T/T_c, \mu_B) = g^2\left(\frac{T^*}{T_c(\mu_B)}, \mu_B = 0\right) \quad \text{with} \quad T^* = \sqrt{T^2 + \mu_q^2/\pi^2}$$

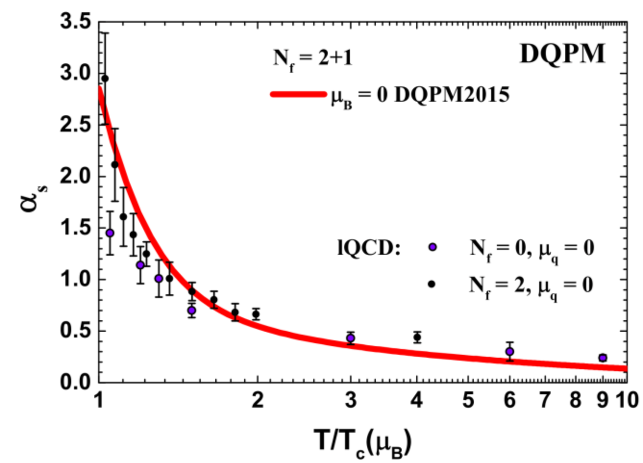

Relation between η/s and $\hat{q}$

In the weak coupling limit:

B. Müller, PRD 104, L071501 (2021)

$$\eta/s \approx 1.25\,\frac{T^3}{\hat{q}}$$

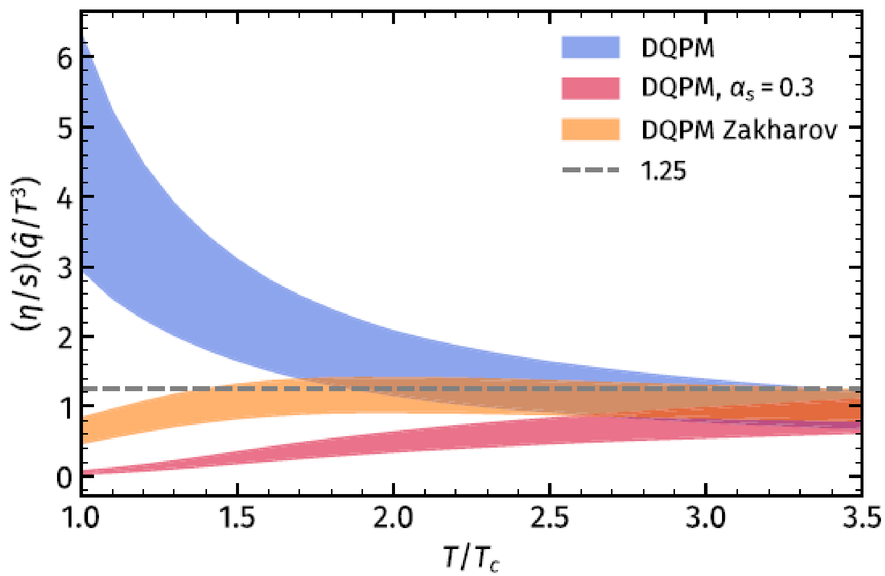

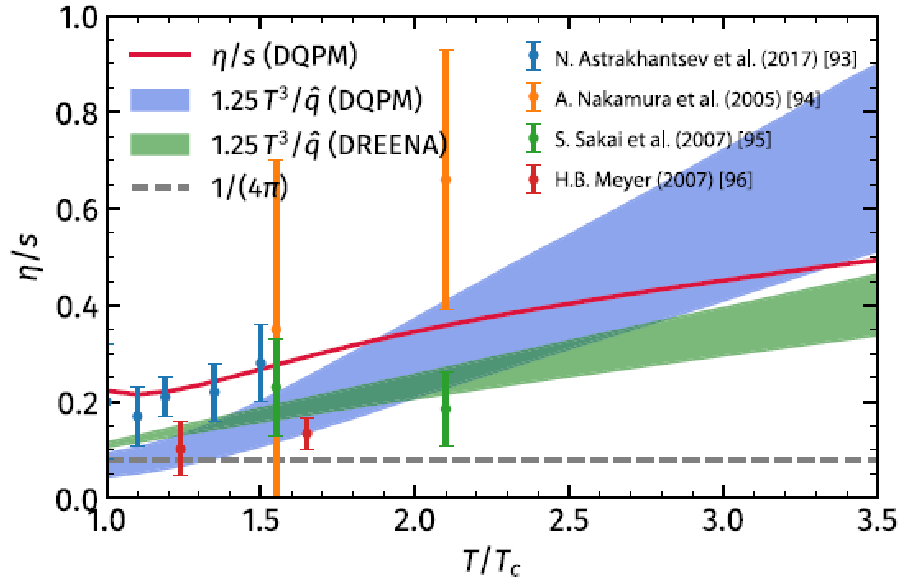

→ **Sensitive to the choice of the strong coupling**

→ **Valid in the weak coupling regime (at high temperatures)**

→ **Violated in the strong coupling regime (at low temperatures)**

Properties of QGP: transport coefficients

EoS(ε,n)
$\sigma(\sqrt{s}, m_q, m_q, T, \mu_B)$
$m(T, \mu_B)$

On practice: effective models
for QGP

Today:

Transport coefficients at finite **T** and $\boldsymbol{\mu_B}$
1.) crossover, CEP and 1st order phase transition (Nf =3 PNJL model)
2.) crossover + CEP (Nf = 3 DQPM)

– Dynamical QPM for partonic phase

W. Cassing, E. Bratkovskaya, PRC 78 (2008) 034919
P. Moreau, O. S , L. Oliva, T. Song, W. Cassing, E. Bratkovskaya, PRC 100 (2019) , 014911;
O. S, P. Moreau, L. Oliva, V. Voronyuk, V. Kireyeu, T. Song, E. Bratkovskaya, Particles 3 (2020), 178-192

Dynamical Quasi-Particle Model

The QGP phase is described in terms of strongly-interacting quasiparticles - quarks and gluons with Lorentzian spectral functions:

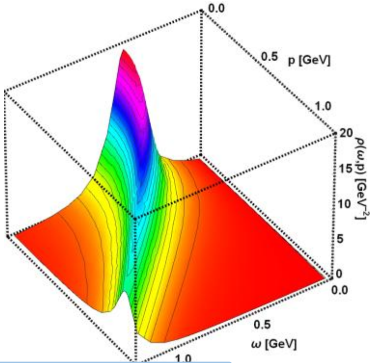

$$\rho_j(\omega,\mathbf{p}) = \frac{\gamma_j}{\tilde{E}_j}\left(\frac{1}{(\omega-\tilde{E}_j)^2+\gamma_j^2} - \frac{1}{(\omega+\tilde{E}_j)^2+\gamma_j^2}\right)$$

$$\equiv \frac{4\omega\gamma_j}{\left(\omega^2-\mathbf{p}^2-M_j^2\right)^2+4\gamma_j^2\omega^2}$$

resummed propagators: $\Delta_i(\omega,\mathbf{p}) = \frac{1}{\omega^2-\mathbf{p}^2-\Pi_i}$ & self-energies: $\Pi_i = m_i^2 - 2i\gamma_i\omega$

Re $\boldsymbol{\Pi_i}$: thermal mass $(\boldsymbol{M_g}, \boldsymbol{M_q})$

$$m^2_{q(\bar{q})}(T,\mu_{\rm B}) = C_q\frac{g^2(T,\mu_{\rm B})}{4}T^2\left[1+\left(\frac{\mu_B}{3\pi T}\right)^2\right]$$

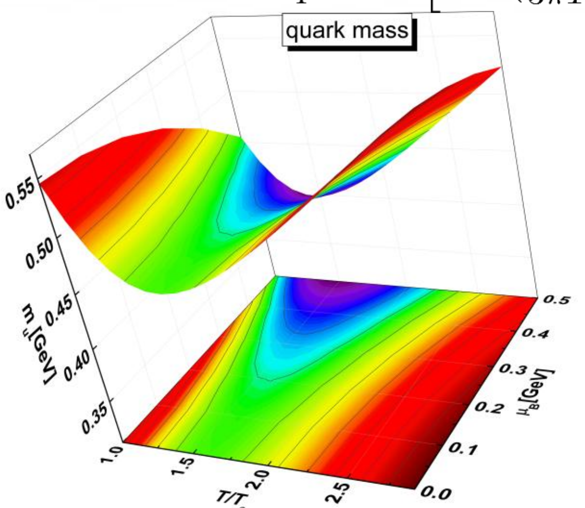

Im $\boldsymbol{\Pi_i}$: interaction width $(\boldsymbol{\gamma_g}, \boldsymbol{\gamma_q})$

$$\gamma_j(T,\mu_{\rm B}) = \frac{1}{3}C_j\frac{g^2(T,\mu_{\rm B})T}{8\pi}\ln\left(\frac{2c_m}{g^2(T,\mu_{\rm B})}+1\right)$$

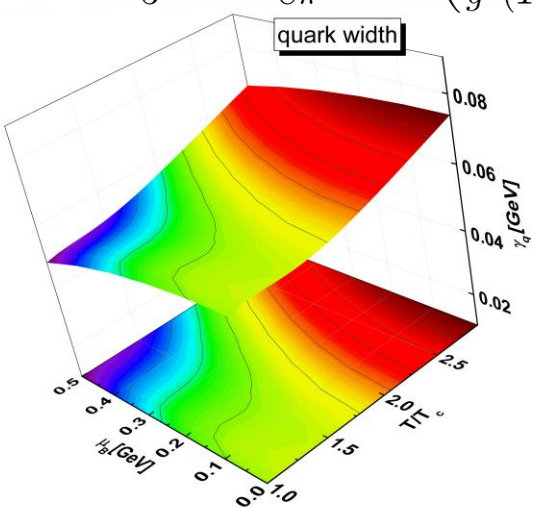

Peshier, Cassing, PRL 94 (2005) 172301; Cassing, NPA 791 (2007) 365; H. Berrehrah, E. Bratkovskaya, T. Steinert, W. Cassing, Int. J. Mod. Phys. E 25 (2016), 164200; P. Moreau, O. Soloveva , L. Oliva, T. Song, W. Cassing, E. Bratkovskaya, PRC 100 (2019) , 014911;

DQPM: EoS

Entropy and baryon density in the quasiparticle limit (G. Baym 1998, Blaizot et al. 2001):

$$s^{dqp} =$$

$$- \int \frac{d\omega}{2\pi} \frac{d^3p}{(2\pi)^3} \Big[d_g \frac{\partial n_B}{\partial T} \left(\mathrm{Im}(\ln -\Delta^{-1}) + \mathrm{Im}\, \Pi\, \mathrm{Re}\, \Delta\right)$$

$$+ \sum_{q=u,d,s} d_q \frac{\partial n_F(\omega - \mu_q)}{\partial T} \left(\mathrm{Im}(\ln -S_q^{-1}) + \mathrm{Im}\, \Sigma_q\, \mathrm{Re}\, S_q\right)$$

$$+ \sum_{\bar q=\bar u,\bar d,\bar s} d_{\bar q} \frac{\partial n_F(\omega + \mu_q)}{\partial T} \left(\mathrm{Im}(\ln -S_{\bar q}^{-1}) + \mathrm{Im}\, \Sigma_{\bar q}\, \mathrm{Re}\, S_{\bar q}\right) \Big]$$

$$n^{dqp} = - \int \frac{d\omega}{2\pi} \frac{d^3p}{(2\pi)^3}$$

$$\Big[\sum_{q=u,d,s} d_q \frac{\partial n_F(\omega - \mu_q)}{\partial \mu_q} \left(\mathrm{Im}(\ln -S_q^{-1}) + \mathrm{Im}\, \Sigma_q\, \mathrm{Re}\, S_q\right)$$

$$+ \sum_{\bar q=\bar u,\bar d,\bar s} d_{\bar q} \frac{\partial n_F(\omega + \mu_q)}{\partial \mu_q} \left(\mathrm{Im}(\ln -S_{\bar q}^{-1}) + \mathrm{Im}\, \Sigma_{\bar q}\, \mathrm{Re}\, S_{\bar q}\right) \Big]$$

- Input: entropy density as a f(T , $\boldsymbol{\mu_B = 0}$)

$$g^2(s/s_{SB}) = d\left((s/s_{SB})^e - 1\right)^f$$

$$s^{DQPM}(\Pi, \Delta, S_q, \Sigma) = s^{lattice}$$

fix the parameters

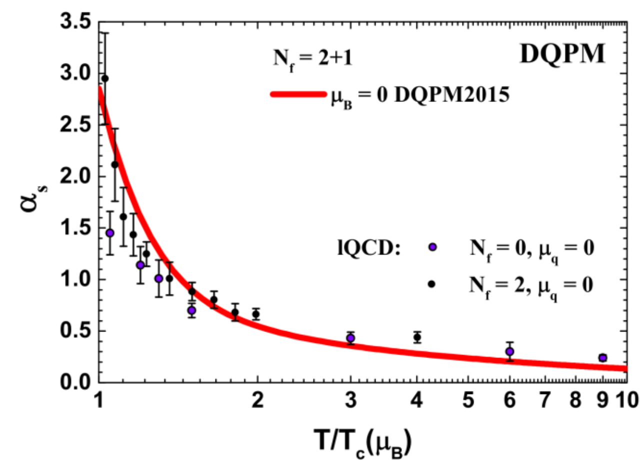

- Scaling hypothesis for the crossover region at finite $\boldsymbol{\mu_B}$

$$g^2(T/T_c, \mu_B) = g^2\left(\frac{T^*}{T_c(\mu_B)}, \mu_B = 0\right) \quad \text{with} \quad T^* = \sqrt{T^2 + \mu_q^2/\pi^2}$$

DQPM: EoS

Input:
lattice EoS
$\mu_B = 0$
(red dots)

Output:
DQPM EoS
$\mu_B \geq 0$
(lines)

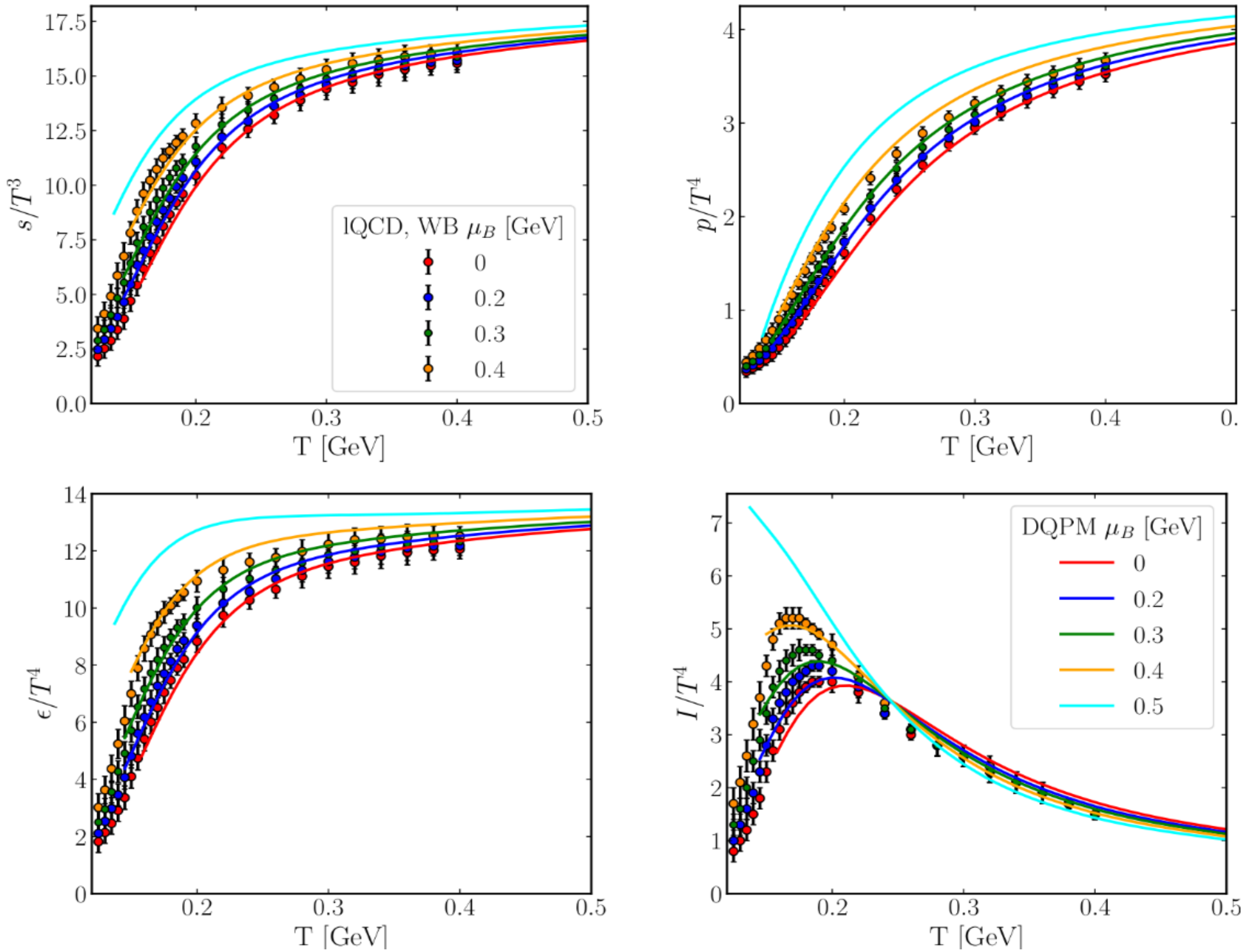

Transport coefficients at finite μ_B

Electric conductivity

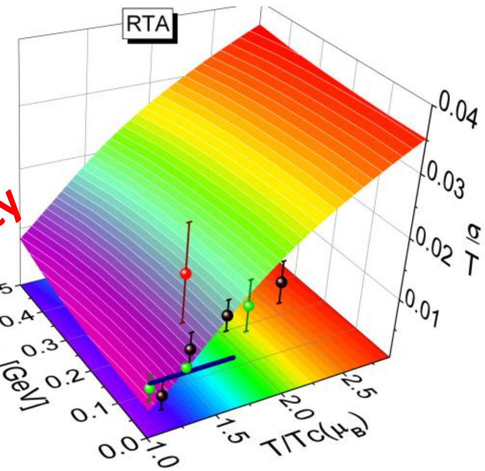

μ_B

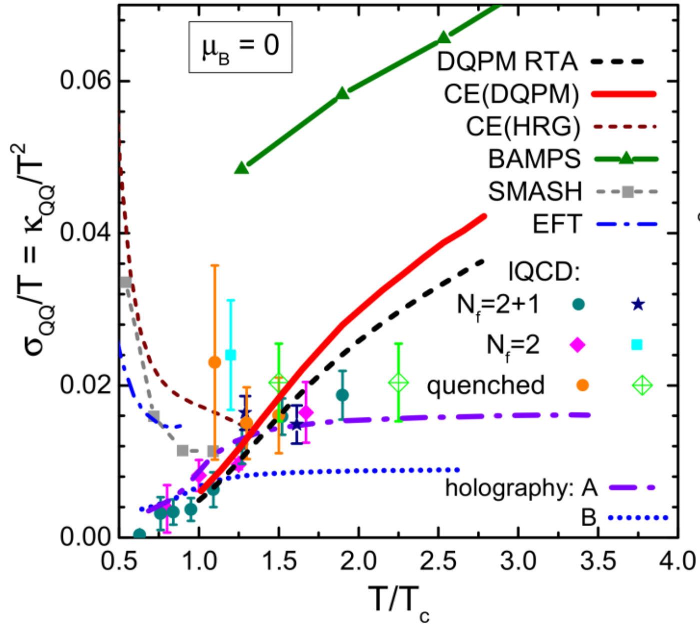

Baryon diffusion coefficient

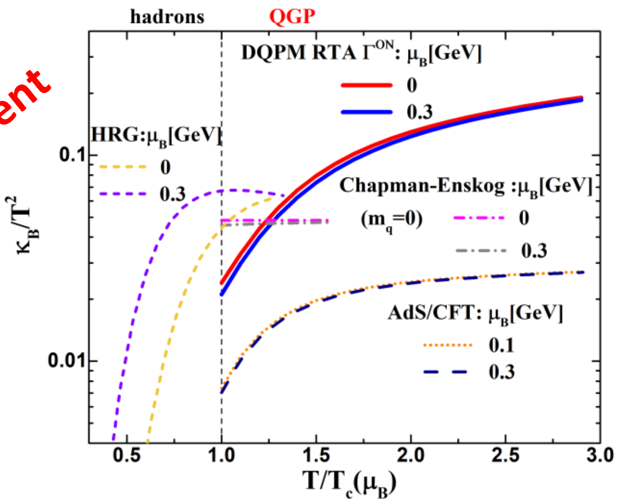

+ Full diffusion coefficient matrix has been evaluated $\sigma_q = \kappa_q/T$

$$\begin{pmatrix} j_B^\mu \\ j_Q^\mu \\ j_S^\mu \end{pmatrix} = \begin{pmatrix} \kappa_{BB} & \kappa_{BQ} & \kappa_{BS} \\ \kappa_{QB} & \kappa_{QQ} & \kappa_{QS} \\ \kappa_{SB} & \kappa_{SQ} & \kappa_{SS} \end{pmatrix} \cdot \begin{pmatrix} \nabla^\mu \alpha_B \\ \nabla^\mu \alpha_Q \\ \nabla^\mu \alpha_S \end{pmatrix}$$

J. A. Fotakis, O. S., C. Greiner, O. Kaczmarek and E. Bratkovskaya PRD 104 (2021) , 034014

- Light increase with μ_B in the crossover region for shear and bulk viscosities and electric conductivity
- Baryon diffusion coefficients decrease with μ_B

O. S., P. Moreau and E. Bratkovskaya, PRC 101 (2020), 045203

QGP in the Polyakov extended NJL model

- PNJL allows for prediction of macroscopic properties of QGP at finite **T** and μ_B
- & QGP transport coefficients for $0 \le \mu_B \le 1.2$ GeV

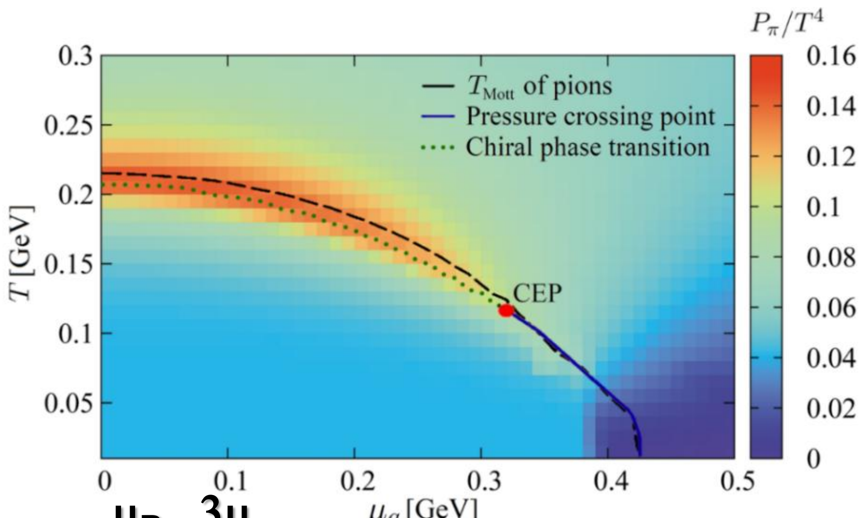

$\mu_B = 3\mu_q$

➢ Parameters fixed, EoS at $\mu_B = 0$:

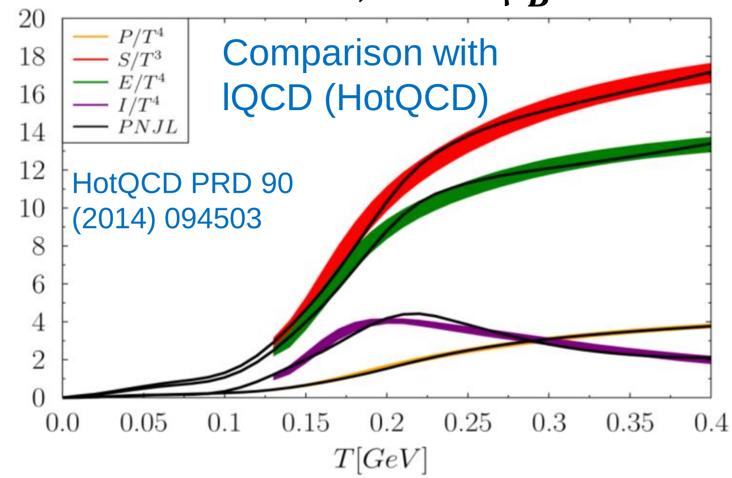

➢ CEP: $(T, \mu_B) = (110{,}960)$ MeV , $\mu_B/T = 8.73$

➢ 1st order PT at high μ_B

➢ same symmetries for the quarks as QCD

Chiral masses (M_l, M_s)

$$m_i = m_{0i} - 4G\langle\langle\bar{\psi}_i\psi_i\rangle\rangle + 2K\langle\langle\bar{\psi}_j\psi_j\rangle\rangle\langle\langle\bar{\psi}_k\psi_k\rangle\rangle$$

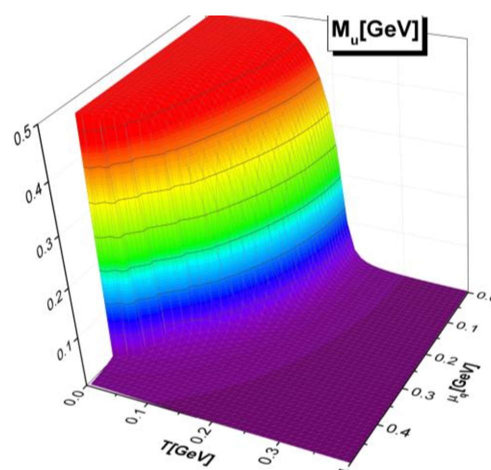

Improved thermodynamics by NNLO in Ω and Polyakov loop

J. M. Torres-Rincon, J. Aichelin PRC 96 (2017) 4 045205

D. Fuseau, T. Steinernert, J. Aichelin PRC 101 (2020) 6 065203

Specific shear viscosity at high μ_B

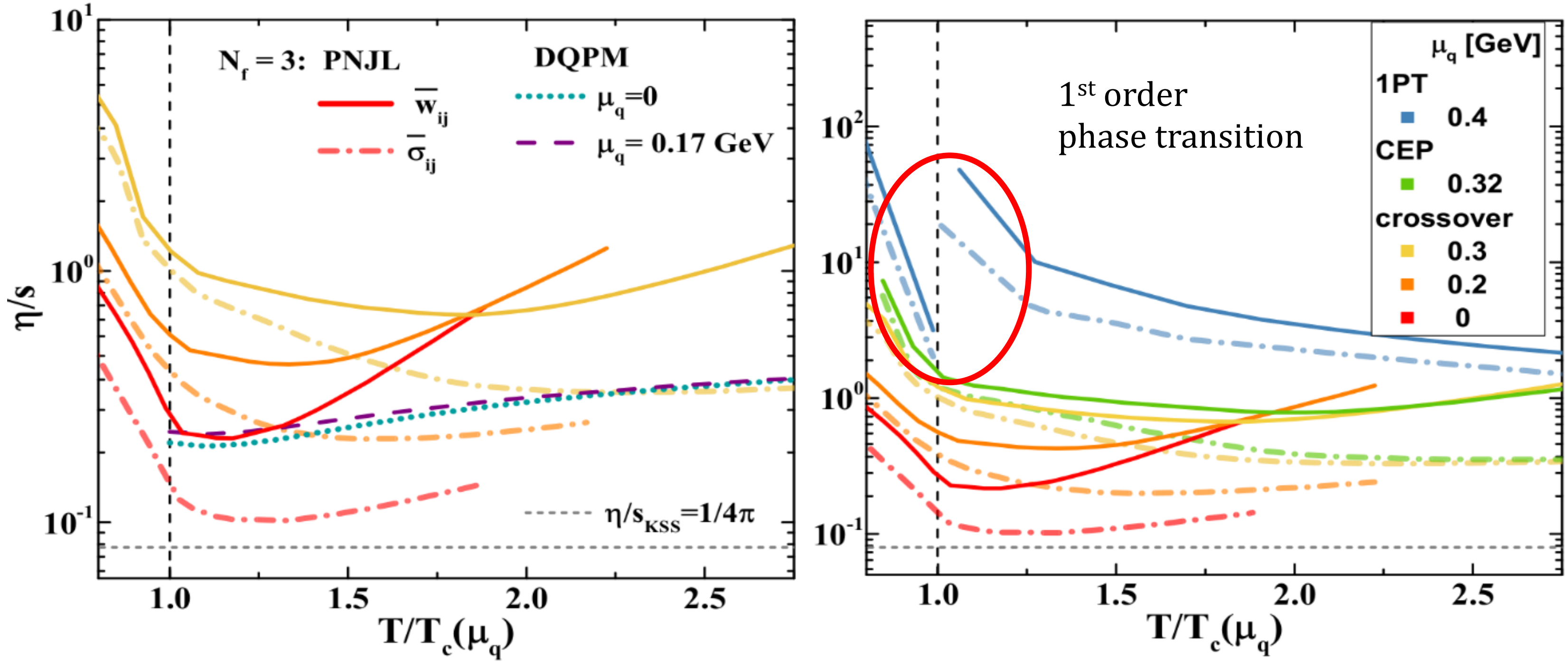

See also Nf=2 NJL results C. Sasaki et al, NPA 832 (2010)

- Two different models have similar increase with μ_B –dependence in the crossover region
- Drastic change of T–dependence for all transport coefficients after 1st order phase transition

O. S., D. Fuseau, J. Aichelin and E. Bratkovskaya, PRC 103 (2021) no.5, 054901

Electric conductivity at high μ_B

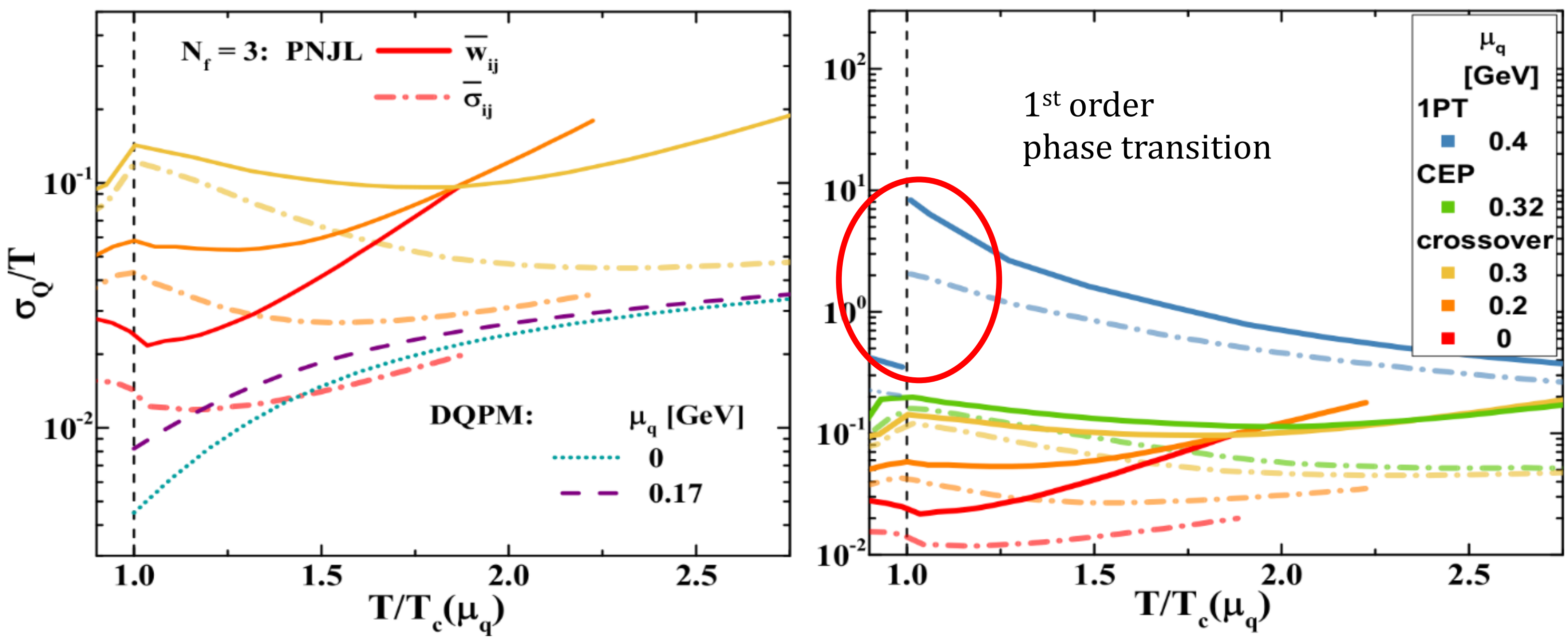

- Two different models have similar increase with μ_B –dependence in the crossover region
- Drastic change of T–dependence for all transport coefficients after 1st order phase transition

O. S., D. Fuseau, J. Aichelin and E. Bratkovskaya, PRC 103 (2021) no.5, 054901

Quasiparticle model with CEP at high μ_B

- DQPM-CP for high μ_B, including the CEP region based on the scaling properties of the entropy density from the PNJL model
- DQPM-CP interpolates EoS and microscopic properties between two asymptotics - high $T \gg T_c$, $\mu_B = 0$ and $T > T_c$, $\mu_B \gg T$
- EoS and transport coefficients of the QGP phase for the wide range of $T > T_c$, μ_B

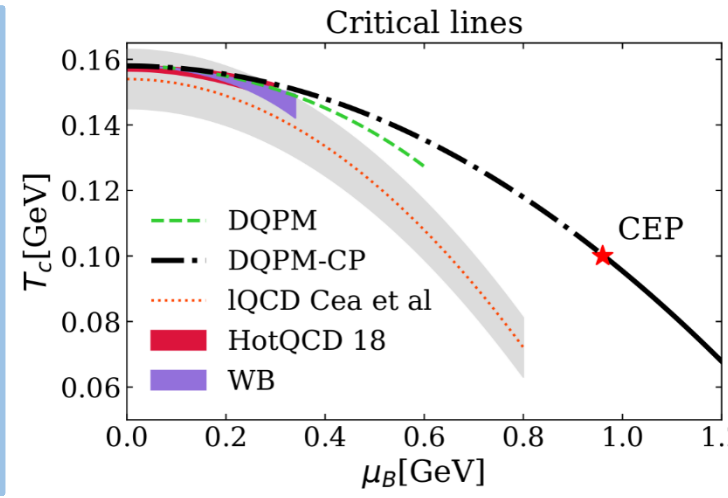

- CEP: $(T, \mu_B) = (100{,}960)$ MeV, $\mu_B/T = 9.6$
- EoS : for $\mu_B/T < 2$ agreement with lQCD for $\mu_B/T > 6$ agreement with pQCD

Near CEP: $g^2 = f(s^{PNJL}(T/T_c)) \to g^2(T/T_c)$

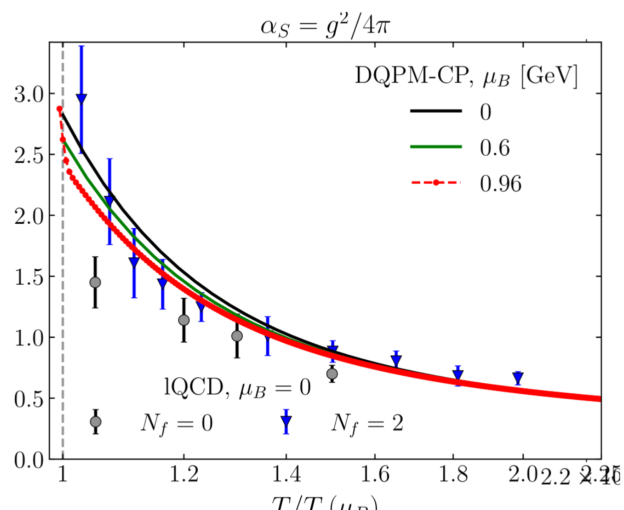

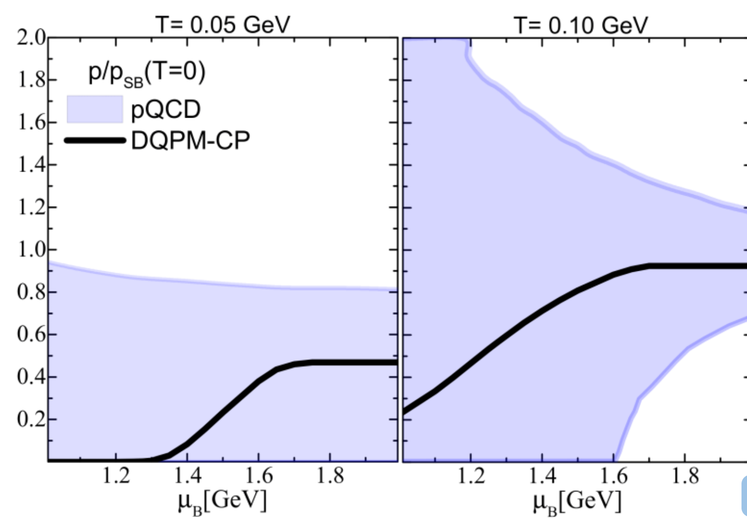

Isentropic trajectories

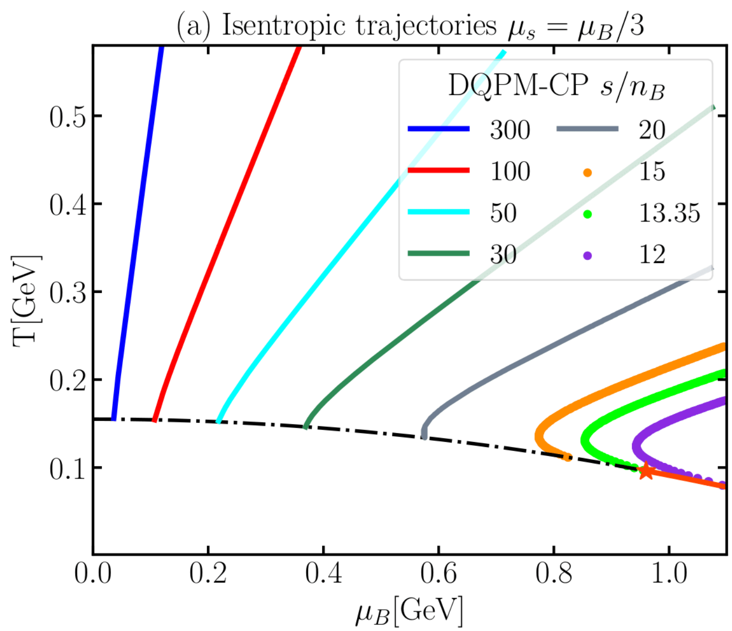

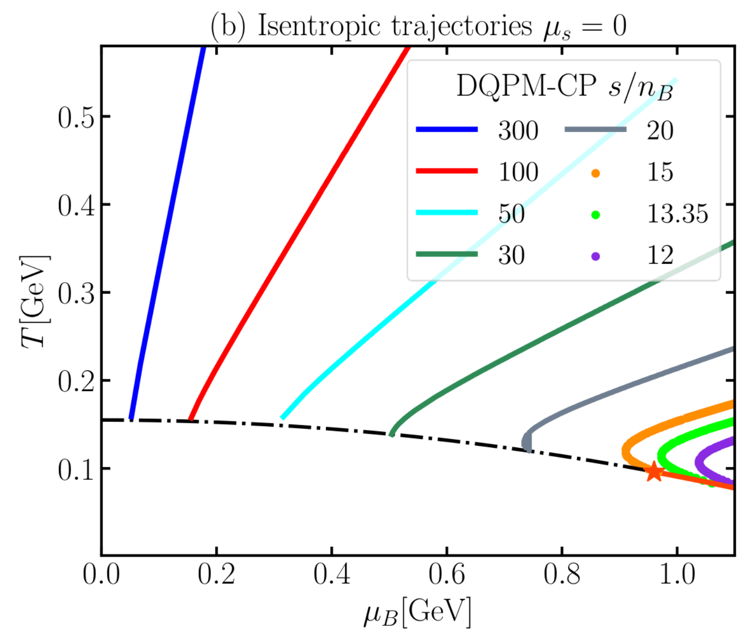

- CEP acts as an attractor of isentropic trajectories (Chiho Nonaka and Masayuki Asakawa PRC 71 (2005), 044904)
- Trajectories of s/n_B =const for <ns> =0 are shifted towards higher μ_B

O. S., J. Aichelin and E. Bratkovskaya, PRD 105 (2022) 054011

Speed of sound

- EoS : for μ_B/T <2 agreement with lQCD for μ_B/T >6 agreement with pQCD

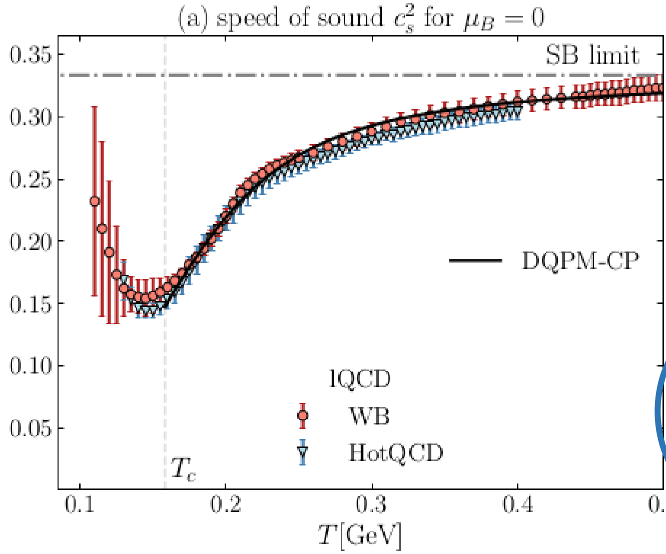

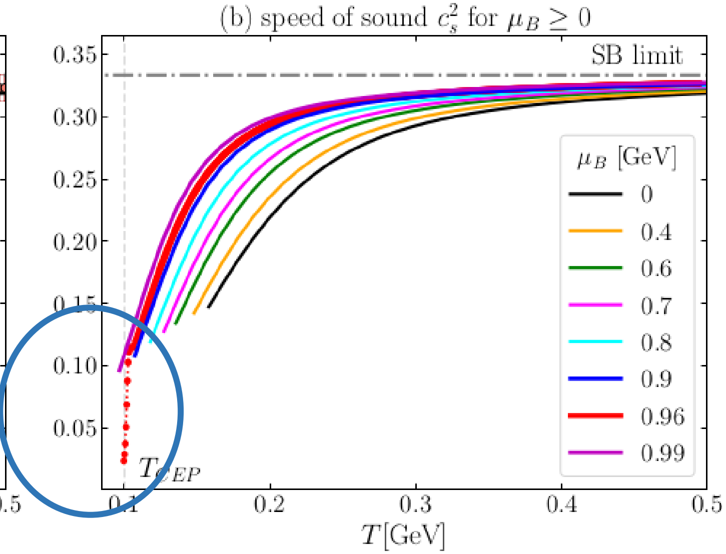

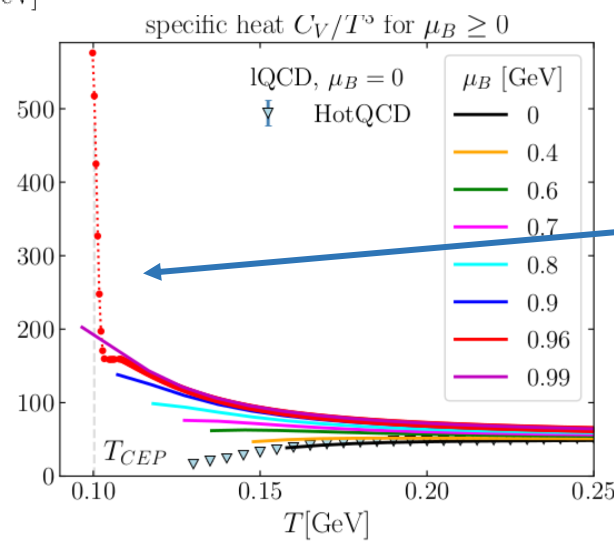

Near CEP critical scaling can be seen:

$$\ln(C_V) = -\alpha \cdot \ln(T - T_{CEP}) + const$$

O. S., J. Aichelin and E. Bratkovskaya, PRD 105 (2022) 054011

Shear and bulk iscosities near the CEP

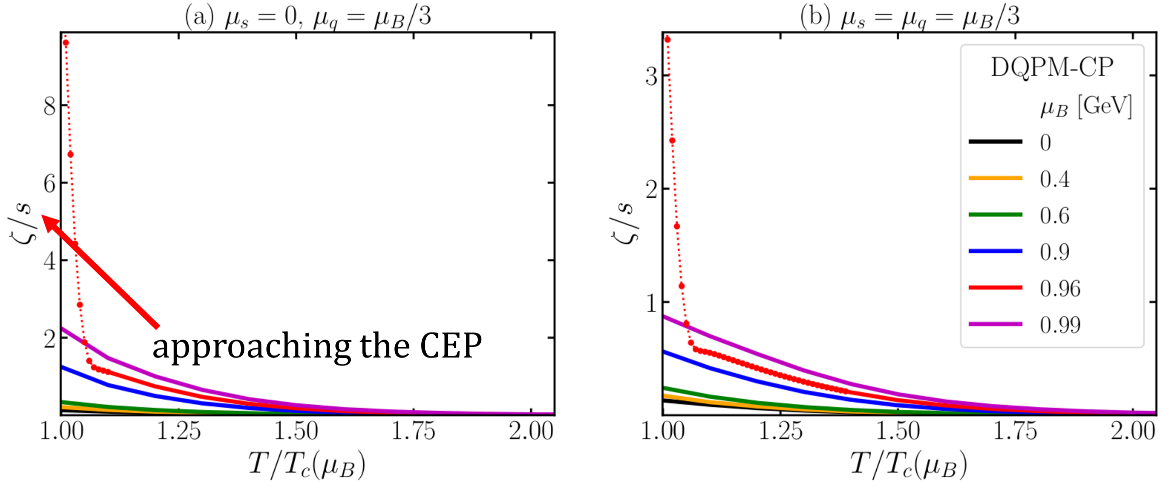

- Sudden rise of specific bulk viscosity approaching the CEP

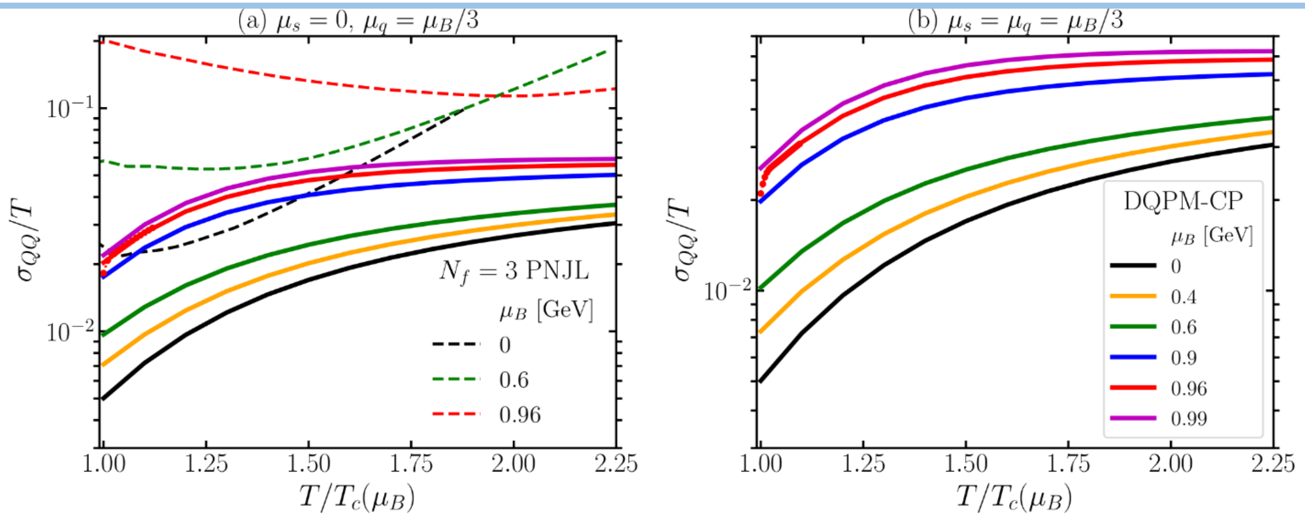

- B,Q,S diffusion coefficients have pronounced $\boldsymbol{\mu_B}$, $\boldsymbol{\mu_S}$-dependence
- Only small increase approaching the CEP

O. S., J. Aichelin and E. Bratkovskaya, PRD 105 (2022) 054011

Modelling HICs: PHSD

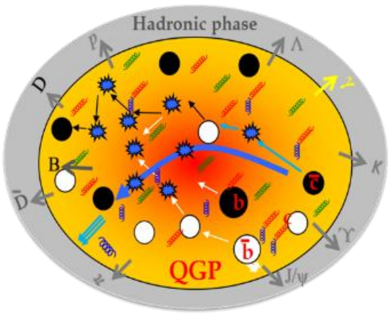

QGP out-of equilibrium ←→ HIC

Parton-Hadron-String-Dynamics (PHSD)

Non-equilibrium microscopic transport approach for the description of strongly-interacting hadronic and partonic matter created in heavy-ion collisions

Dynamics: based on the solution of generalized off-shell transport equations derived from Kadanoff-Baym many-body theory

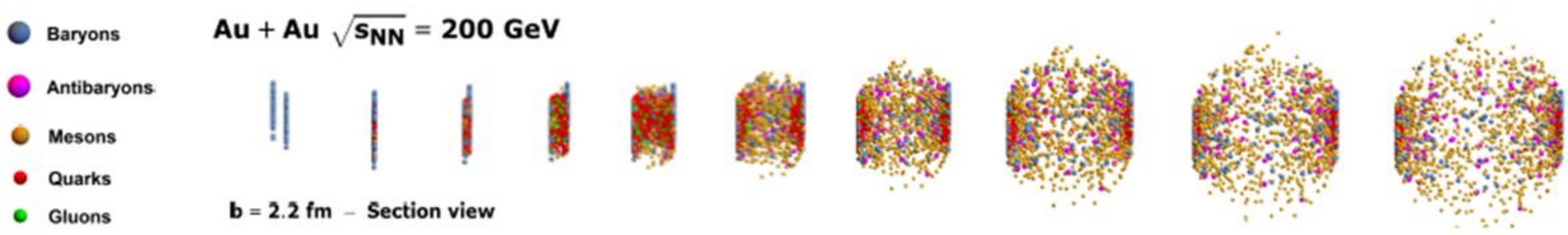

W. Cassing, E. Bratkovskaya, PRC 78 (2008) 034919; NPA831 (2009) 215; W. Cassing, EPJ ST 168 (2009) 3; …….;
P. Moreau, O. Soloveva , L. Oliva, T. Song, W. Cassing, E. Bratkovskaya, PRC 100 (2019) , 014911;
O. Soloveva, P. Moreau, L. Oliva, V. Voronyuk, V. Kireyeu, T. Song, E. Bratkovskaya, Particles 3 (2020), 178-192;….

PHSD

- **PHSD 4.0 : only isotropic $\sigma(T)$ and $\rho(T)$**

  parton cross sections

  parton spectral function (masses and widths)

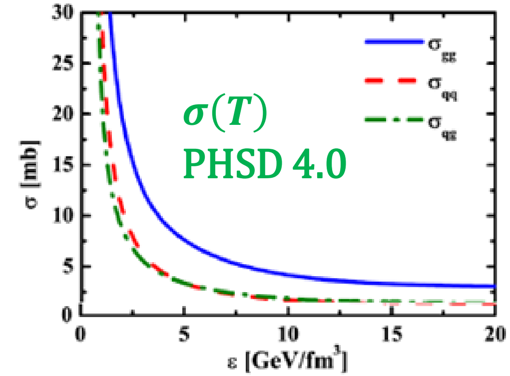

new PHSD 5 : angular dependence of $d\sigma/d\cos\theta$

- **PHSD 5.0 : with $\sigma(\sqrt{s}, m_1, m_2, T, \mu_B = 0)$ and $\rho(T, \mu_B = 0)$**
- **PHSD 5.0 : with $\sigma(\sqrt{s}, m_1, m_2, T, \mu_B)$ and $\rho(T, \mu_B)$**

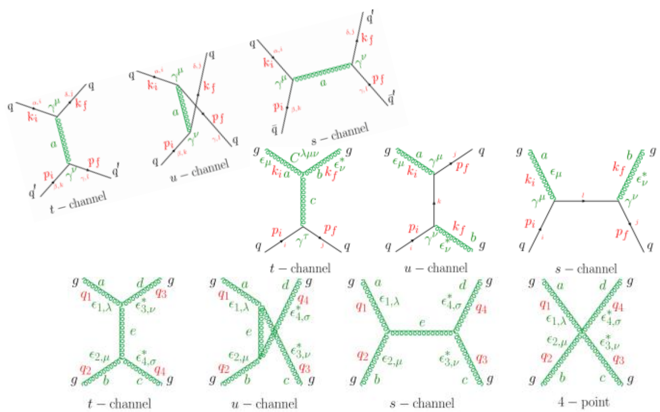

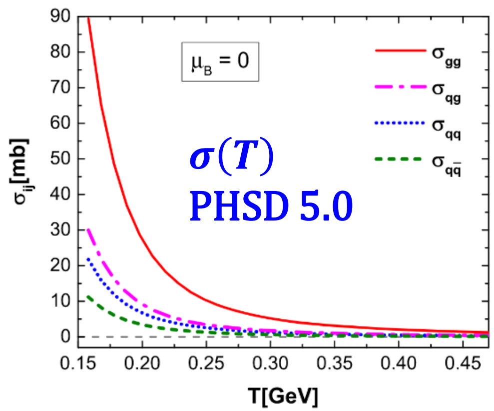

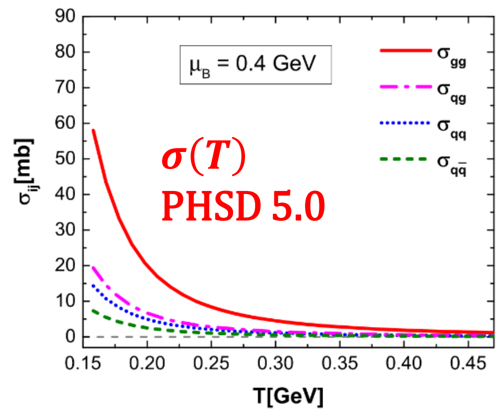

P. Moreau, O. Soloveva , L. Oliva, T. Song, W. Cassing, E. Bratkovskaya, PRC 100 (2019) , 014911;
O. Soloveva, P. Moreau, L. Oliva, V. Voronyuk, V. Kireyeu, T. Song, E. Bratkovskaya, Particles 3 (2020), 178-192

PHSD: extraction of T and μ_B

For each space-time cell of the PHSD: $T^{\mu\nu} = \sum_i \frac{p_i^\mu p_i^\nu}{E_i}$ → **Diagonalize in LRF** → ε^{PHSD}

1. Calculate the local energy density ε^{PHSD} and baryon density n_B^{PHSD}

2. use lQCD relations (up to 6th order):

$$\begin{cases} \frac{n_B}{T^3} \approx \chi_2^B(T)\left(\frac{\mu_B}{T}\right) + \ldots \\ \Delta\epsilon/T^4 \approx \frac{1}{2}\left(T\frac{\partial\chi_2^B(T)}{\partial T} + 3\chi_2^B(T)\right)\left(\frac{\mu_B}{T}\right)^2 + \ldots \end{cases}$$

Use baryon number susceptibilities χ_n from lQCD
Obtain T, μ_B by solving sistem of coupled eqs using ε, n_B

$e(x, y, z = 0)$

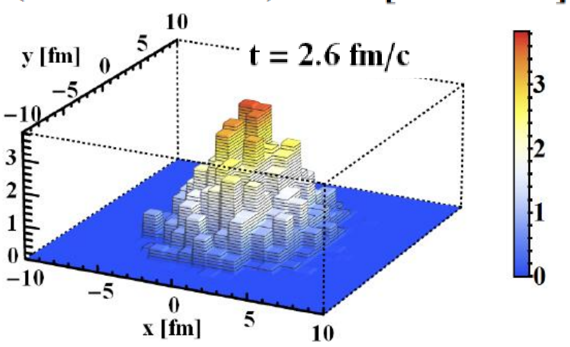

Input:

ε^{PHSD} and n_B^{PHSD}

Output:

T, μ_B

for details see P. Moreau, O. S., L. Oliva, T. Song, W. Cassing, E. Bratkovskaya
arXiv:1903.10157, PRC 100 (2019) no. 1, 014911

PHSD: QGP evolution in HICs

Input:

ε^{PHSD} and n_B^{PHSD}

Output:

T, μ_B

The T -profile in (x;y) & μ_B profile in (x;y)

at midrapidity ($|y_{cell}|$< 1) at fixed times(1 and 4 fm/c)

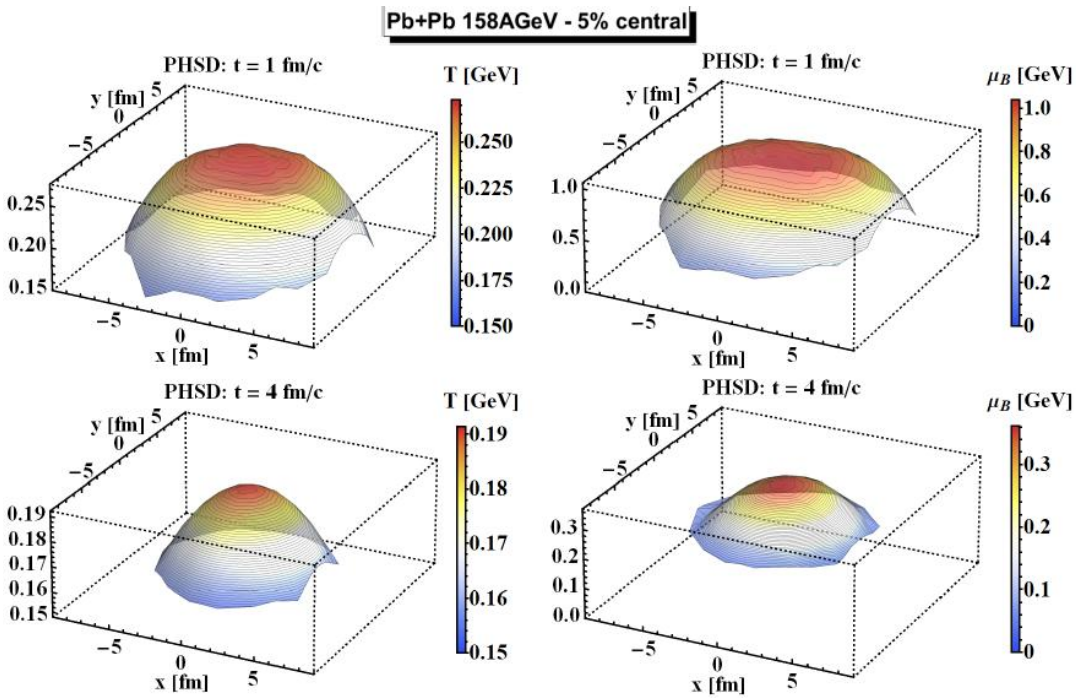

time evolution

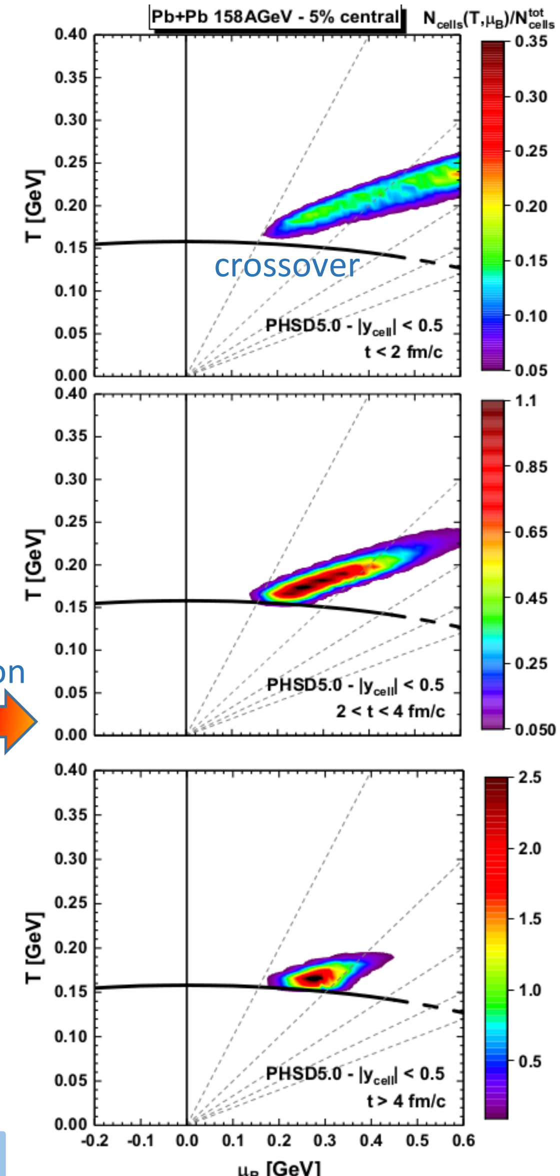

Path through the phase diagram is not trivial and localized

Specific shear viscosity compilation

Model predictions:

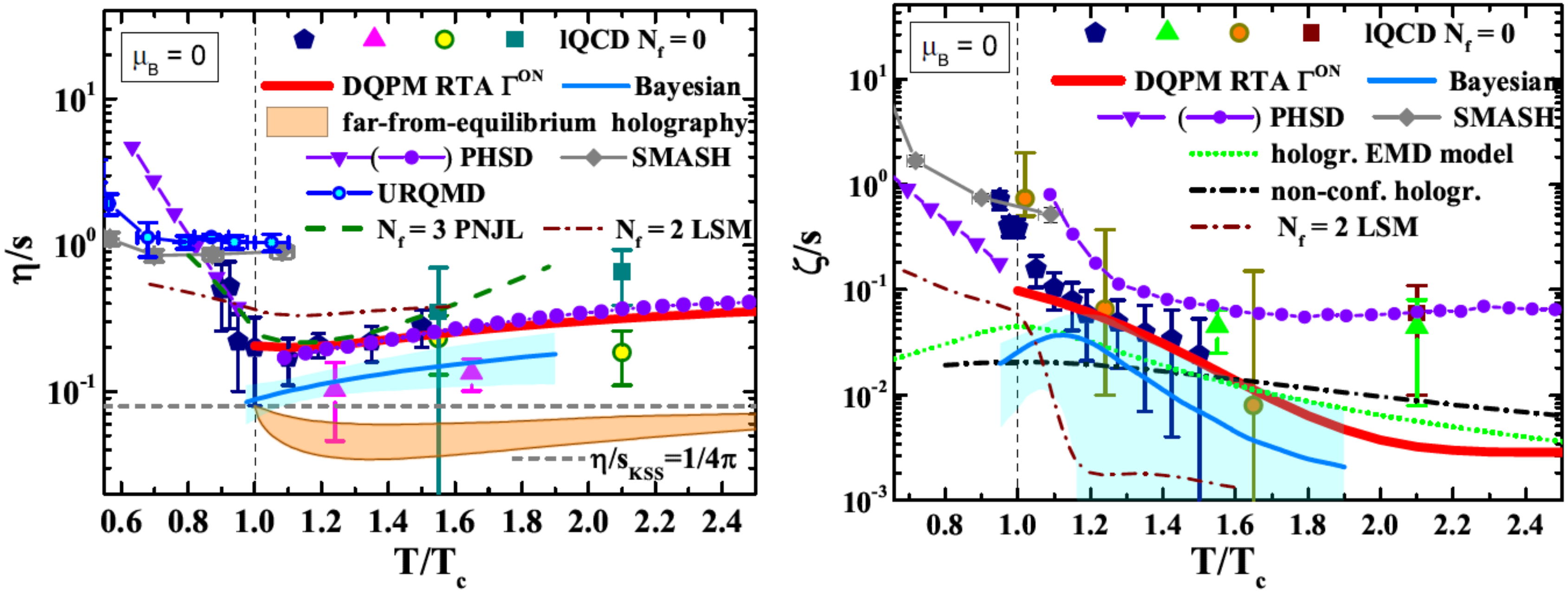

! Different models using the same EoS can have completely different transport coefficients!

Backup slides

Results for ($\sqrt{s_{NN}}$ = 200 GeV - 7 GeV)

- No visible effects on p_T-spectra, dN/dy of μ_B -dependence
- Small effect of the angular dependence of **dσ/dcosθ**

at high $\sqrt{s_{NN}}$ - low μ_B

! QGP fraction is small at low $\sqrt{s_{NN}}$

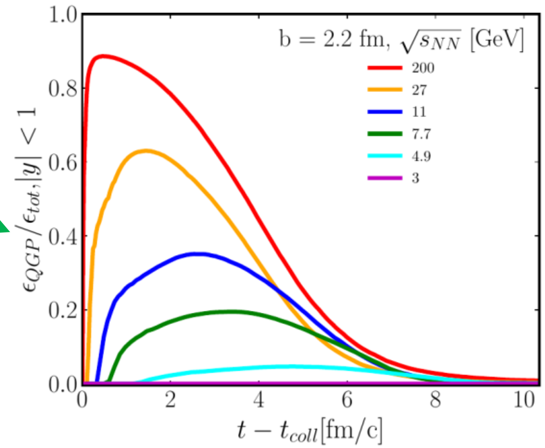

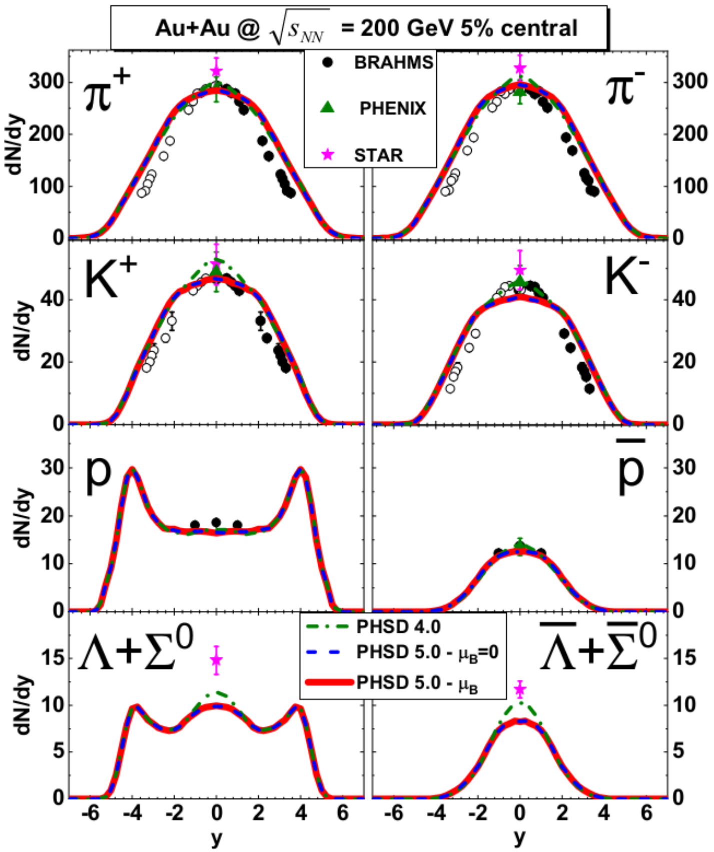

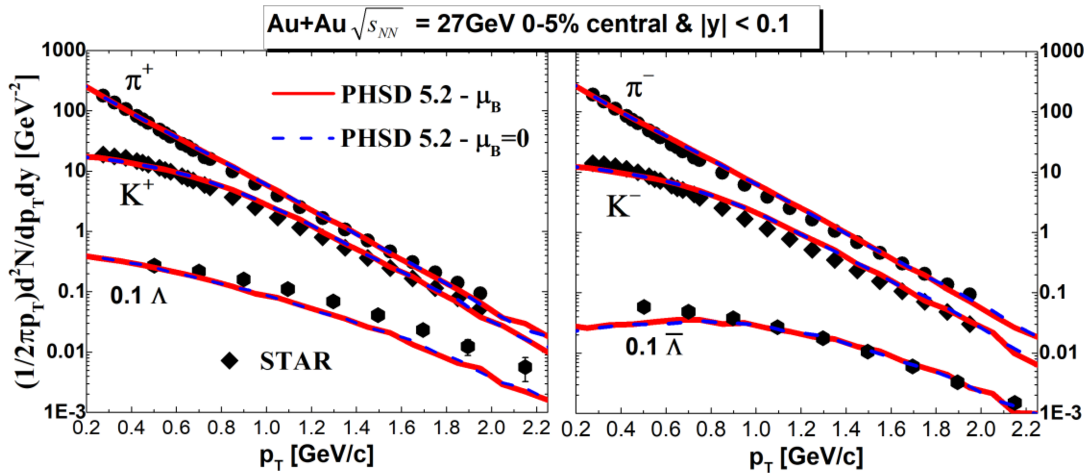

P. Moreau, O. Soloveva , L. Oliva, T. Song, W. Cassing, E. Bratkovskaya, PRC 100 (2019) , 014911;
O. Soloveva, P. Moreau, L. Oliva, V. Voronyuk, V. Kireyeu, T. Song, E. Bratkovskaya, Particles 3 (2020), 178-192

Anisotropic flow coefficients

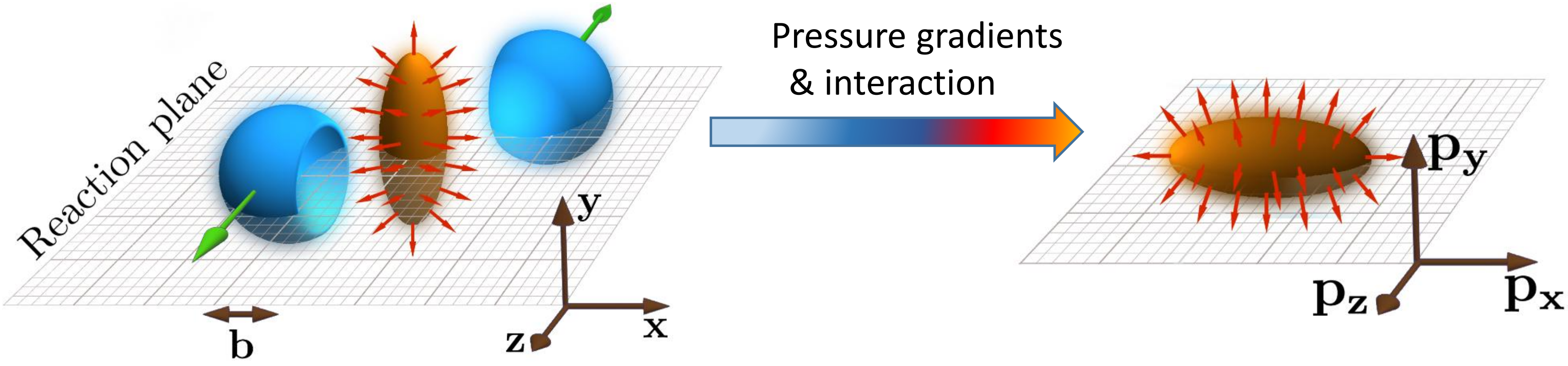

Quantify the anisotropic flow using Fourier expansion

$$\frac{dN}{d\varphi} \propto \left(1 + 2\sum_{n=1}^{+\infty} v_n \cos\left[n(\varphi - \psi_n)\right]\right)$$

$$v_n = \left\langle \cos n\left(\varphi - \psi_n\right)\right\rangle, \quad n = 1,2,3..,$$

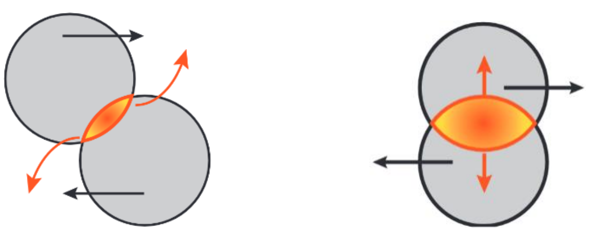

$$v_1 = \left\langle \frac{p_x}{p_T} \right\rangle \qquad v_2 = \left\langle \frac{p_x^2 - p_y^2}{p_T^2} \right\rangle$$

Anisotropic flow

- Assess the transport properties of the QGP
- Sensitive to the QGP EoS and initial state
- Validate models of bulk evolution that are used in the computation of other observables

Directed flow ($\sqrt{s_{NN}} = 200\ GeV\ vs\ 27\ GeV$)

$$v_1 = \left\langle \frac{p_x}{p_T} \right\rangle$$

- Influence of the QGP dynamics on final particles observables
- Weak μ_B –dependence – small fraction of QGP or low μ_B

Particles 3 (2020) no.1, 178-192

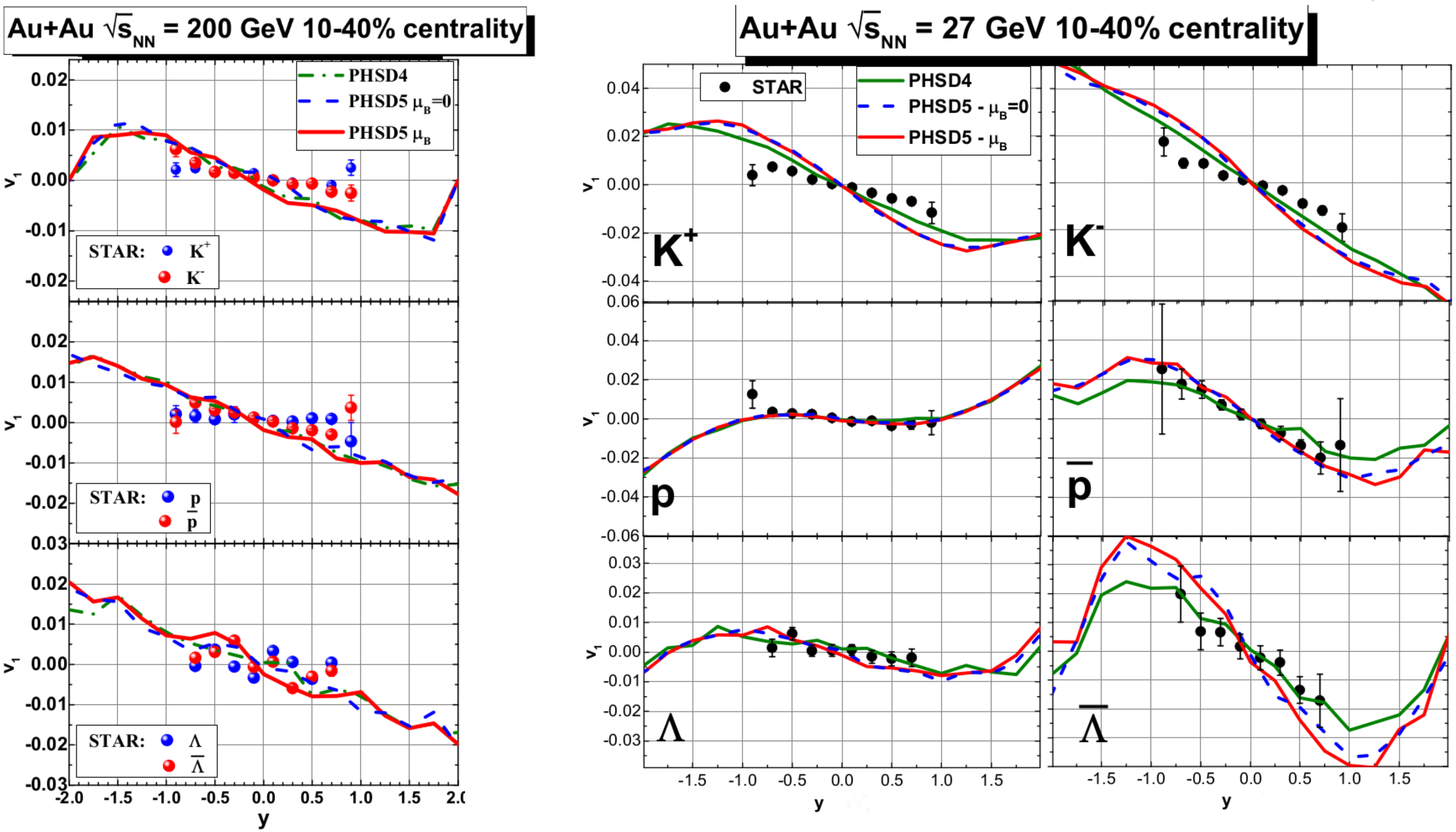

Elliptic flow ($\sqrt{s_{NN}} = 200\ GeV\ vs\ 27 GeV$)

$$v_2 = \left\langle \frac{p_x^2 - p_y^2}{p_T^2} \right\rangle$$

- Weak μ_B -dependence
- Small effect of the angular dependence of **dσ/dcosθ**
- Strong flavor dependence

Particles 3 (2020) no.1, 178-192

200GeV, 10-20%

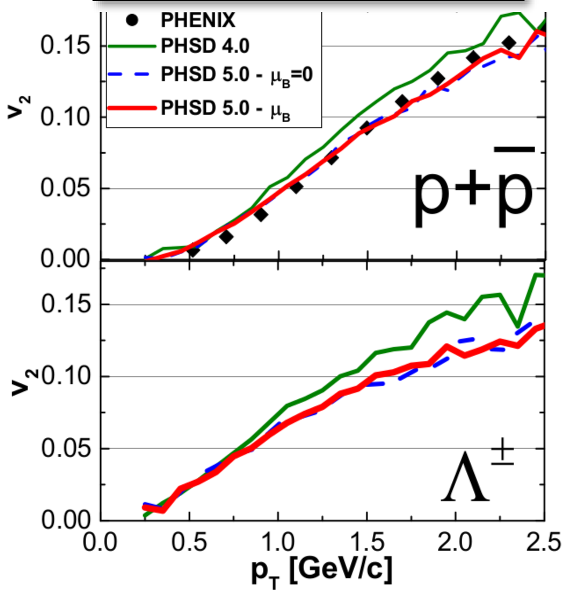

27GeV, 10-40%

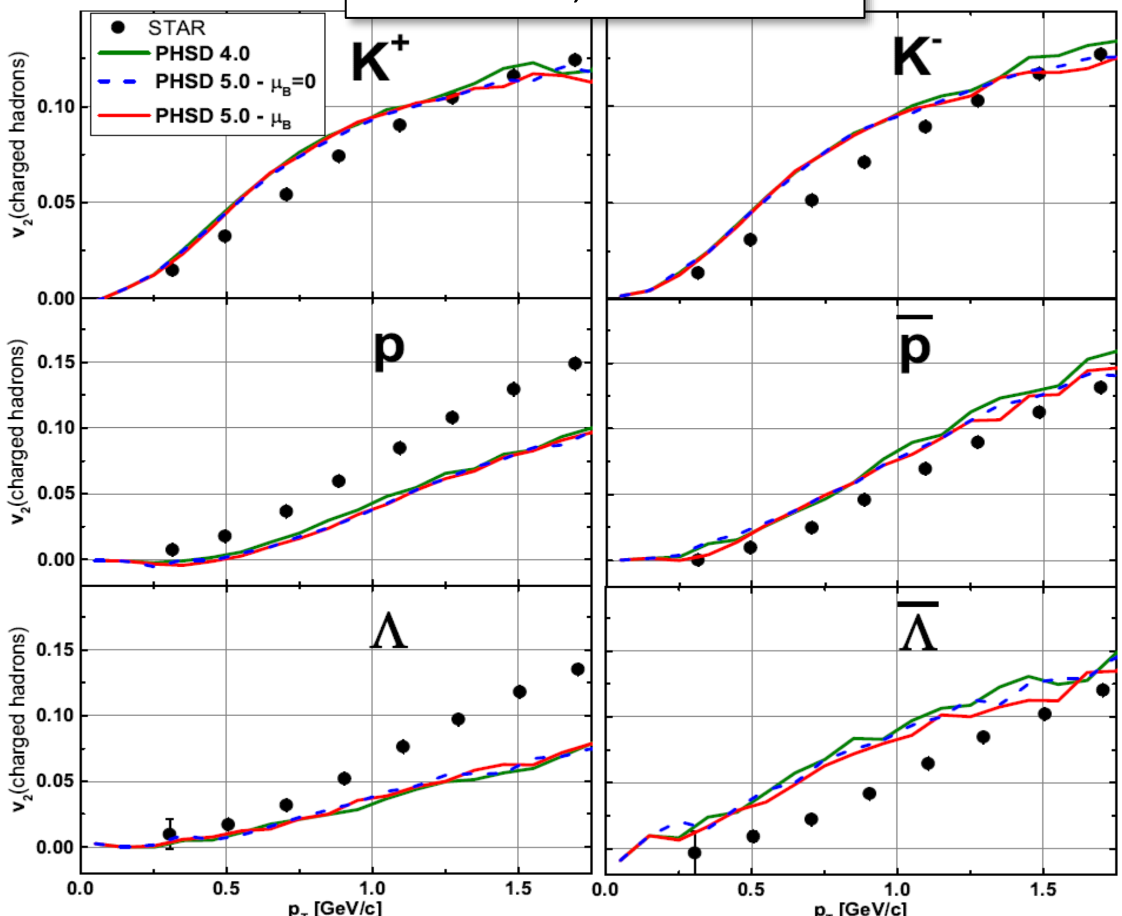

Summary

Transport properties of the strongly-interacting QGP matter at finite **T** and $\boldsymbol{\mu_B}$ have been investigated.
Influence of an order of a phase transition on thermodynamic and transport properties has been studied.

- Transport coefficients can differ among the models, which have similar phase structures and EoS

Evolution of the QGP matter created in HICs and the sensitivity of the bulk and flow observables on the QGP interactions and transport properties have been explored by the simulations within the PHSD transport approach

- High-$\boldsymbol{\mu_B}$ regions are probed at low $\sqrt{\boldsymbol{s_{NN}}}$ or high rapidity regions
  Moreover, QGP fraction is small at low $\sqrt{\boldsymbol{s_{NN}}}$: small effect seen in observables
- $\boldsymbol{\mu_B}$-dependence of QGP interactions is more pronounced in observables for strange hadrons and antiprotons

Outlook:

- Phase transition in PHSD
- Possible effects of phase transitions on flow/dileptons

Summary

Transport properties of the strongly-interacting QGP matter at finite **T** and μ_B have been investigated.
Influence of an order of a phase transition on thermodynamic and transport properties has been studied.

- Transport coefficients can differ among the models, which have similar phase structures and EoS

Evolution of the QGP matter created in HICs and the sensitivity of the bulk and flow observables on the QGP interactions and transport properties have been explored by the simulations within the PHSD transport approach

- High-μ_B regions are probed at low $\sqrt{s_{NN}}$ or high rapidity regions
  Moreover, QGP fraction is small at low $\sqrt{s_{NN}}$: small effect seen in observables
- μ_B-dependence of QGP interactions is more pronounced in observables for strange hadrons and antiprotons

Thank you for your attention!

Elliptic flow ($\sqrt{s_{NN}} = 200\ GeV\ vs\ 27GeV$)

$$v_2 = \left\langle \frac{p_x^2 - p_y^2}{p_T^2} \right\rangle$$

- Weak μ_B -dependence
- Small effect of the angular dependence of **dσ/dcosθ**
- Strong flavor dependence

Particles 3 (2020) no.1, 178-192

Channel decomposition :

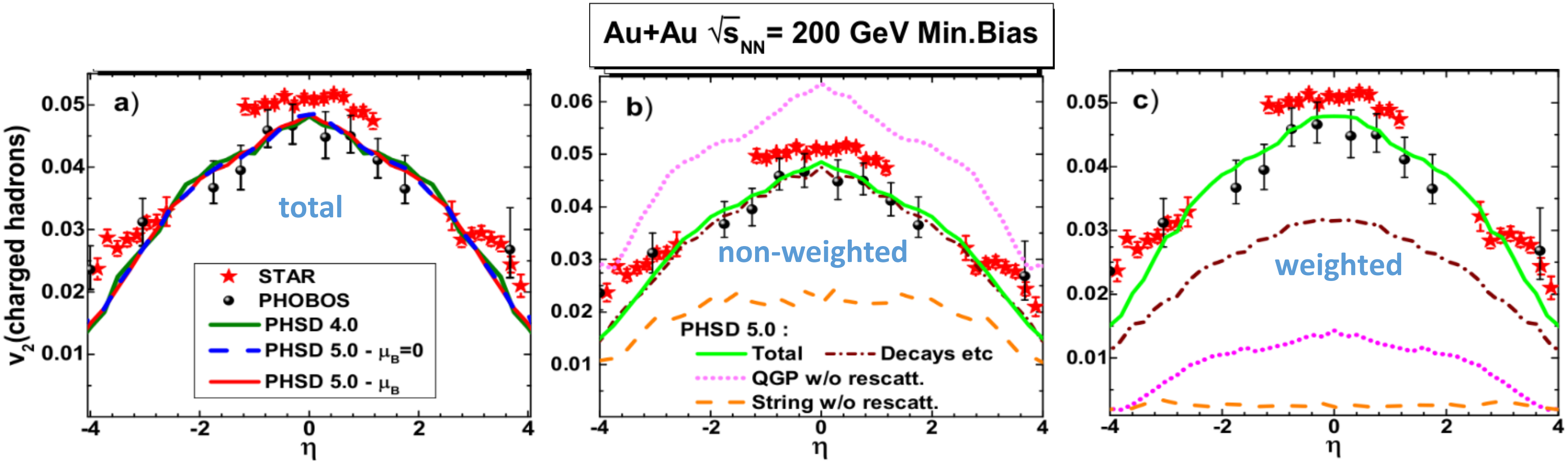

Elliptic flow ($\sqrt{s_{NN}} = 200\ GeV\ - 27GeV$)

- Weak μ_B –dependence – small fraction of QGP or low μ_B
- Small effect of the angular dependence of **dσ/dcosθ**
- Strong flavor dependence

27GeV, 10-40%

$$v_1 = \left\langle \frac{p_x}{p_T} \right\rangle$$

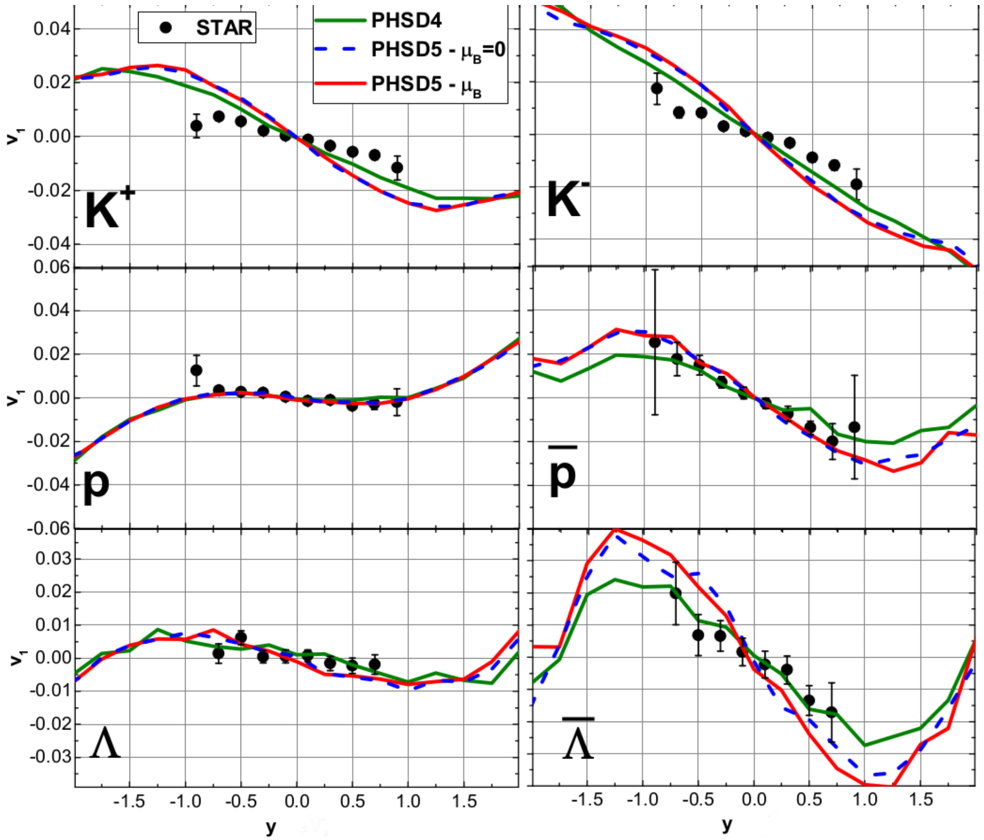

$$v_2 = \left\langle \frac{p_x^2 - p_y^2}{p_T^2} \right\rangle$$

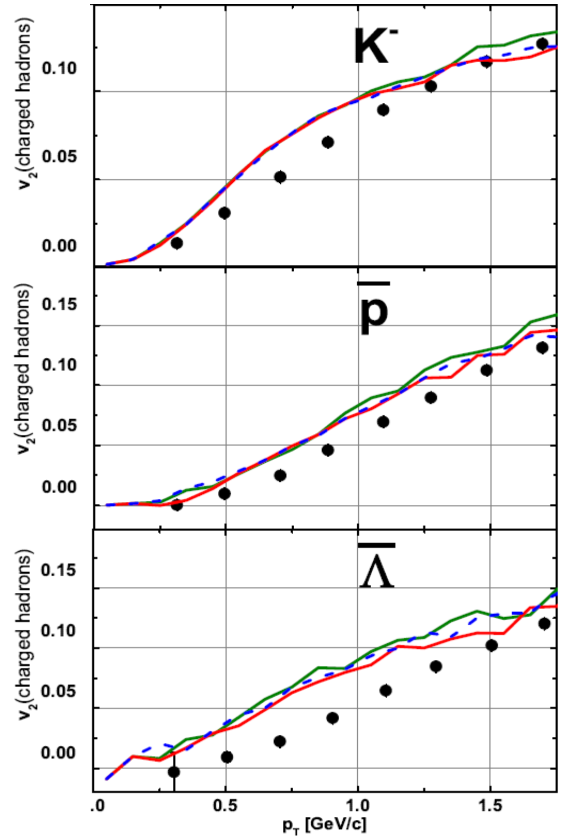

O. Soloveva, P. Moreau, L. Oliva, V. Voronyuk, V. Kireyeu, T. Song, E. Bratkovskaya, Particles 3 (2020), 178-192

PNJL relaxation times

$$\boxed{\tau_i(\mathbf{p},T,\mu_B) = \frac{1}{\Gamma_i(\mathbf{p},T,\mu_B)}}$$

$$\Gamma_i^{\rm on}(\mathbf{p}_i,T,\mu_q) = \frac{1}{2E_i}\sum_{j=q,\bar{q},g}\int \frac{d^3p_j}{(2\pi)^3 2E_j}\, d_j\ f_j(E_j,T,\mu_q)$$
$$\int \frac{d^3p_3}{(2\pi)^3 2E_3}\int \frac{d^3p_4}{(2\pi)^3 2E_4}(1\pm f_3)(1\pm f_4)$$
$$\boxed{|\bar{\mathcal{M}}|^2(p_i,p_j,p_3,p_4)}\,(2\pi)^4\delta^{(4)}\,(p_i+p_j-p_3-p_4)$$

Relaxation times(PNJL vs NJL)

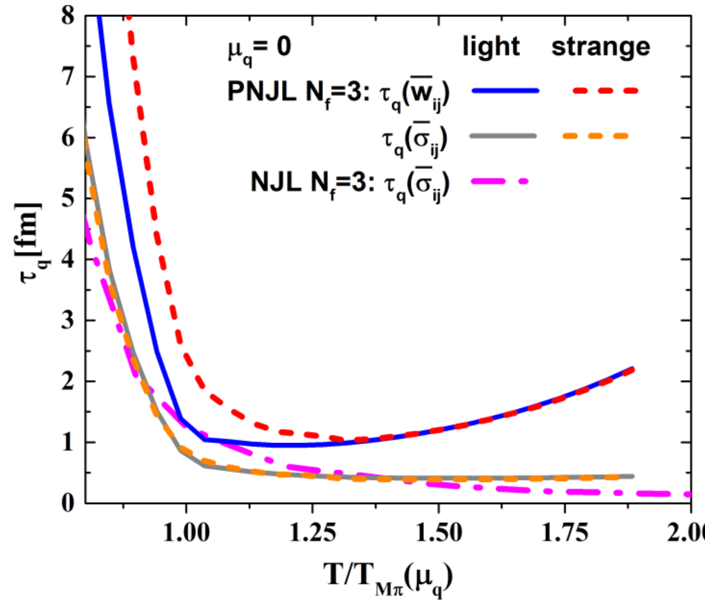

qq - interactions:

4 point interaction -> meson exchange(π,Ϭ,η,η',K,.. for s,t,u channels)

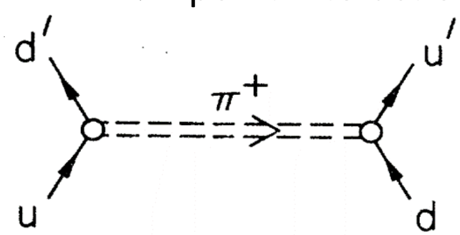

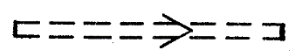

$$=(i\gamma_5)\tau^{(-)}\frac{-ig^2_{\pi qq}}{k^2-m^2_\pi}(i\gamma_5)\tau^{(+)}$$

meson propagator $\quad \mathscr{D} = \dfrac{2ig_m}{1-2g_m\Pi^{\pm}_{ff'}(k_0,\vec{k})}$

Effective interaction in RPA

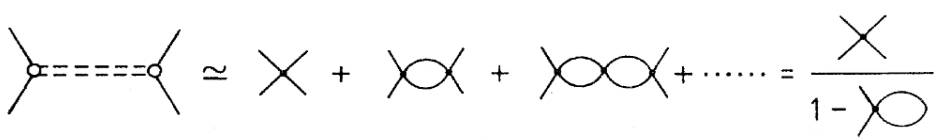

PNJL relaxation times

$$\boxed{\tau_i(\mathbf{p},T,\mu_B) = \frac{1}{\Gamma_i(\mathbf{p},T,\mu_B)}}$$

$$\Gamma_i^{\rm on}(\mathbf{p}_i,T,\mu_q) = \frac{1}{2E_i}\sum_{j=q,\bar{q},g}\int\frac{d^3p_j}{(2\pi)^3 2E_j}\, d_j \boxed{f_j(E_j,T,\mu_q)}$$
$$\int\frac{d^3p_3}{(2\pi)^3 2E_3}\int\frac{d^3p_4}{(2\pi)^3 2E_4}(1\pm f_3)(1\pm f_4)$$
$$|\bar{\mathcal{M}}|^2(p_i,p_j,p_3,p_4)\ (2\pi)^4\delta^{(4)}\ (p_i+p_j-p_3-p_4)$$

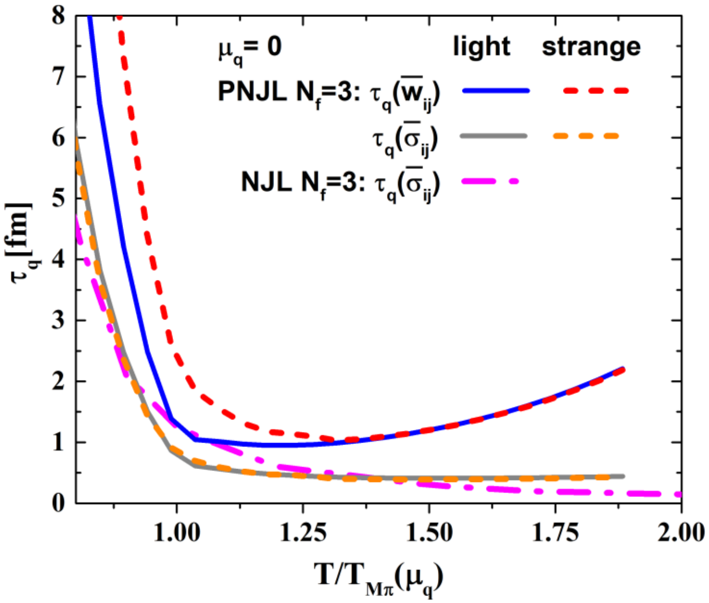

Modified distribution functions:
Polyakov loop contributions

$$f_q \rightarrow f_q^{\Phi}(\mathbf{p},T,\mu)$$
$$= \frac{(\bar{\Phi}+2\Phi e^{-(E_{\mathbf{p}}-\mu)/T})e^{-(E_{\mathbf{p}}-\mu)/T}+e^{-3(E_{\mathbf{p}}-\mu)/T}}{1+3(\bar{\Phi}+\Phi e^{-(E_{\mathbf{p}}-\mu)/T})e^{-(E_{\mathbf{p}}-\mu)/T}+e^{-3(E_{\mathbf{p}}-\mu)/T}},$$

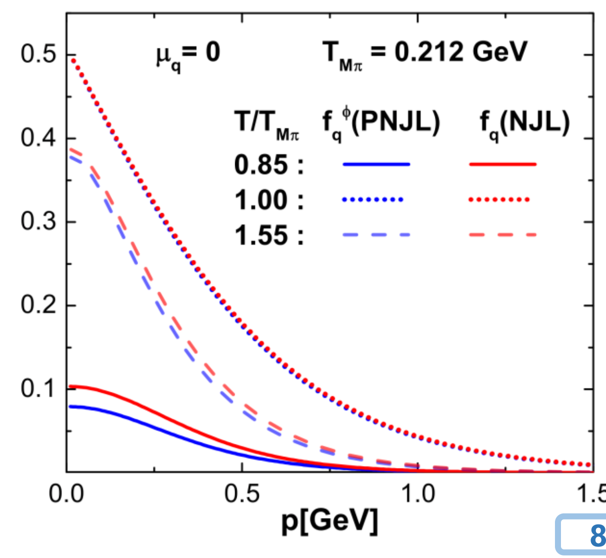

QGP in the Polyakov extended NJL model

- PNJL model based on effective Lagrangian with the same symmetries for the quark dof as QCD

$$
\begin{aligned}
\mathscr{L}_{PNJL} = & \sum_i \bar{\psi}_i (iD - m_{0i} + \mu_i \gamma_0)\psi_i \\
& + G \sum_a \sum_{ijkl} \left[(\bar{\psi}_i \; i\gamma_5 \tau^a_{ij} \psi_j)\; (\bar{\psi}_k \; i\gamma_5 \tau^a_{kl} \psi_l) + (\bar{\psi}_i \tau^a_{ij} \psi_j)\; (\bar{\psi}_k \tau^a_{kl} \psi_l) \right] \\
& - K \det_{ij} \left[\bar{\psi}_i \; (-\gamma_5)\psi_j \right] - K \det_{ij} \left[\bar{\psi}_i \; (+\gamma_5)\psi_j \right] \\
& - \mathcal{U}(T; \Phi, \bar{\Phi})
\end{aligned}
$$

Polyakov-loop effective potential fitted to the YM

5 parameters fixed by vacuum values K,π masses, η-η'mass splitting , π decay constant, Chiral condensate

Improvements:

- Next to leading order in Nc(O(1/Nc)$^{\mathbf{0}}$) of the grand-canonical potential : presence of the mesons below Tc

$$
\Omega_{\mathrm{PNJL}}(T,\mu_i) = \Omega_q^{(-1)}(T,\mu_i) + \boxed{\sum_{M \in J^\pi = \{0^+,0^-\}} \Omega_M^{(0)}(T,\mu_M(\mu_i))} + \mathcal{U}_{glue}(T) \; ,
$$

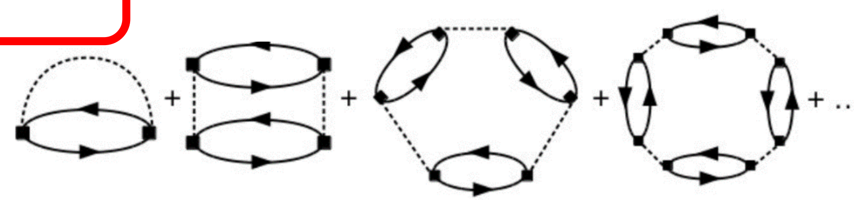

J. M. Torres-Rincon, J. Aichelin PRC 96 (2017) 4 045205
D. Fuseau, T. Steinernert, J. Aichelin PRC 101 (2020) 6 065203

- Modification of the gluon potential due to the presence of the quark

Specific shear viscosity to conductivity

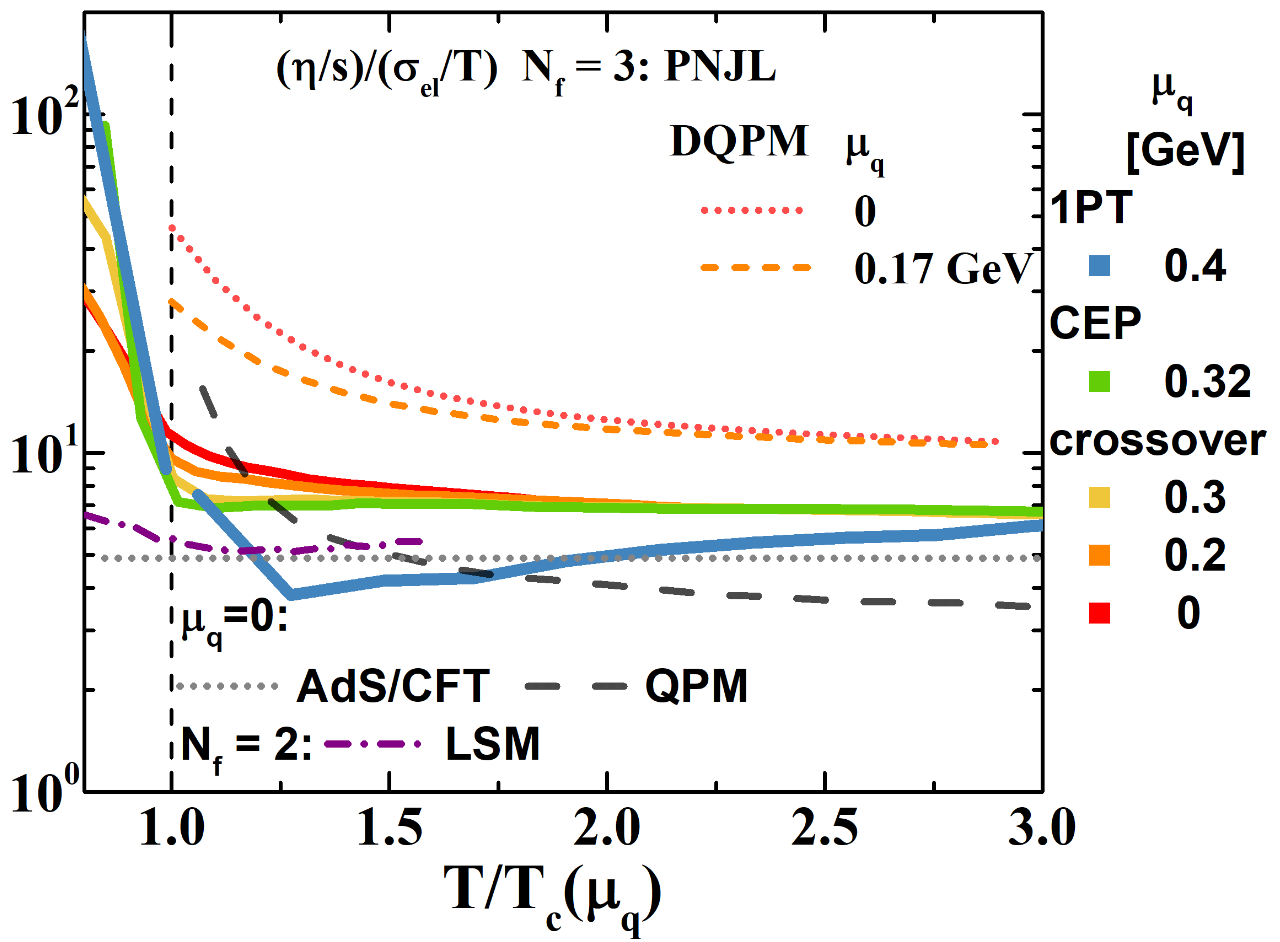

QGP in the Polyakov extended NJL model

- PNJL allows for prediction of macroscopic properties of QGP at finite **T** and μ_B
- & QGP transport coefficients for $0 \leq \boldsymbol{\mu_B} \leq 1.2$ GeV

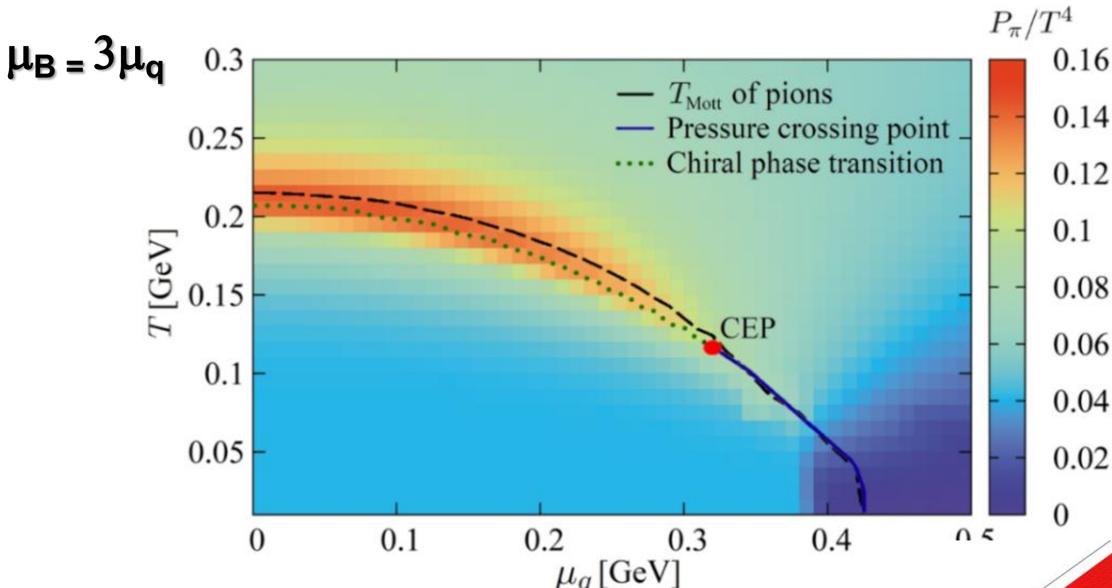

D. Fuseau, T. Steinert, J. Aichelin PRC 101 (2020) 6 065203

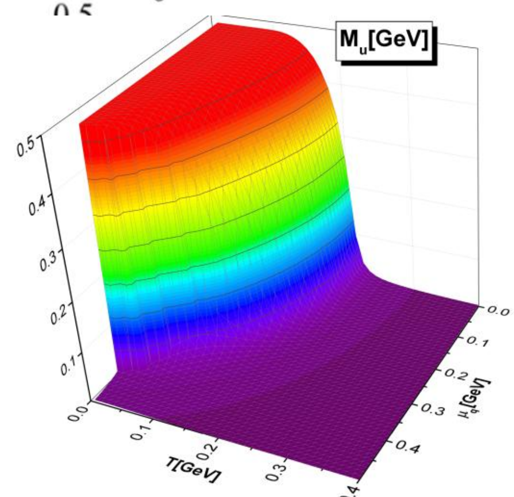

- CEP: (T , $\boldsymbol{\mu_B}$) = (110,960) MeV , $\boldsymbol{\mu_B}$/T = 8.73
- 1st order PT at high $\boldsymbol{\mu_B}$
- same symmetries for the quarks as QCD

Chiral masses ($\boldsymbol{M_l}, \boldsymbol{M_s}$)

$$m_i = m_{0i} - 4G\langle\langle\bar{\psi}_i\psi_i\rangle\rangle + 2K\langle\langle\bar{\psi}_j\psi_j\rangle\rangle\langle\langle\bar{\psi}_k\psi_k\rangle\rangle$$

Specific shear viscosity compilation

- **Kubo formalism: transport coefficients are expressed through correlation functions of stress-energy tensor**

used in lattice QCD, transport approaches(hadrons), effective models

$$\eta = \frac{1}{20} \lim_{\omega\to 0} \frac{1}{\omega} \int d^4x \, e^{i\omega t} \left\langle \left[\mathcal{S}^{ij}(t,\mathbf{x}), \, \mathcal{S}^{ij}(0,\mathbf{0}) \right] \right\rangle \theta(t) \qquad \mathcal{S}^{ij} = T^{ij} - \delta^{ij}\mathcal{P}$$

$$\zeta = \frac{1}{2} \lim_{\omega\to 0} \frac{1}{\omega} \int d^4x \, e^{i\omega t} \langle [\mathcal{P}(t,\mathbf{x}), \, \mathcal{P}(0,\mathbf{0})] \rangle \theta(t) \qquad \mathcal{P} = -\tfrac{1}{3} T^{i}{}_{i}$$

R. Lang and W. Weise, EPJ. A 50, 63 (2014) (NJL model)
A. Harutyunyan et al,PRD 95, 114021, (2017)

Kinetic theory:

- **Relaxation time approximation(RTA) : consider relaxation time** $\dfrac{df_a^{\mathrm{eq}}}{dt} = \mathcal{C}_a = -\dfrac{f_a^{\mathrm{eq}}\phi_a}{\tau_a}$

P. Chakraborty and J. I. Kapusta, PRC 83,014906 (2011)

- **Chapman-Enskog : expand the distribution in terms of the Knudsen number**

J. A. Fotakis et al, PRD 101 (2020) 7, 076007 (HRG)

And more!

Holographic models: AdS/CFT correspondence

D. T. Son and A. O. Starinets, JHEP 0603, 052 (2006)
M. Attems et al , JHEP 10 (2016), 155.

Elliptic flow ($\sqrt{s_{NN}} = 200\ GeV\ - 27GeV$)

- Weak μ_B –dependence – small fraction of QGP or low μ_B
- Small effect of the angular dependence of **dσ/dcosθ**
- Strong flavor dependence

27GeV, 10-40%

$$v_1 = \left\langle \frac{p_x}{p_T} \right\rangle$$

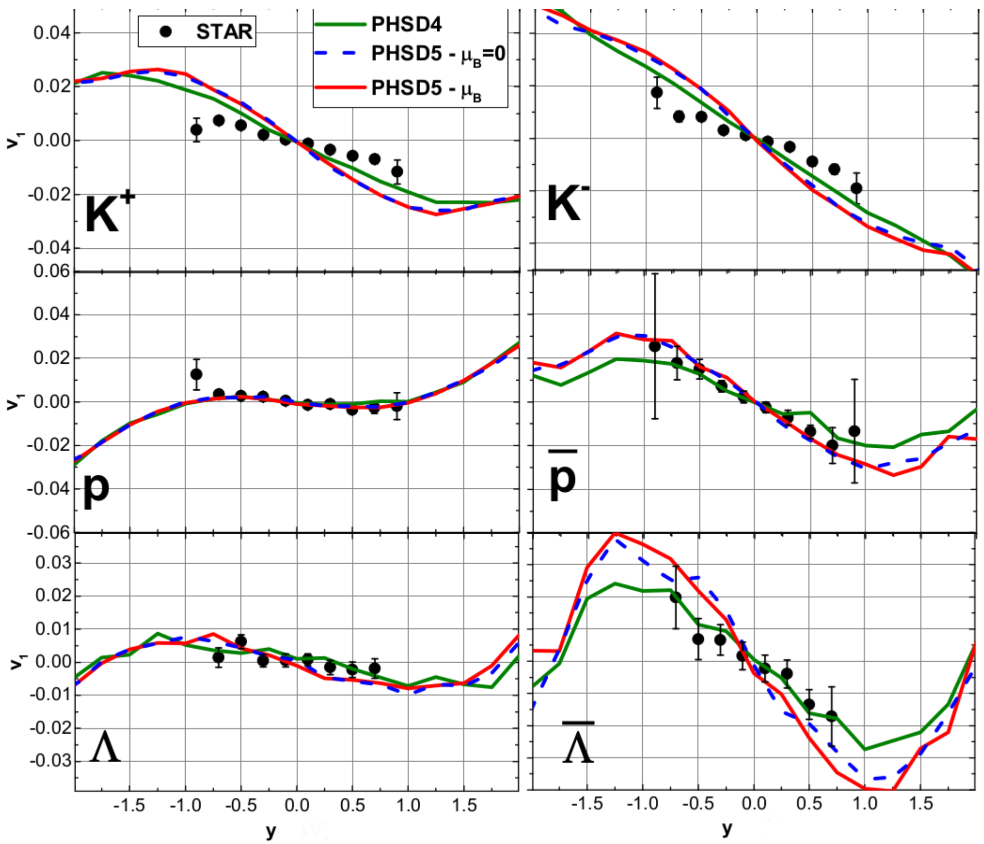

$$v_2 = \left\langle \frac{p_x^2 - p_y^2}{p_T^2} \right\rangle$$

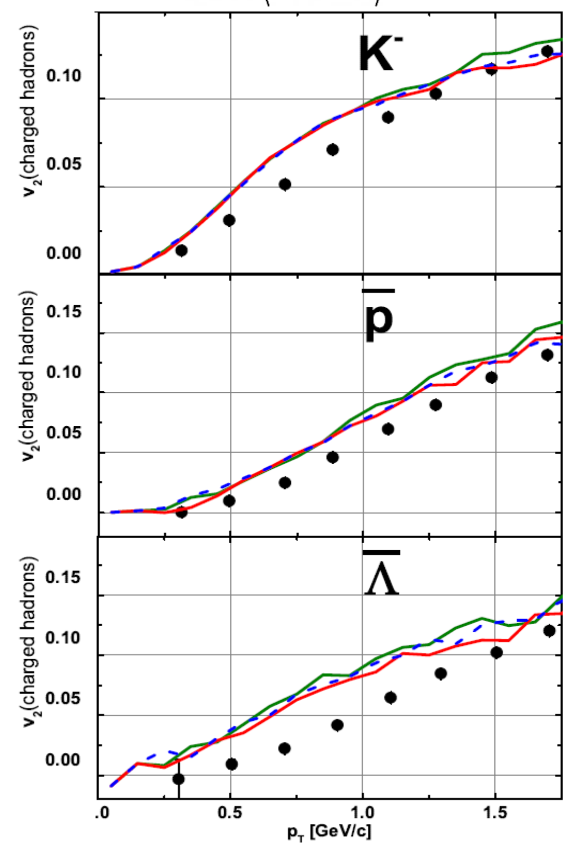

O. Soloveva, P. Moreau, L. Oliva, V. Voronyuk, V. Kireyeu, T. Song, E. Bratkovskaya, Particles 3 (2020), 178-192

PNJL improvements

- **Next to leading order in Nc (O(1/Nc)^0) of the grand-canonical potential :** **presence of the mesons below Tc**

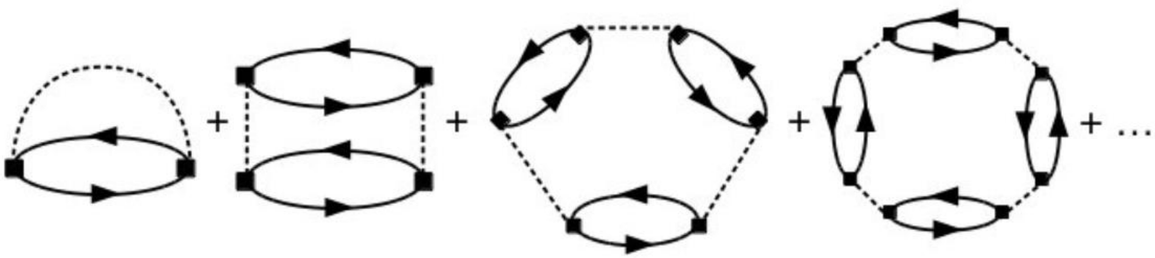

J. M. Torres-Rincon, J. Aichelin PRC 96 (2017) 4 045205

- **Modification of the gluon potential due to the presence of the quark**

$$\frac{U(\phi,\bar{\phi},T)}{T^4} = -\frac{b_2(T)}{2}\bar{\phi}\phi - \frac{b_3}{6}(\bar{\phi}^3+\phi^3) + \frac{b_4}{4}(\bar{\phi}\phi)^2$$

$$b_2(T) = a_0 + \frac{a_1}{1+\tau} + \frac{a_2}{(1+\tau)^2} + \frac{a_3}{(1+\tau)^3}$$ where $$\tau_{\text{phen}} = 0.57\frac{T - T^{\text{cr}}_{\text{phen}}(T)}{T^{\text{cr}}_{\text{phen}}(T)}$$

$$T_{phen}(T) = a + bT + cT^2 + dT^3 + \boxed{e\frac{1}{T}}$$

D. Fuseau, T. Steinernert, J. Aichelin PRC 101 (2020) 6 065203

Stages of collisions in PHSD

Initial A+A collision

- **String formation** in primary NN collisions

  → **decays** to pre-hadrons (baryons and mesons)

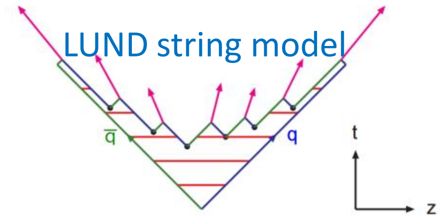

Partonic phase

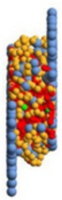

- Formation of a **QGP** state if $\varepsilon > \varepsilon_{critical}$:
  Dissolution of pre-hadrons → DQPM

  → massive quarks/gluons and mean-field energy

  (quasi-)elastic collisions :

  $$q+q \to q+q \quad g+q \to g+q$$
  $$q+\bar{q} \to q+\bar{q} \quad g+\bar{q} \to g+\bar{q}$$
  $$\bar{q}+\bar{q} \to \bar{q}+\bar{q} \quad g+g \to g+g$$

  inelastic collisions:

  $$q+\bar{q} \to g$$
  $$g \to q+\bar{q}$$

Hadronization

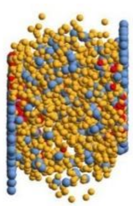

- **Hadronization** to colorless off-shell mesons and baryons

  $$g \to q+\bar{q}, \quad q+\bar{q} \leftrightarrow meson \ ('\,string\,')$$
  $$q+q+q \leftrightarrow baryon \ ('\,string\,')$$

  Strict 4-momentum and quantum number conservation

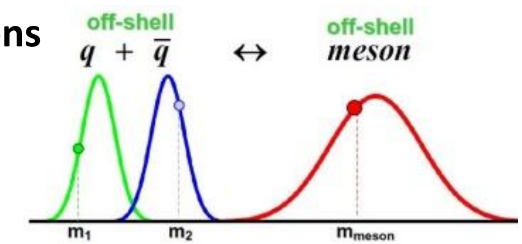

Hadronic phase

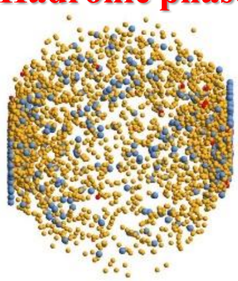

- **Hadron-string interactions** – off-shell HSD

W. Cassing, E. Bratkovskaya, PRC 78 (2008) 034919; NPA831 (2009) 215;
W. Cassing, EPJ ST 168 (2009) 3

Stages of HIC

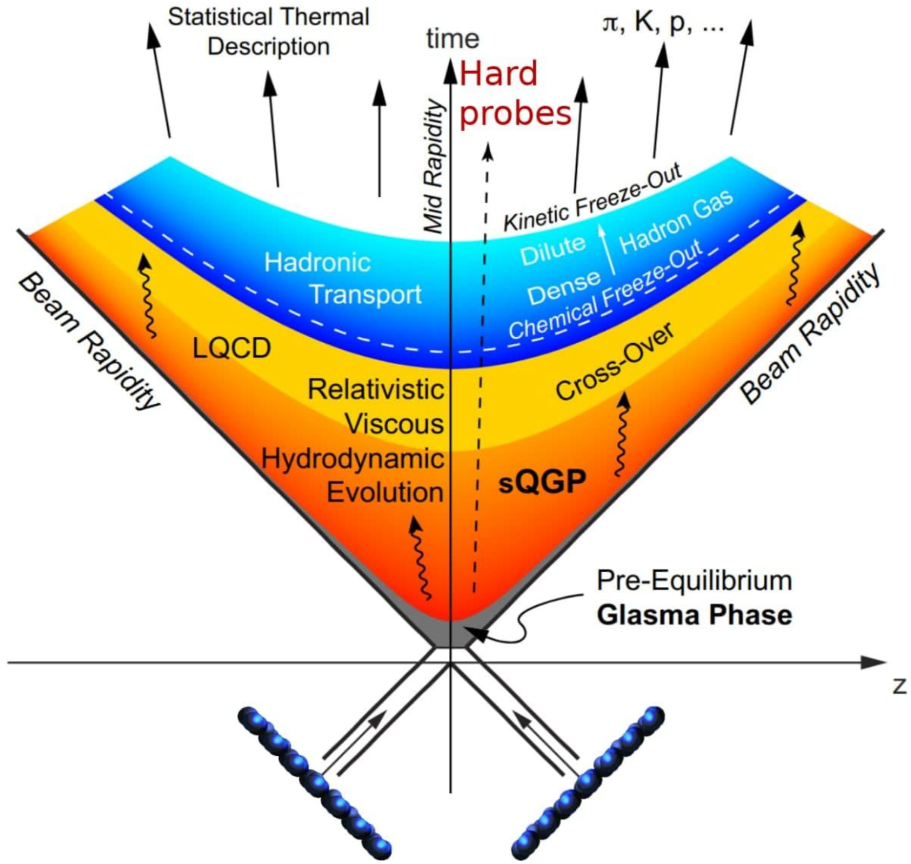

t > 10 fm - hadronisation and free streem to detectors

10 fm > t > 1 fm - QGP expansion

t ≈ 1 fm - Equilibration

t << 1 fm - Initial state

QGP out-of equilibrium ↔ HIC

Results for ($\sqrt{s_{NN}}$ = 200 GeV - 7 GeV)

- No visible effects on p_T-spectra, dN/dy of μ_B -dependence
- Small effect of the angular dependence of **dσ/dcosθ**

at high $\sqrt{s_{NN}}$ - low μ_B

! QGP fraction is small at low $\sqrt{s_{NN}}$

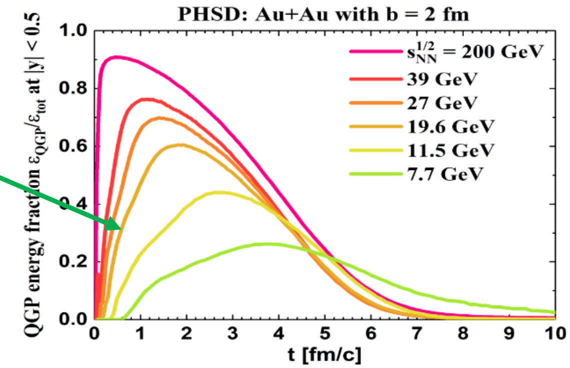

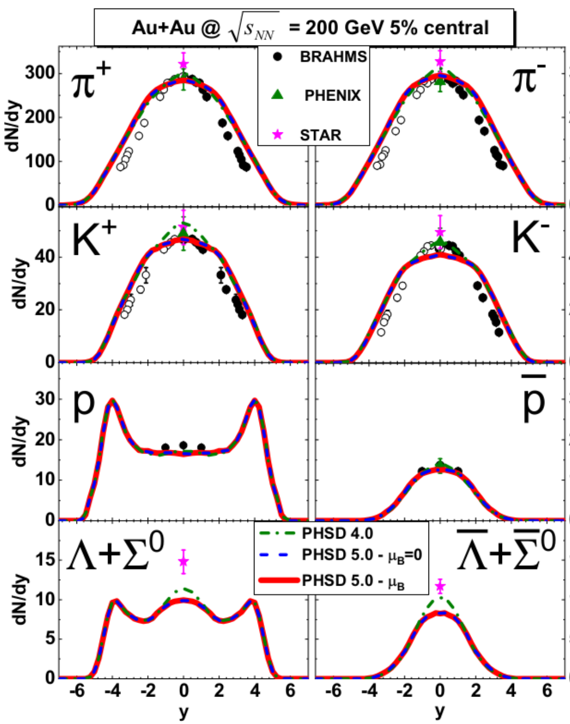

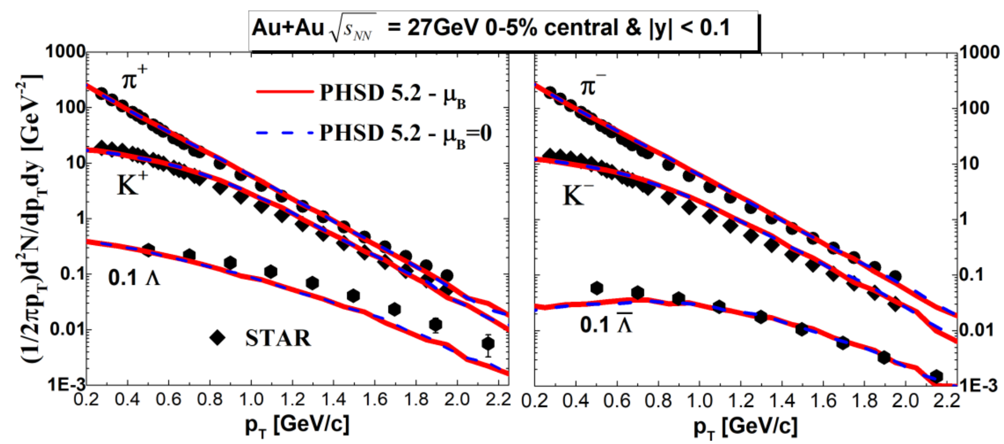

P. Moreau, O. Soloveva , L. Oliva, T. Song, W. Cassing, E. Bratkovskaya, PRC 100 (2019) , 014911;
O. Soloveva, P. Moreau, L. Oliva, V. Voronyuk, V. Kireyeu, T. Song, E. Bratkovskaya, Particles 3 (2020), 178-192

Directed flow ($\sqrt{s_{NN}} = 200\ GeV\ vs\ 27\ GeV$)

$$v_1 = \left\langle \frac{p_x}{p_T} \right\rangle$$

- Influence of the QGP dynamics on final particles observables
- Weak μ_B –dependence – small fraction of QGP or low μ_B

Particles 3 (2020) no.1, 178-192

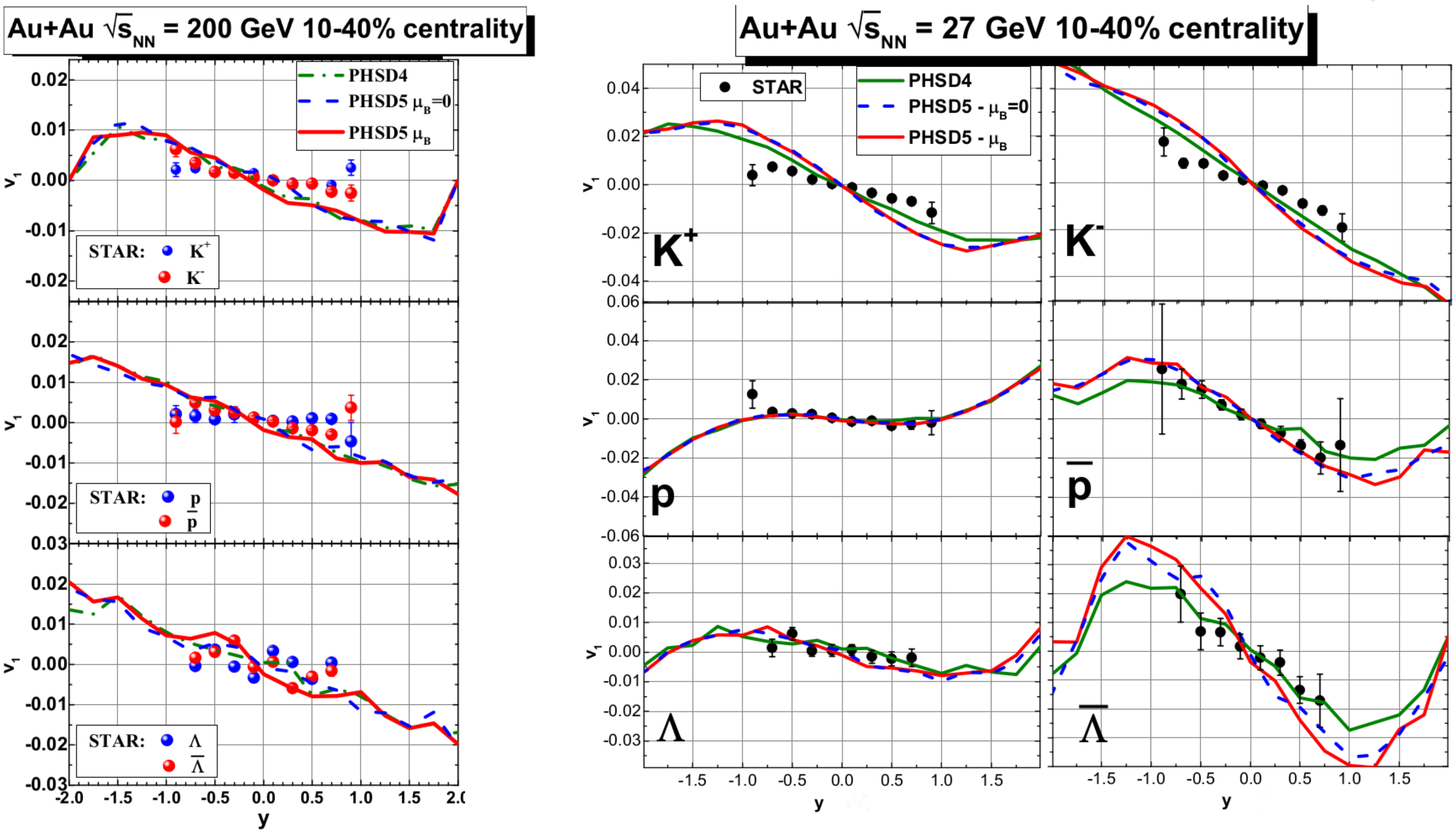

Elliptic flow ($\sqrt{s_{NN}} = 200\ GeV\ vs\ 27 GeV$)

$$v_2 = \left\langle \frac{p_x^2 - p_y^2}{p_T^2} \right\rangle$$

- Weak μ_B -dependence
- Small effect of the angular dependence of **dσ/dcosθ**
- Strong flavor dependence

Particles 3 (2020) no.1, 178-192

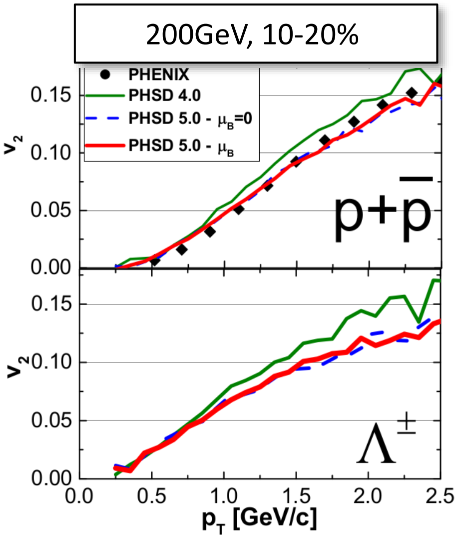

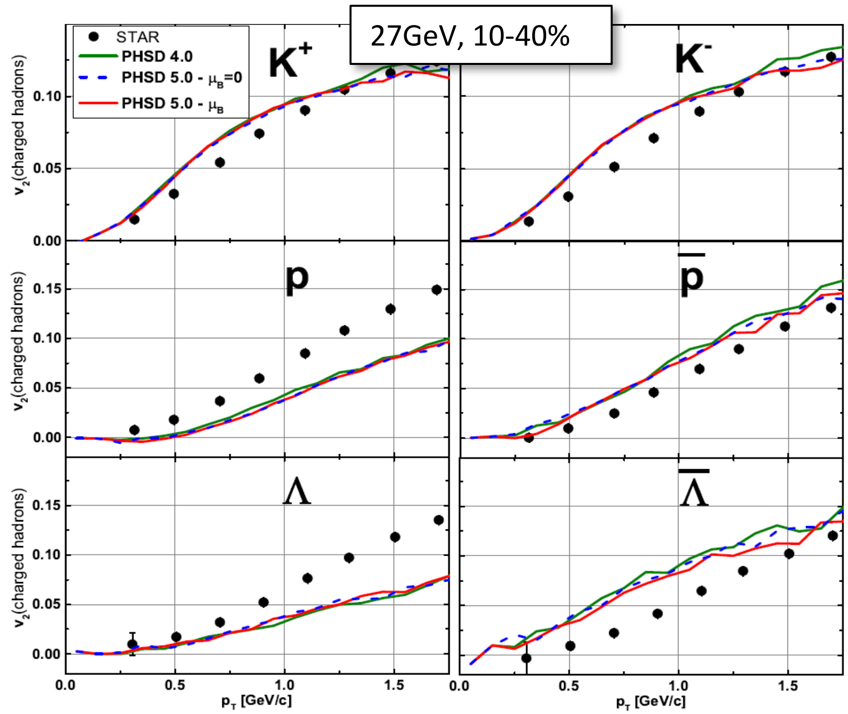

Channel decomposition :